

Evolution of a 4-Benzyloxy-benzylamino Chemotype to Provide Efficacious, Potent, and Isoform Selective PPAR α Agonists as Leads for Retinal Disorders

Xiaozheng Dou,^{†,§} Dinesh Nath,^{†,§} Henry Shin,[‡] Elmar Nurmemmedov,[‡] Philip C. Bourne,[§] Jian-Xing Ma,[‡] and Adam S. Duerfeldt^{*†,§}

[†]*Institute for Natural Products Applications and Research Technologies and* [§]*Department of Chemistry & Biochemistry, University of Oklahoma, 101 Stephenson Parkway, Stephenson Life Sciences Research Center, Norman, Oklahoma 73019, United States*

[‡]*Department of Physiology, University of Oklahoma Health Sciences Center, 941 Stanton L. Young Boulevard, Oklahoma City, Oklahoma 73104, United States*

[‡]*John Wayne Cancer Institute & Pacific Neuroscience Institute at Providence Saint John's Health Center, 2200 Santa Monica Boulevard, Santa Monica, California 90404, United States*

Supporting information –Two-concentration luciferase data, PPAR α expression and purification, cellular thermal shift western blots, cytotoxicity, *in silico* metabolic predictions, isothermal titration calorimetry thermograms and curve fits, ¹H and ¹³C NMR spectra for final compounds, HPLC traces for select leads, and pharmacokinetic data sets.

*to whom correspondence should be addressed. Department of Chemistry and Biochemistry, University of Oklahoma, 101 Stephenson Parkway, Stephenson Life Sciences Research Center, Norman, Oklahoma 73019. Phone: 1-405-325-2232. Email: adam.duerfeldt@ou.edu.

Table of Contents

PPAR α Luciferase Two-Concentration Assessment	S4
Isothermal Calorimetry.....	S5
PPAR α Expression and Purification.....	S5
CETSA Western Blot Data	S6
LDH Cytotoxicity Assay	S7
<i>In silico</i> Metabolic Predictions	S8
NMR Spectra for Final Compounds	
^1H and ^{13}C NMR Spectra for 4b.....	S9
^1H and ^{13}C NMR Spectra for 4b*	S10
^1H and ^{13}C NMR Spectra for 4c	S11
^1H and ^{13}C NMR Spectra for 4d.....	S12
^1H and ^{13}C NMR Spectra for 4e	S13
^1H and ^{13}C NMR Spectra for 4f.....	S14
^1H and ^{13}C NMR Spectra for 4g.....	S15
^1H and ^{13}C NMR Spectra for 4h.....	S16
^1H and ^{13}C NMR Spectra for 4i.....	S17
^1H and ^{13}C NMR Spectra for 4j.....	S18
^1H and ^{13}C NMR Spectra for 4k.....	S19
^1H and ^{13}C NMR Spectra for 4l.....	S20
^1H and ^{13}C NMR Spectra for 4m.....	S21
^1H and ^{13}C NMR Spectra for 4n.....	S22
^1H and ^{13}C NMR Spectra for 4o	S23
^1H and ^{13}C NMR Spectra for 4p.....	S24
^1H and ^{13}C NMR Spectra for 4q.....	S25
^1H and ^{13}C NMR Spectra for 4r	S26
^1H and ^{13}C NMR Spectra for 4s.....	S27
^1H and ^{13}C NMR Spectra for 4t.....	S28
^1H and ^{13}C NMR Spectra for 4u	S29
^1H and ^{13}C NMR Spectra for 4v	S30
^1H and ^{13}C NMR Spectra for 4w	S31
^1H and ^{13}C NMR Spectra for 4x	S32

¹H and ¹³C NMR Spectra for 4y	S33
¹H and ¹³C NMR Spectra for 4z	S34
¹H and ¹³C NMR Spectra for 5a	S35
¹H and ¹³C NMR Spectra for 5b	S36
¹H and ¹³C NMR Spectra for 5b*	S37
¹H and ¹³C NMR Spectra for 5f	S38
¹H and ¹³C NMR Spectra for 19a	S39
¹H and ¹³C NMR Spectra for 19b	S40
¹H and ¹³C NMR Spectra for 19c	S41
¹H and ¹³C NMR Spectra for 19d	S42
¹H and ¹³C NMR Spectra for 19e	S43
¹H and ¹³C NMR Spectra for 19f	S44
¹H and ¹³C NMR Spectra for 20	S45
¹H and ¹³C NMR Spectra for 21	S46
¹H and ¹³C NMR Spectra for 22	S47
¹H and ¹³C NMR Spectra for 23	S48
¹H and ¹³C NMR Spectra for 24	S49
¹H and ¹³C NMR Spectra for 25	S50
¹H and ¹³C NMR Spectra for 26	S51
¹H and ¹³C NMR Spectra for 27	S52
¹H and ¹³C NMR Spectra for 28	S53
¹H and ¹³C NMR Spectra for 29	S54
¹H and ¹³C NMR Spectra for 30	S55
¹H and ¹³C NMR Spectra for 31	S56
¹H and ¹³C NMR Spectra for 32	S57
¹H and ¹³C NMR Spectra for 33	S58
HPLC Traces for Key Analogues	S59
Pharmacokinetic Data (Eurofins)	S62

PPARα LUCIFERASE TWO-CONCENTRATION ASSESSMENT

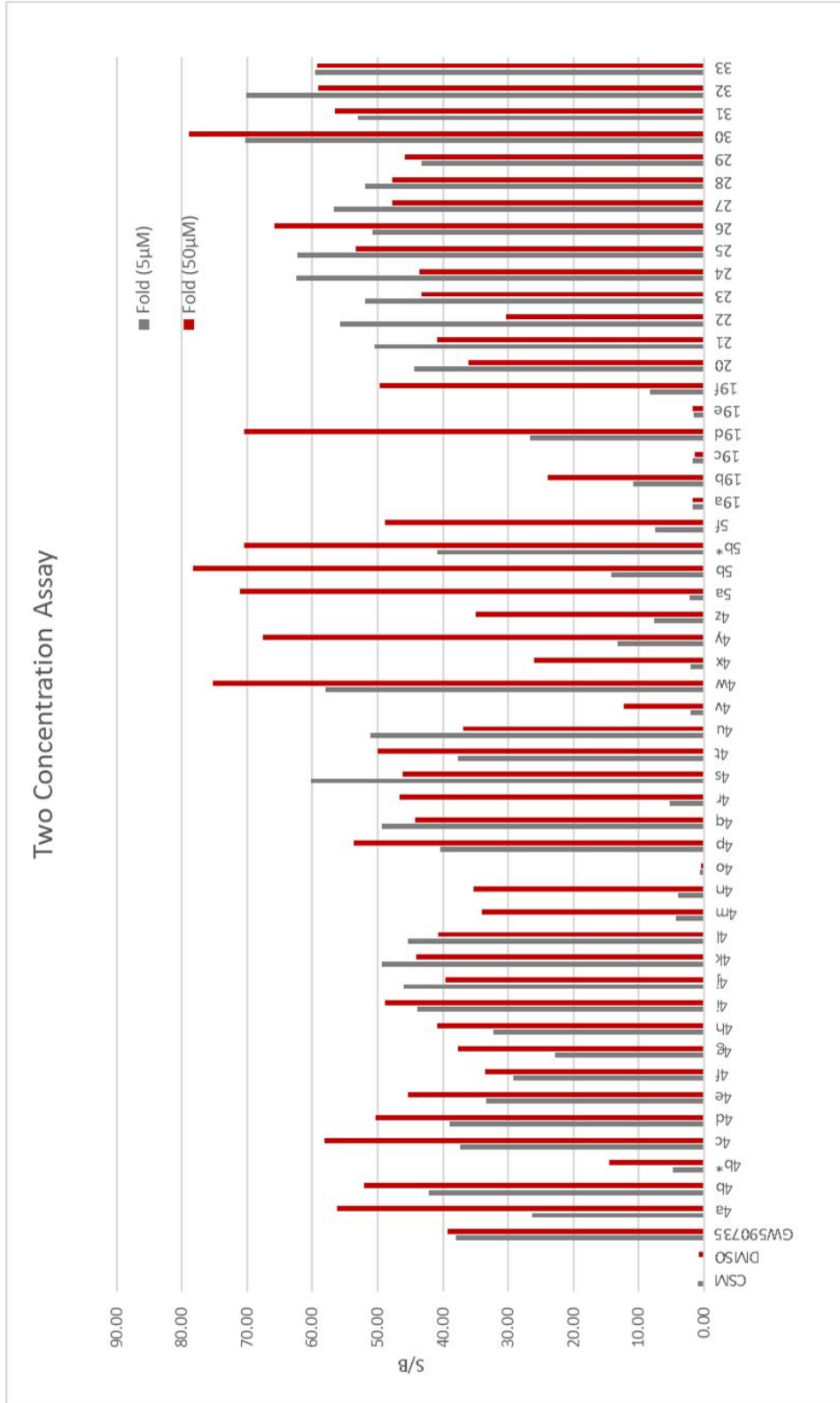


Figure 1. Initial two-concentration assessment of 4a-4z, 5a, 5b, 5b*, 5f, 20a-20f, and 21-34 for PPARα agonism in a luciferase-based cellular assay (Indigo). Results presented from a single experiment as mean signal/mean background (S/B). GW590735 was evaluated at 5 μM and 40 μM due to observed cytotoxicity at higher concentrations.

ISOTHERMAL CALORIMETRY

ITC experiments were performed using a MicroCal PEAQ ITC (MicroCal Inc., Northampton, MA, USA). PPAR α was concentrated down to a final concentration of 3.27 mg/mL using an Amicon Ultra-15 centrifugal concentrator (Millipore). Buffer (20 mM HEPES, 150 mM NaCl, pH 7.4) was used to dilute the ligand stock solution (10, 12.5, or 25 mM in DMSO). DMSO was added to the protein solution at the same percentage (0.8-10%) of the ligand solution. Samples were centrifuged before the experiment to eliminate possible aggregates. The protein solution (30-85 μ M) was placed in the sample cell, and the ligand solution (2.3-15 times more concentrated than the protein) was loaded into the syringe injector. The detailed experimental parameters are shown below. The titrations involved 19 injections of 2 μ L at 150 s intervals or 13 injections of 3 μ L at 150 s intervals. The experiment was set at 25 $^{\circ}$ C and the syringe stirring speed was set at 750 rpm. Titration of ligand at same concentration into buffer with same percentage DMSO were used as a reference control. The thermodynamic data were processed with MicroCal PEAQ-ITC Analysis Software provided by Malvern. The one-site binding model was selected to calculate the value of the dissociation constant (K_d), the enthalpy (ΔH), the binding free energy (ΔG), and the entropy ($-T\Delta S$).

Ligand	[PPAR α] μ M	[Ligand] nM	DMSO% (v/v)
4a (A91)	85	0.2	0.8%
4b	60	0.5	2%
4u	30	0.25	2%
GW590735	80	0.5	2%

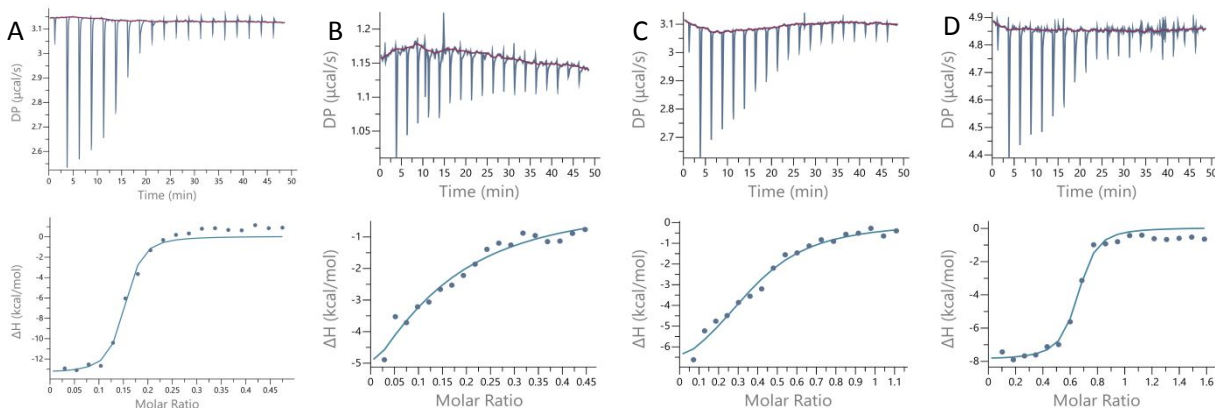


Figure S2. Isothermal titration calorimetry thermograms of select ligands to PPAR α -LBD. The upper panel shows the raw data of a representative ITC experiment. The lower panel shows the corresponding binding isotherm fit according to the “one binding site” model. A) GW590735; B) compound **4a**; C) compound **4b**; and D) compound **4u**

PROTEIN EXPRESSION, PURIFICATION

Protein was expressed from the pET28c vector (Novagen) in *Escherichia coli* strain RosettaTM (DE3) grown in LB media to an OD of 0.6 and then induced with 1 mM IPTG for 20 h at 18 $^{\circ}$ C. Cells were harvested and resuspended in Buffer A (20 mM Tris, 150 mM NaCl, 5% glycerol, 5 mM imidazole, pH 8.0) at 5 ml/g pellet weight. Cultures were lysed using an Emulsiflex C-3 homogenizer (Avestin), and the lysate clarified by centrifugation (22,000 \times g, 40 min). The supernatant was loaded onto a 5ml HisTrap FF Crude column (GE Life Sciences) and eluted with a linear gradient of 5-500 mM imidazole over 20 column volumes. Fractions containing PPAR α were identified by sodium dodecyl sulfate–polyacrylamide gel electrophoresis analysis. The His-Tag was removed by thrombin cleavage (10 U thrombin/mg) dialyzed overnight at 4 $^{\circ}$ C against buffer B (20 mM Tris, 150 mM NaCl, 5% glycerol, pH 8.0). The uncleaved protein was removed by reloading the sample onto the 5 ml HisTrap FF Crude column (GE Life Sciences). The flow through was concentrated to a final volume of 5 ml using an Amicon Ultra-15 centrifugal concentrator (Millipore),

and loaded on to a HiLoad Superdex 200PG size exclusion chromatography column (GE Life Sciences) pre-equilibrated with Buffer C (20 mM HEPES, 150 mM NaCl, pH 7.4).

CETSA DATA

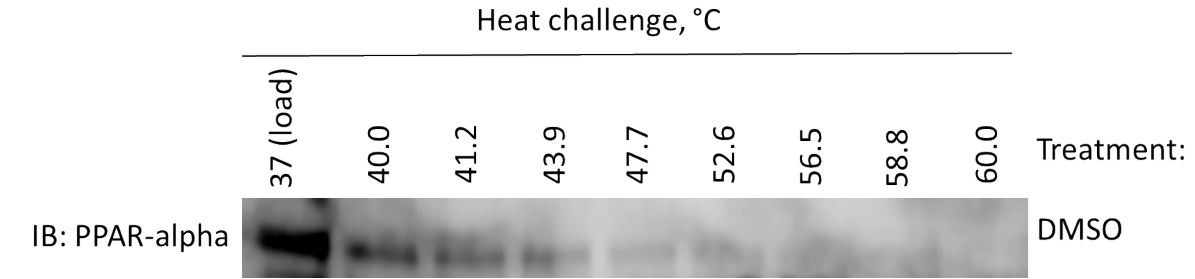


Figure S3. Melting profile of hPPAR α . MIO-M1 cells were subjected to a heat gradient to determine the thermal melting profile of hPPAR α . Band intensity of remaining stable protein at each temperature was quantified, and subsequently the temperature of aggregation ($T_{agg,50}$ and $T_{agg,75}$) was determined as 40.8 °C and 45.5 °C, respectively.

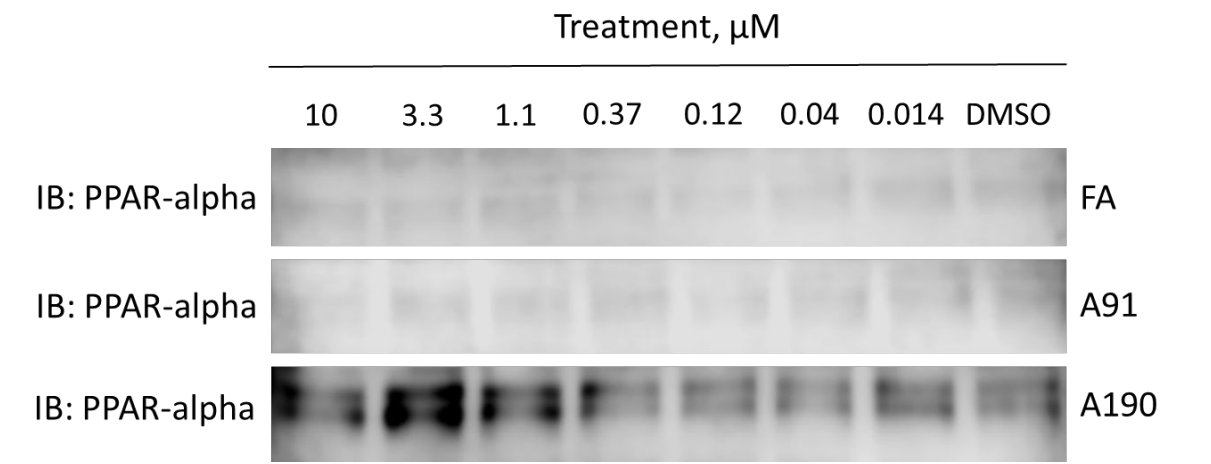


Figure S4. Dose-response CETSA at 45.5 °C. MIO-M1 cells treated with increasing doses of inhibitors were subjected to heat challenge at $T_{agg,75}$ of 45.5 °C. Band intensity of remaining stabilized protein at each dose was quantified, and subsequently the EC_{50} for each inhibitor was determined.

LDH Cytotoxicity Data

661W mouse photoreceptor cells were cultured on 96-well plate (6700 cells per well) with varying concentrations of DMSO, GW7647, or A91 (0 to 200 μM) to induce cytotoxicity. Following overnight incubation with the compounds, culture media from the 96-well plate was collected for the LDH quantification assay, which performed following the manufacturer's instructions (Thermo Scientific, #88953). In short, 50 μL of culture medium was mixed and incubated with 50 μL of Reaction Mixture at 25 $^{\circ}\text{C}$ for 30 minutes. 50 μL of Stop Solution was added and the absorbance was measured at 490 nm and 680 nm. Cell death (percentage of maximum LDH release control) was then determined following the manufacturer's protocols.

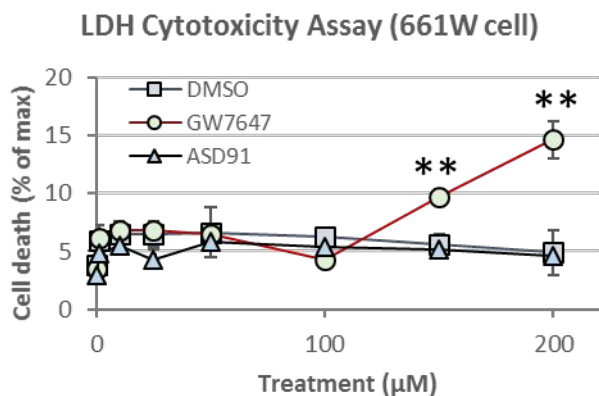


Figure S5. Cytotoxicity of A91 in a retinal epithelium photoreceptor cell-line 661W. LDH activities were measured to determine dose-dependent cytotoxicity of ASD091. No significant LDH activities were detected in all concentrations of ASD091 tested, whereas GW7647 began to induce cell death 150 μM (mean \pm SD; $n=3$). $**P<0.01$.

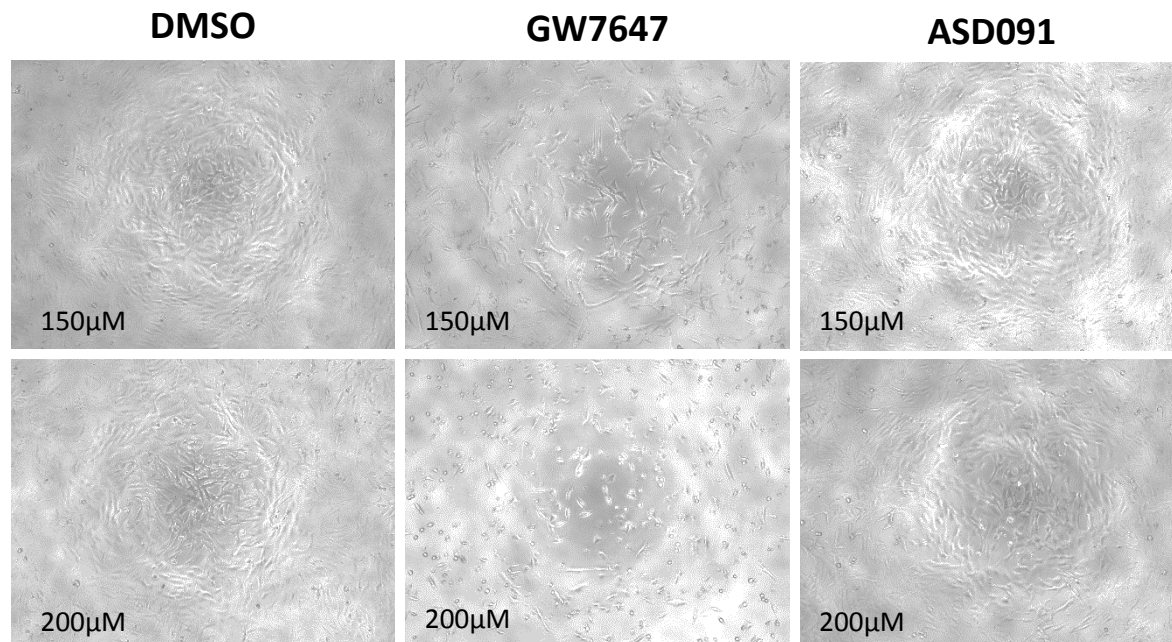


Figure S6. Cellular morphology after compound treatment under light microscopy. Unlike GW7647, ASD091-treated cells did not exhibit any obvious signs of cellular morphology changes at all concentrations tested.

In silico Metabolic Predictions

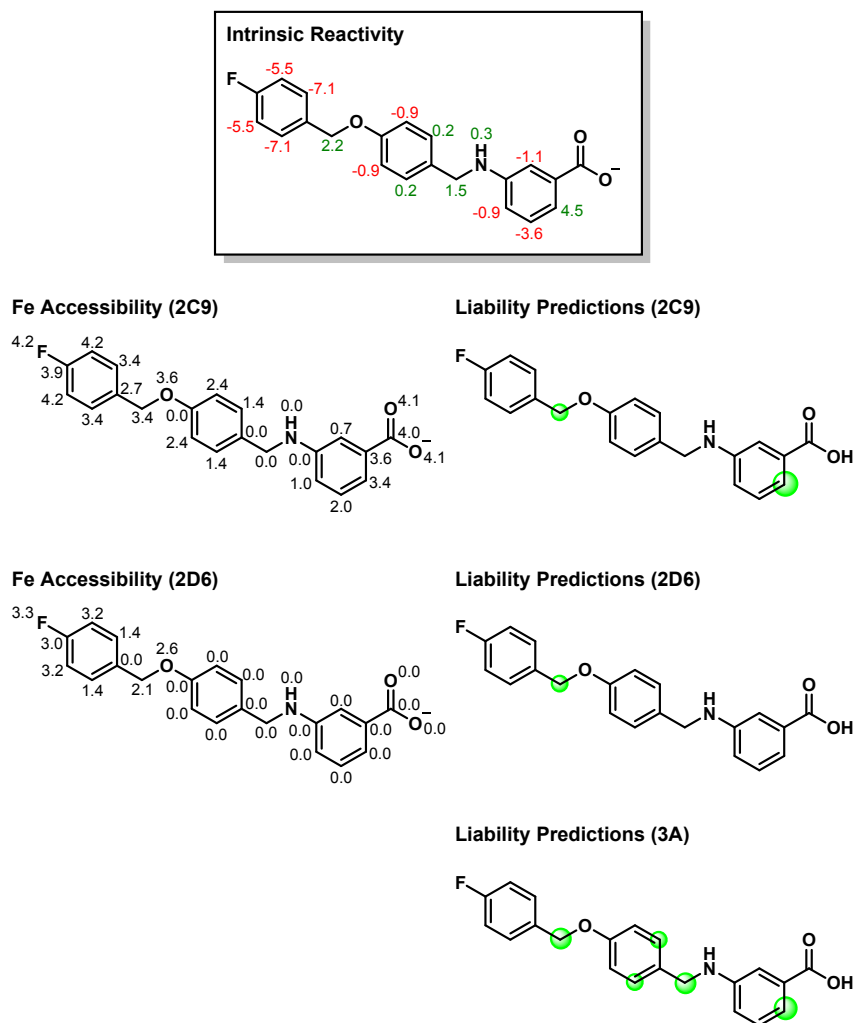
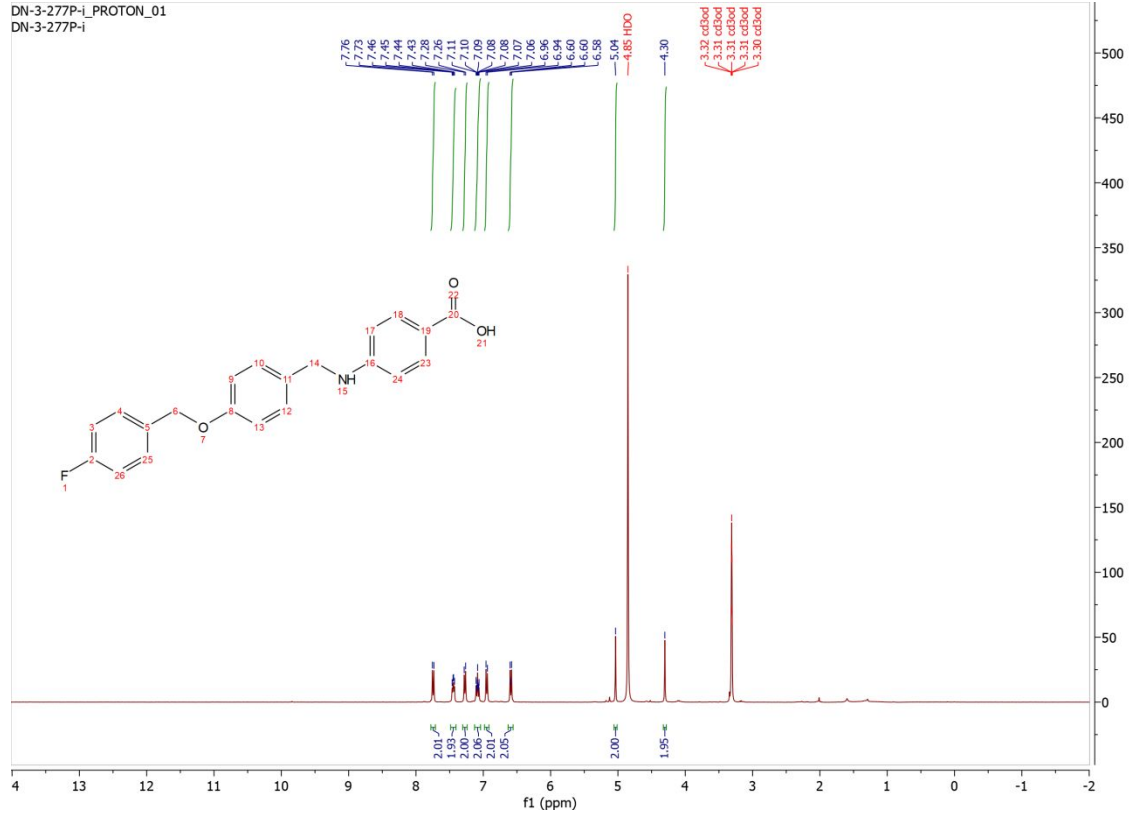


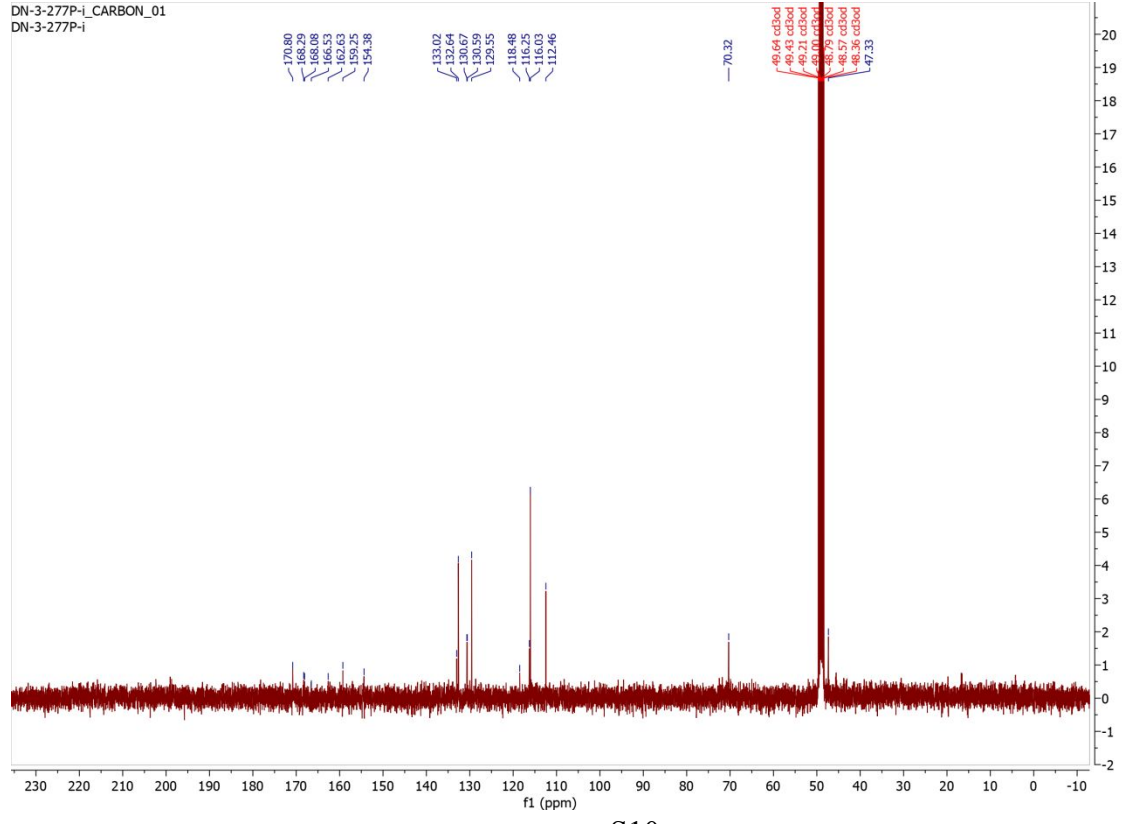
Figure S7. *In silico* metabolic predictions determined by Schrodinger's P450 Site of Metabolism Module. Predictions calculated for **4b** against 2C9, 2D6, and 3A4 CYPs. Components are described as transcribed directly from the manufacturer's manual. **Intrinsic Reactivity** = atoms are labeled with the intrinsic reactivity calculated with Hammett and Taft methodology. Positive values are predicted to be more reactive, negative values are predicted to be less reactive. **Fe Accessibility** = atoms are labeled with accessibility to the iron. This is defined as the natural logarithm of the number of poses for the atom in which the atom was within 5 Å of Fe. Larger values indicate greater accessibility. **Liability Predictions** = linear combination of the accessibility and the intrinsic reactivity. Results are displayed as green circles, in which the radius is proportional to the score. Larger circles mean higher reactivity.

4b*

DN-3-277P-i_PROTON_01
DN-3-277P-i

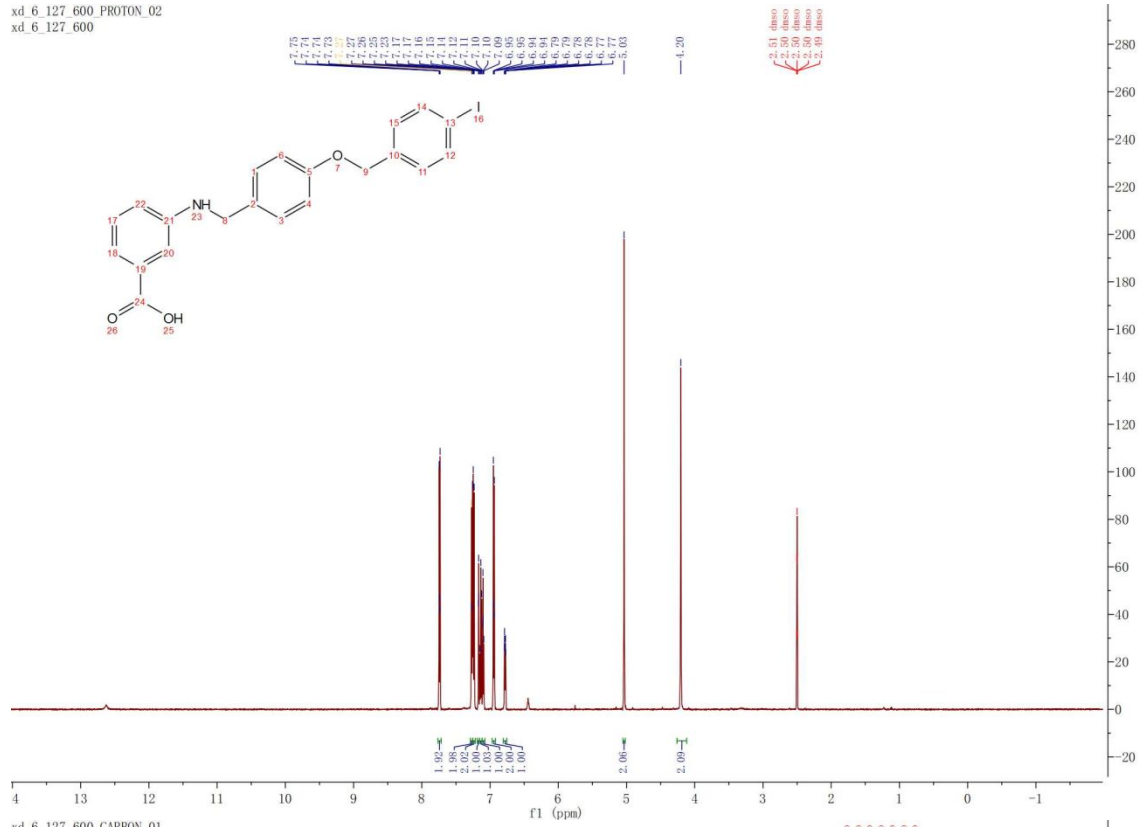


DN-3-277P-i_CARBON_01
DN-3-277P-i

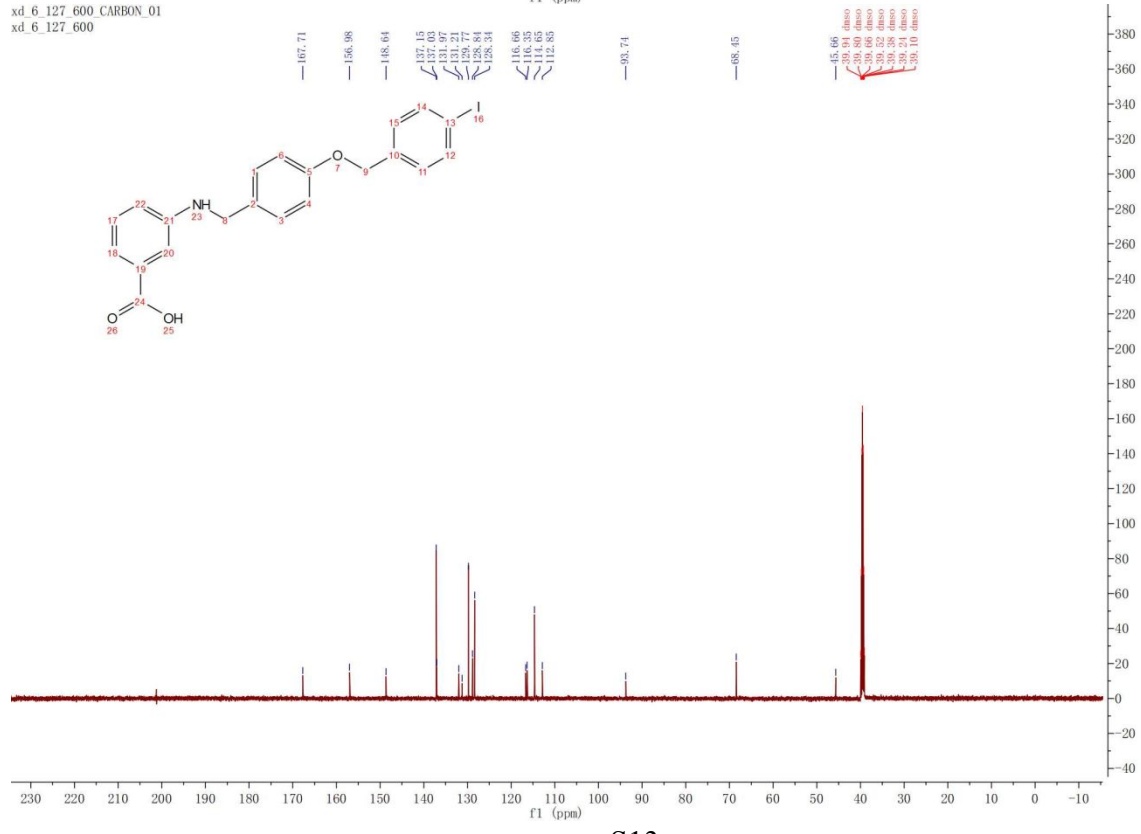


4e

xd_6_127_600_PROTON_02
xd_6_127_600

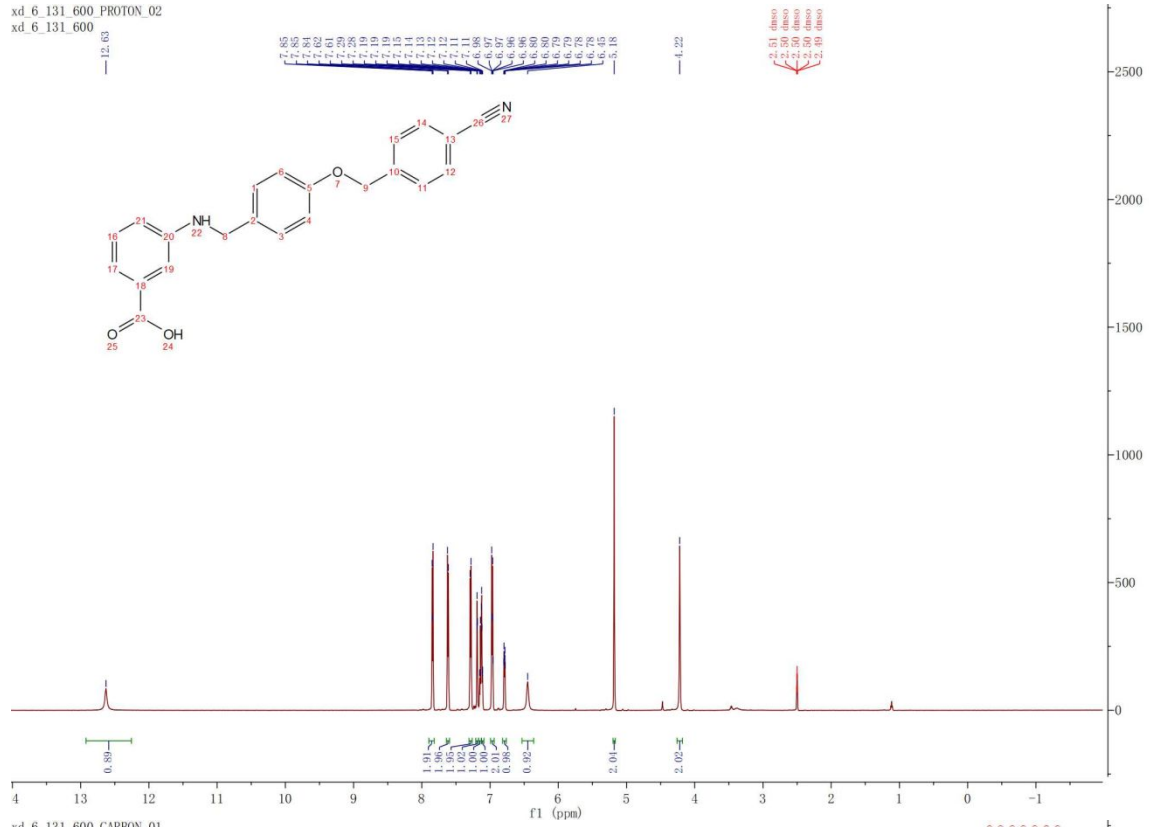


xd_6_127_600_CARBON_01
xd_6_127_600

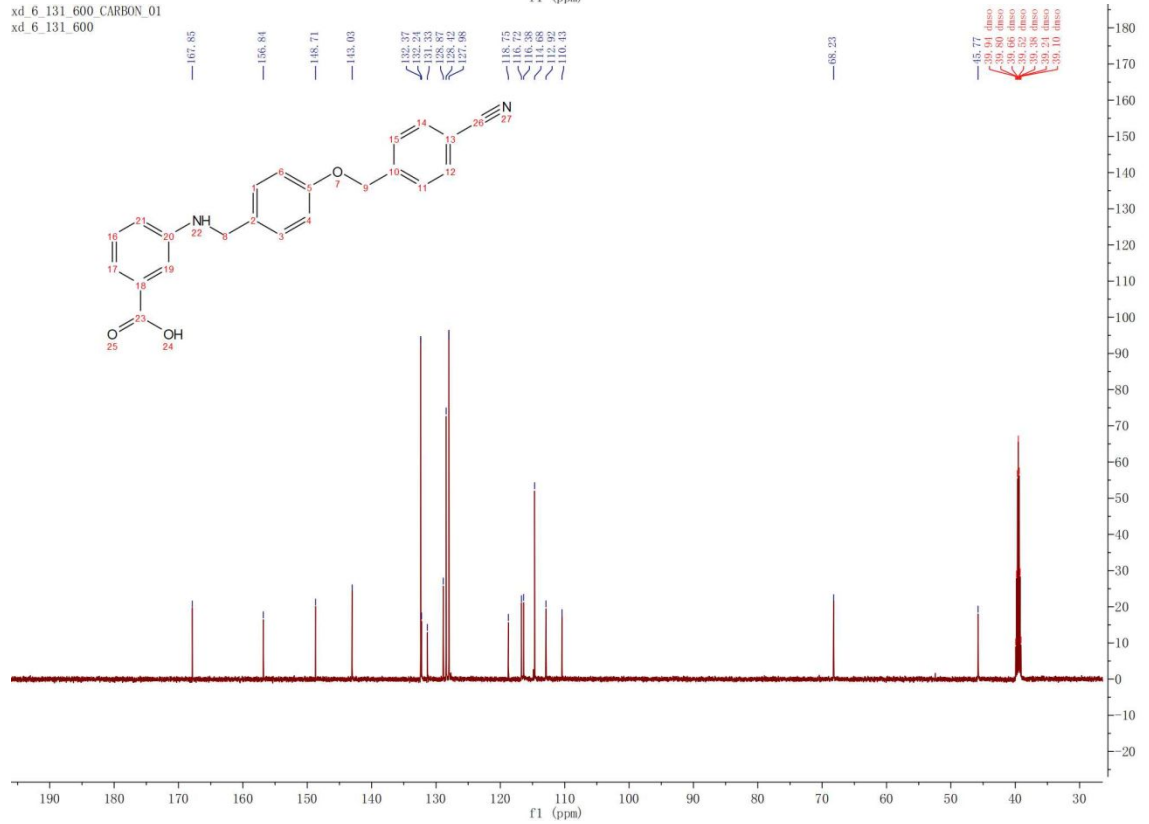


4g

xd_6_131_600_PROTON_02
xd_6_131_600

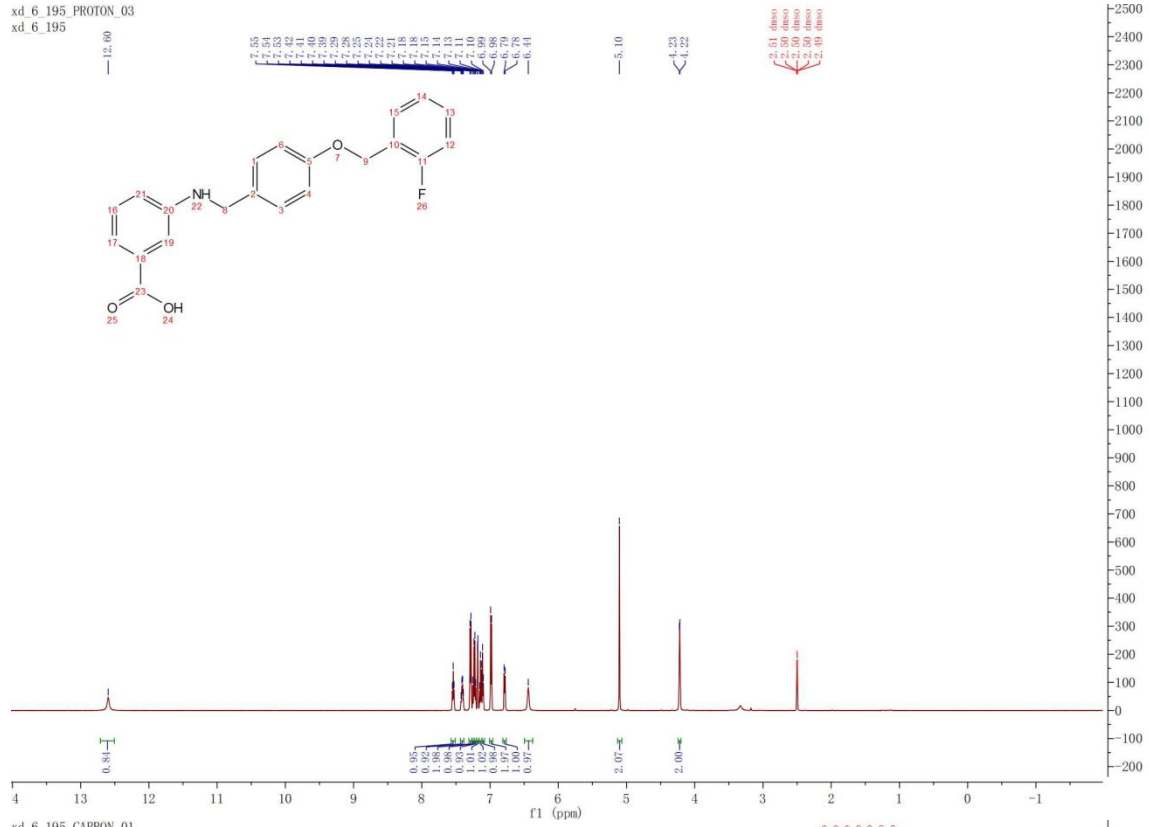


xd_6_131_600_CARBON_01
xd_6_131_600

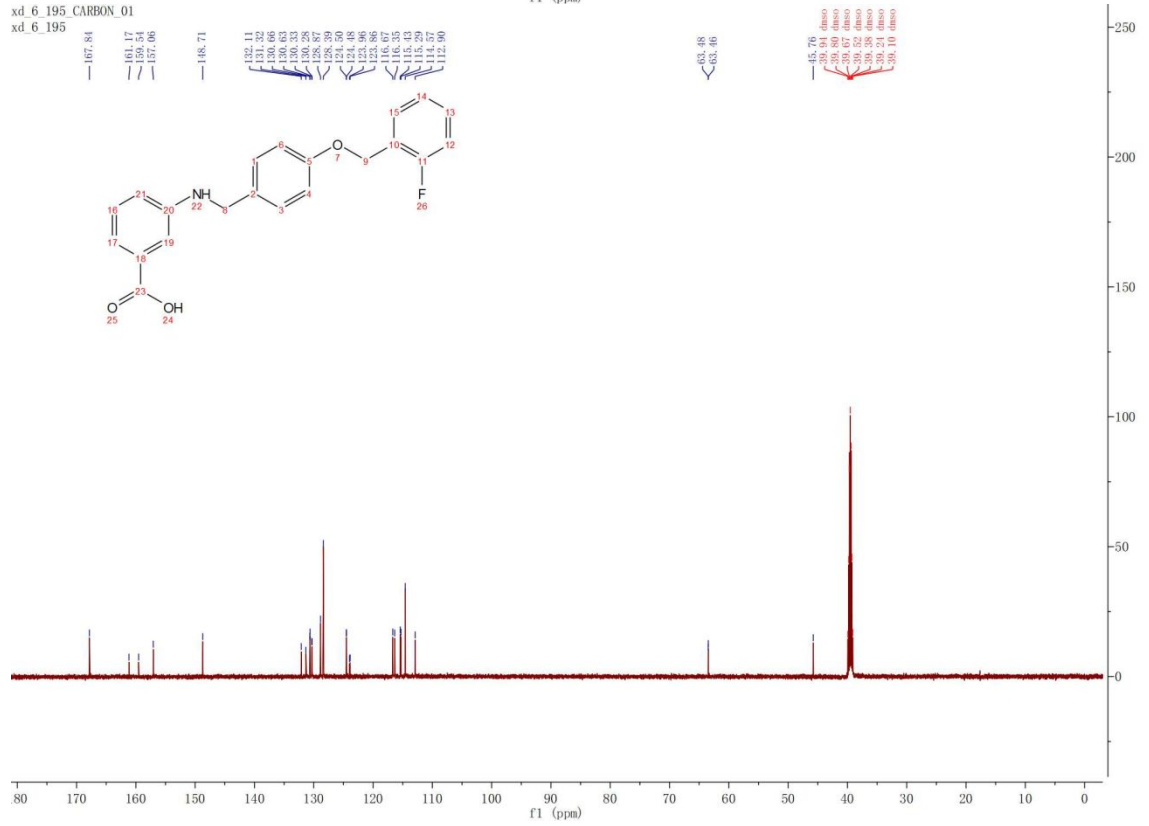


4h

xd_6_195 PROTON_03
xd_6_195

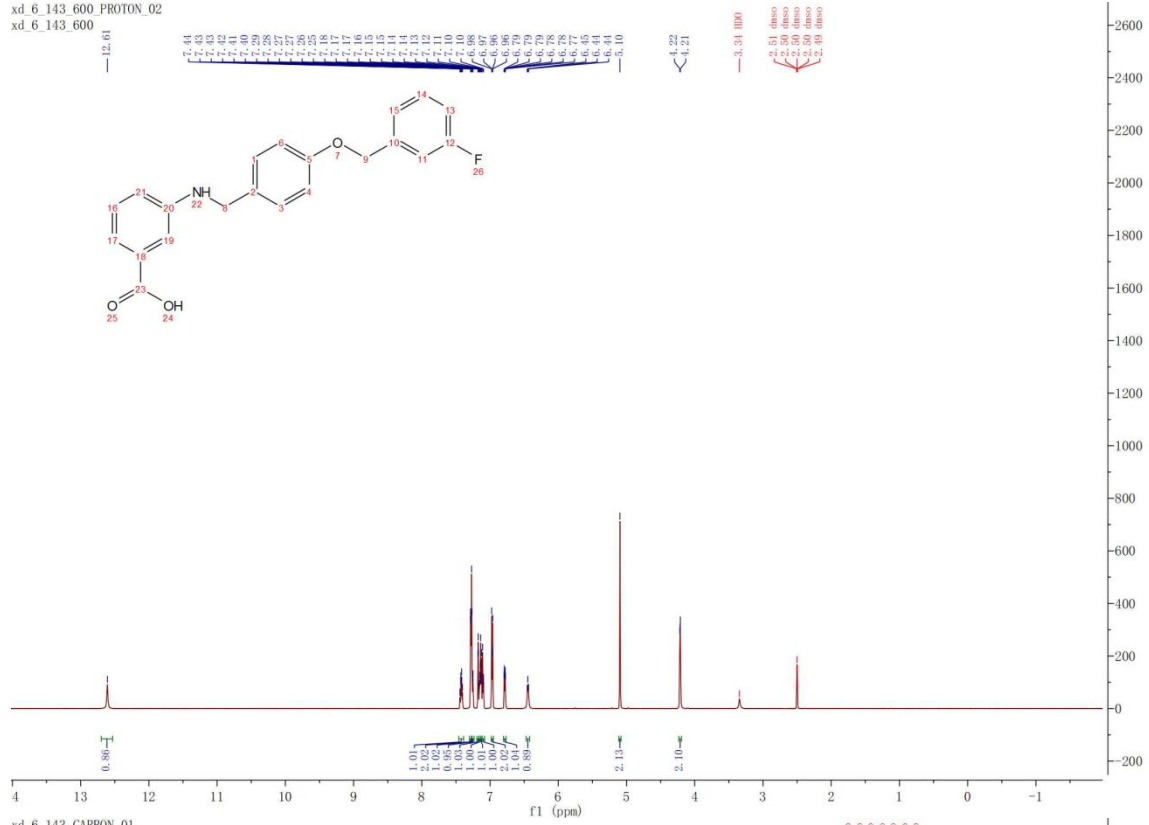


xd_6_195 CARBON_01
xd_6_195

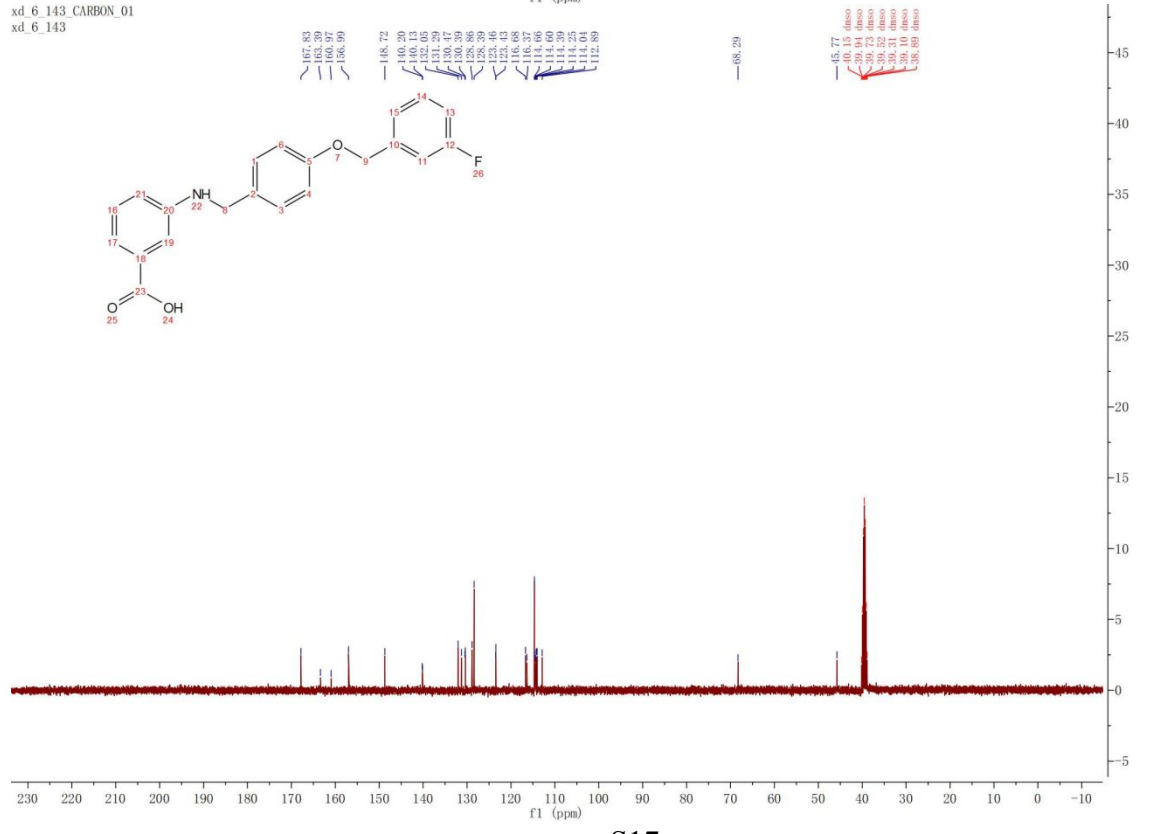


4i

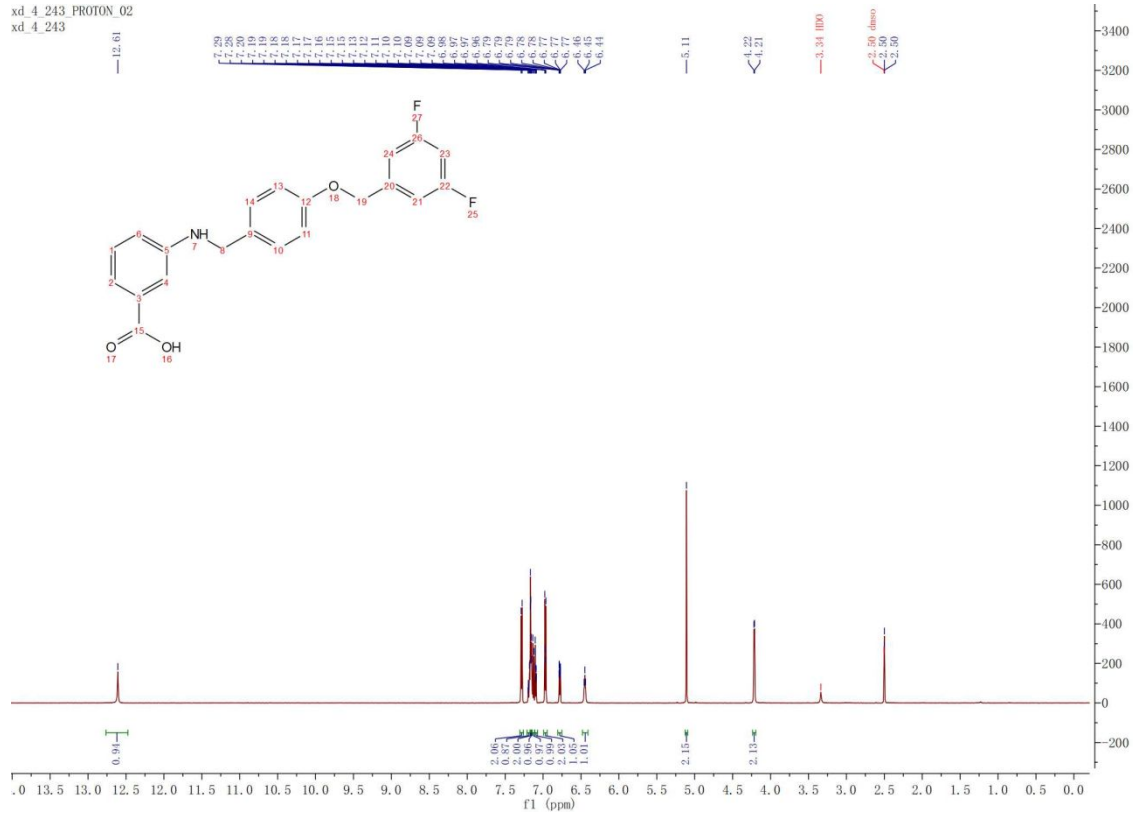
xd_6_143_600 PROTON_02
xd_6_143_600



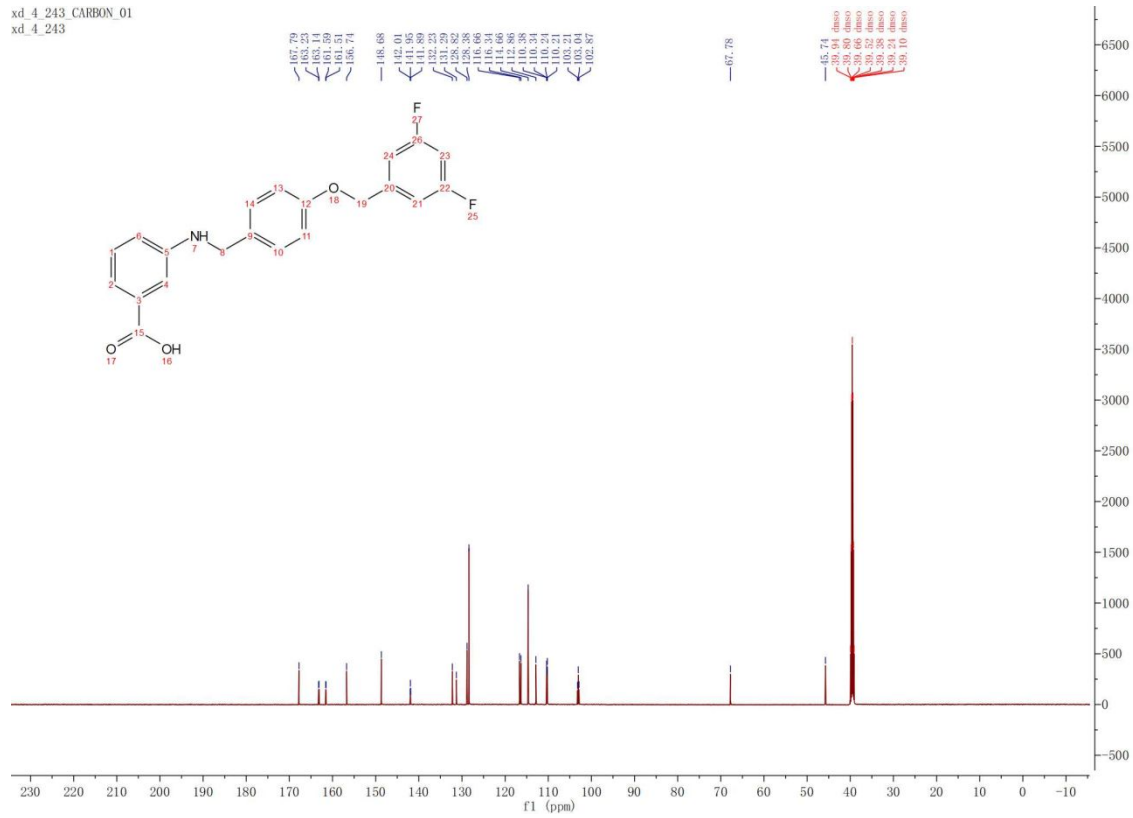
xd_6_143 CARBON_01
xd_6_143



xd_4_243 PROTON_02
xd_4_243

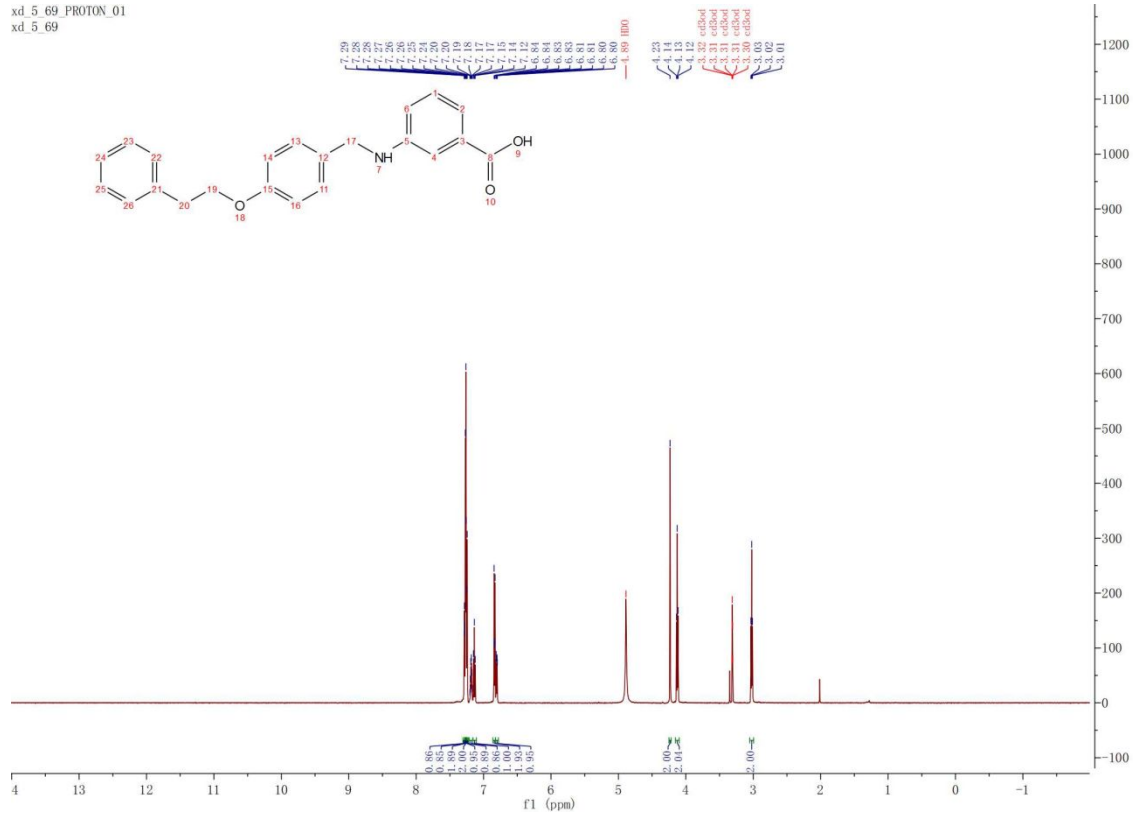


xd_4_243 CARBON_01
xd_4_243

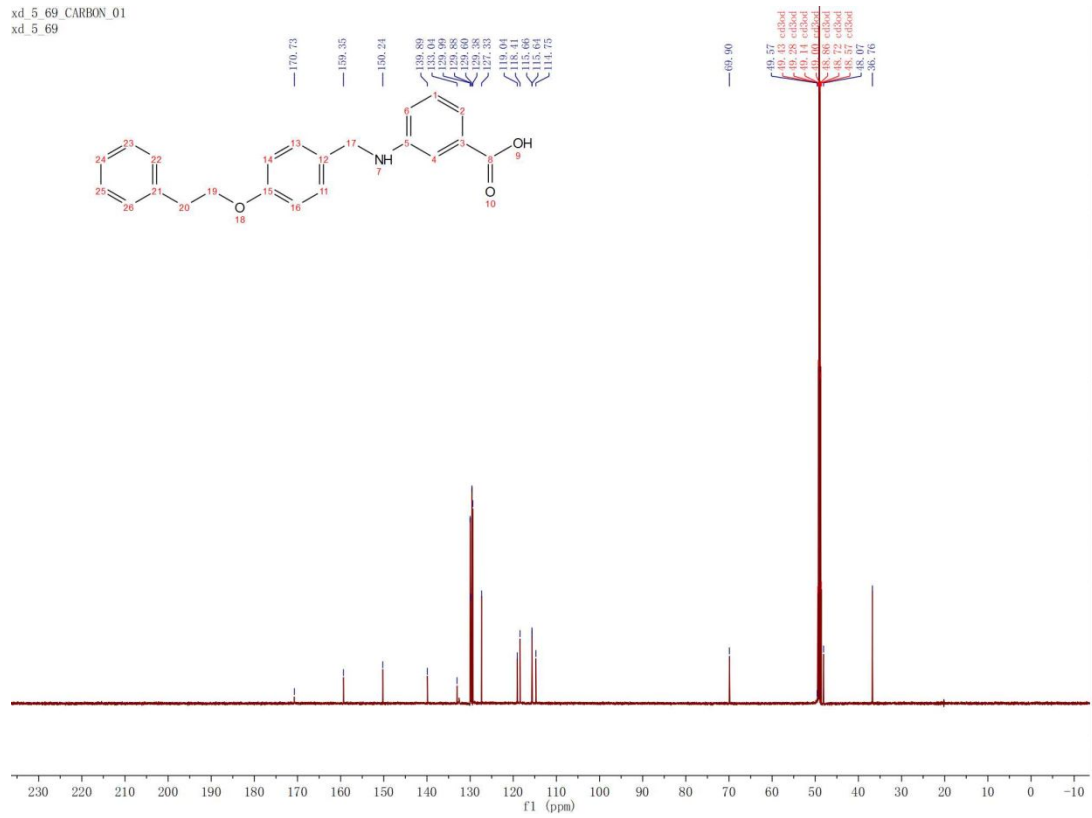


4m

xd_5_69_PROTON_01
xd_5_69

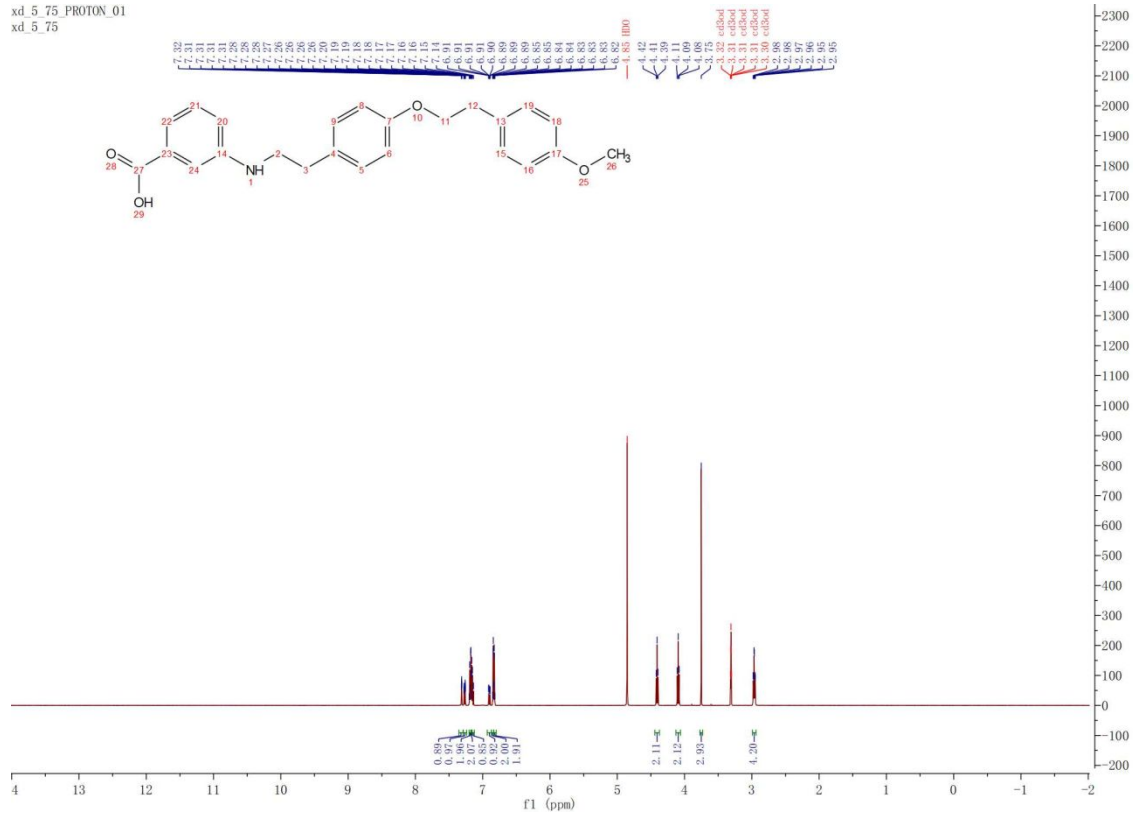


xd_5_69_CARBON_01
xd_5_69

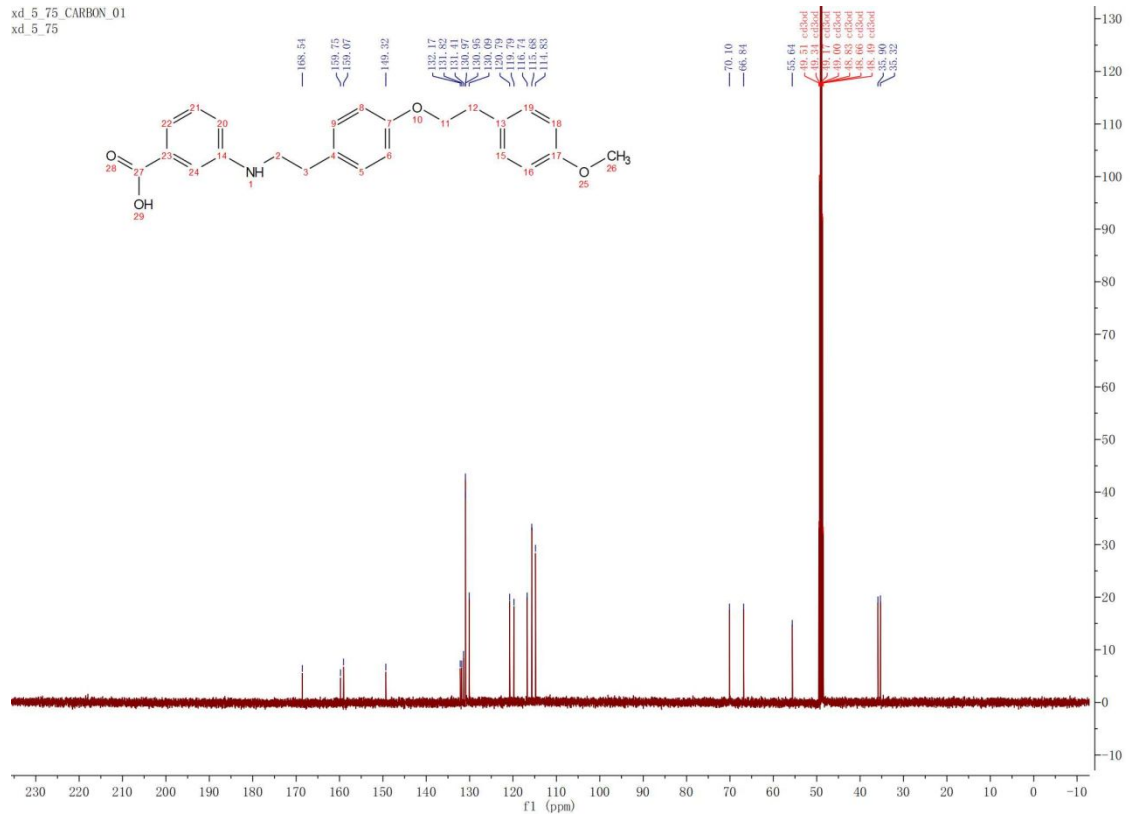


4o

xd_5_75_PROTON_01
xd_5_75

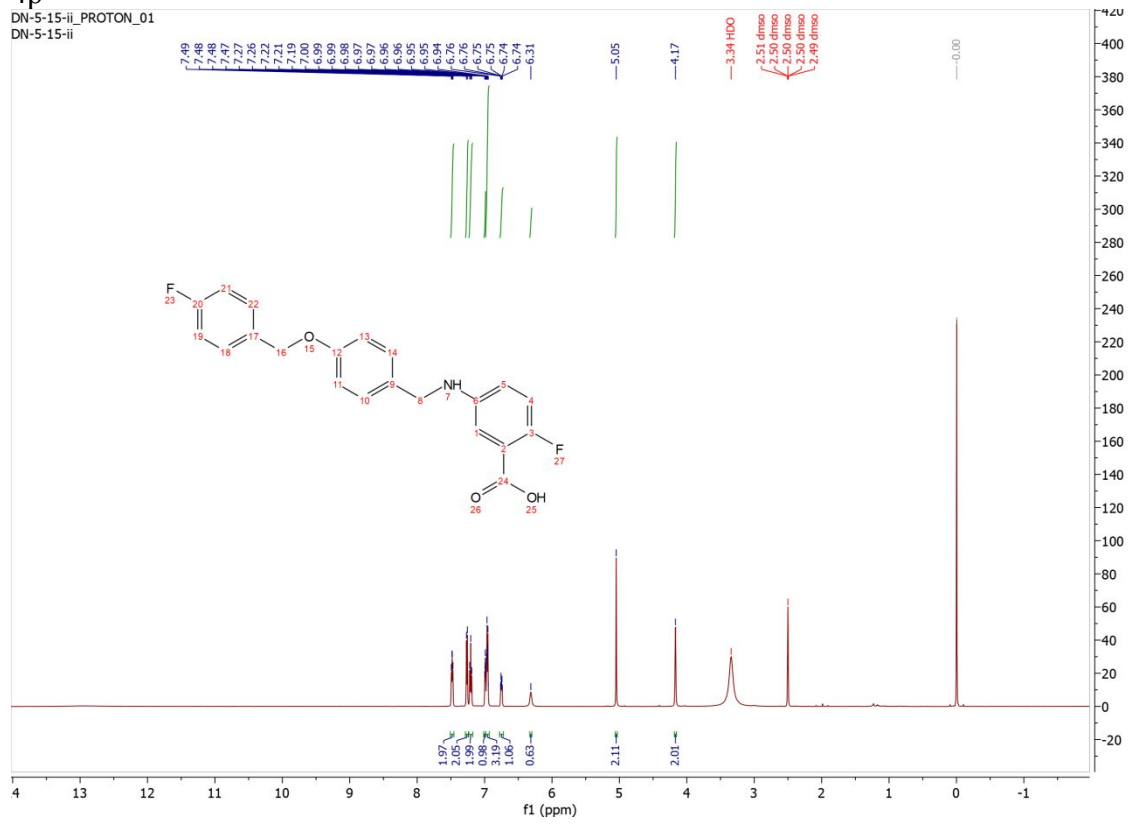


xd_5_75_CARBON_01
xd_5_75

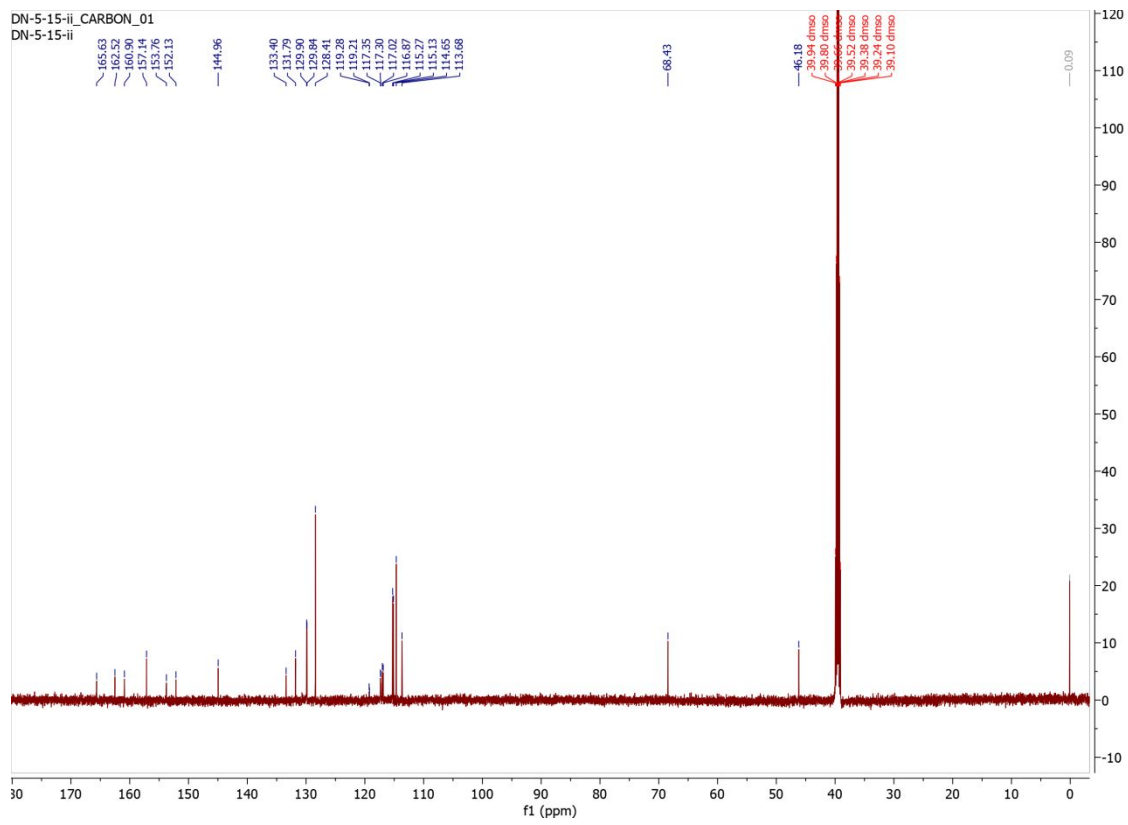


4p

DN-5-15-ii_PROTON_01
DN-5-15-ii

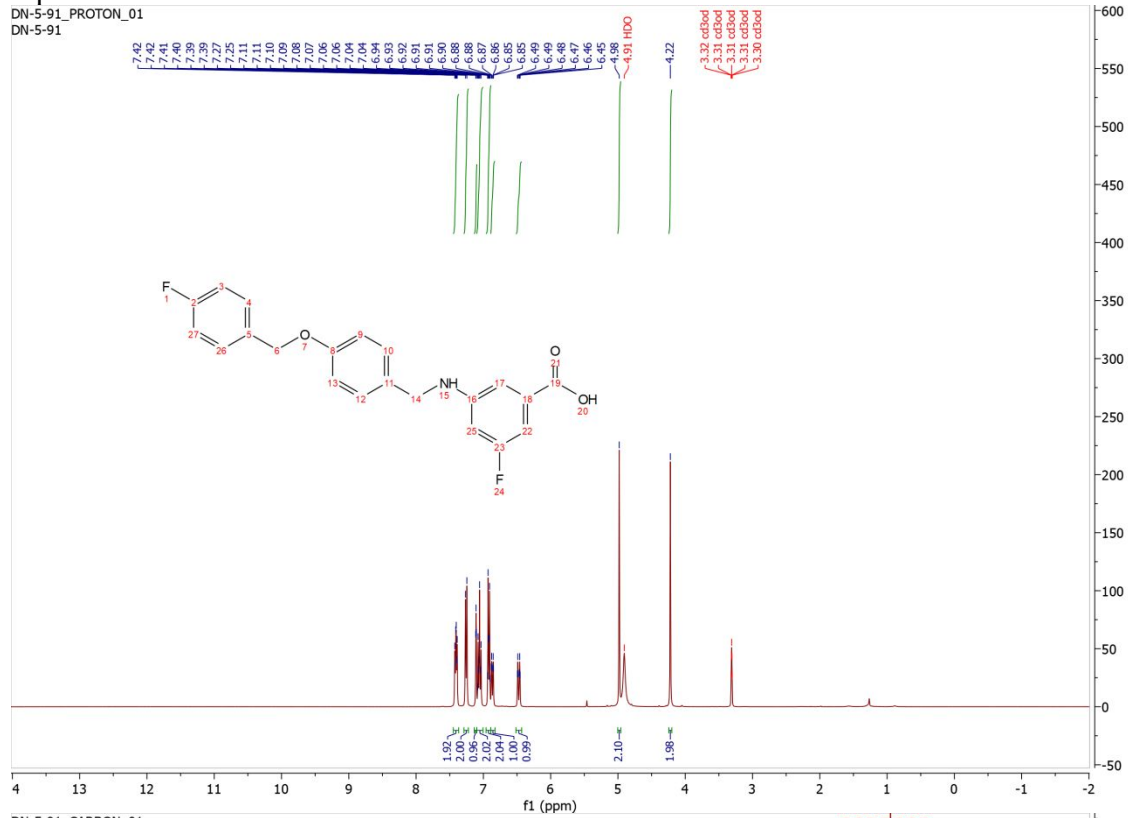


DN-5-15-ii_CARBON_01
DN-5-15-ii

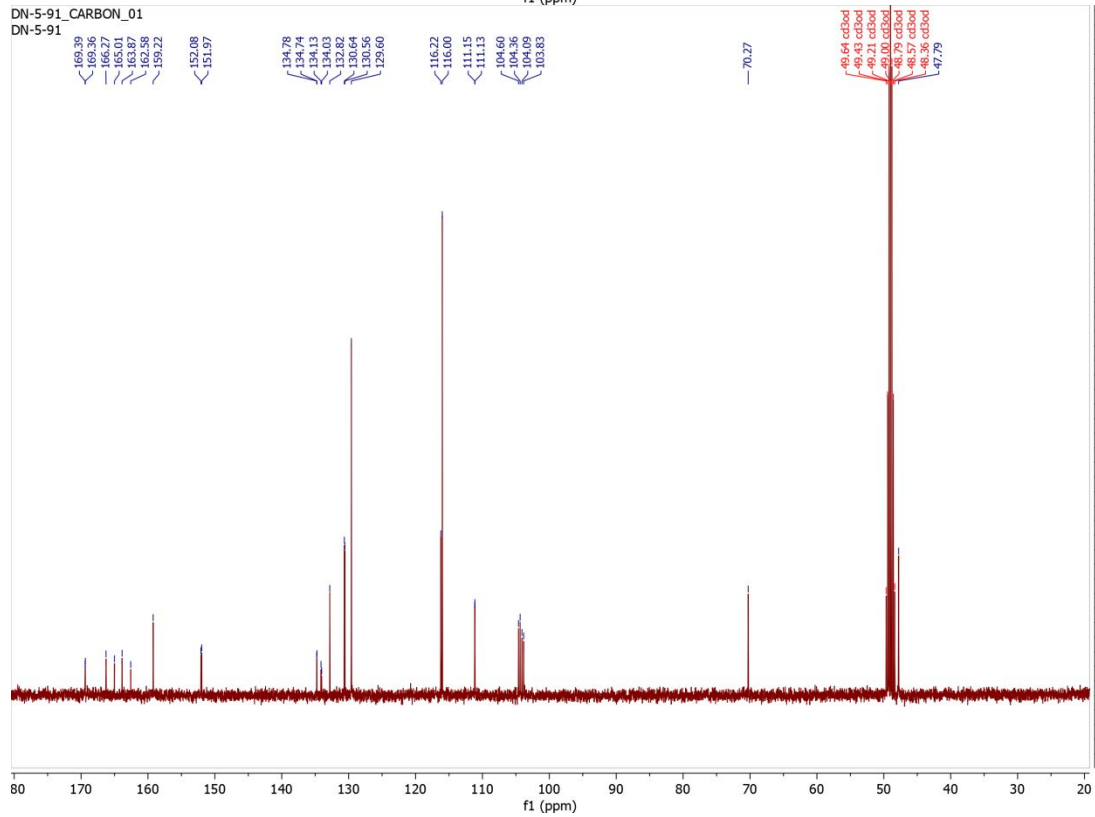


4q

DN-5-91_PROTON_01
DN-5-91

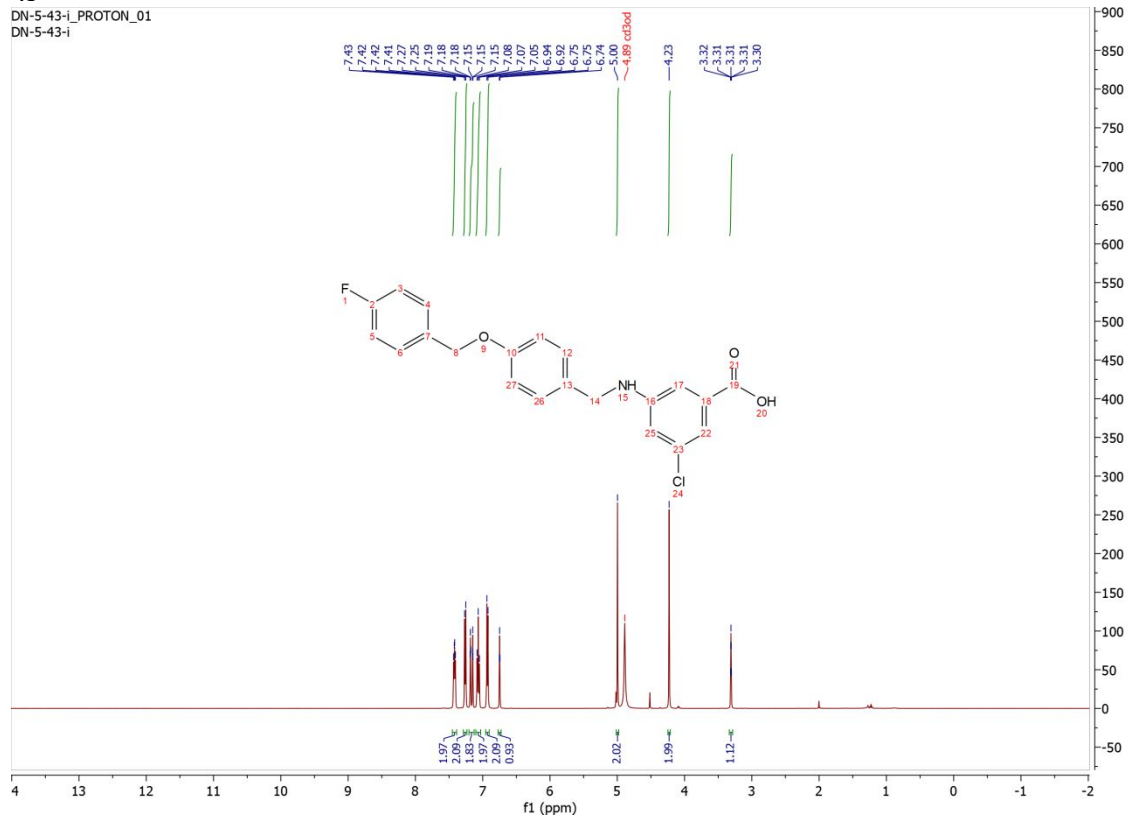


DN-5-91_CARBON_01
DN-5-91

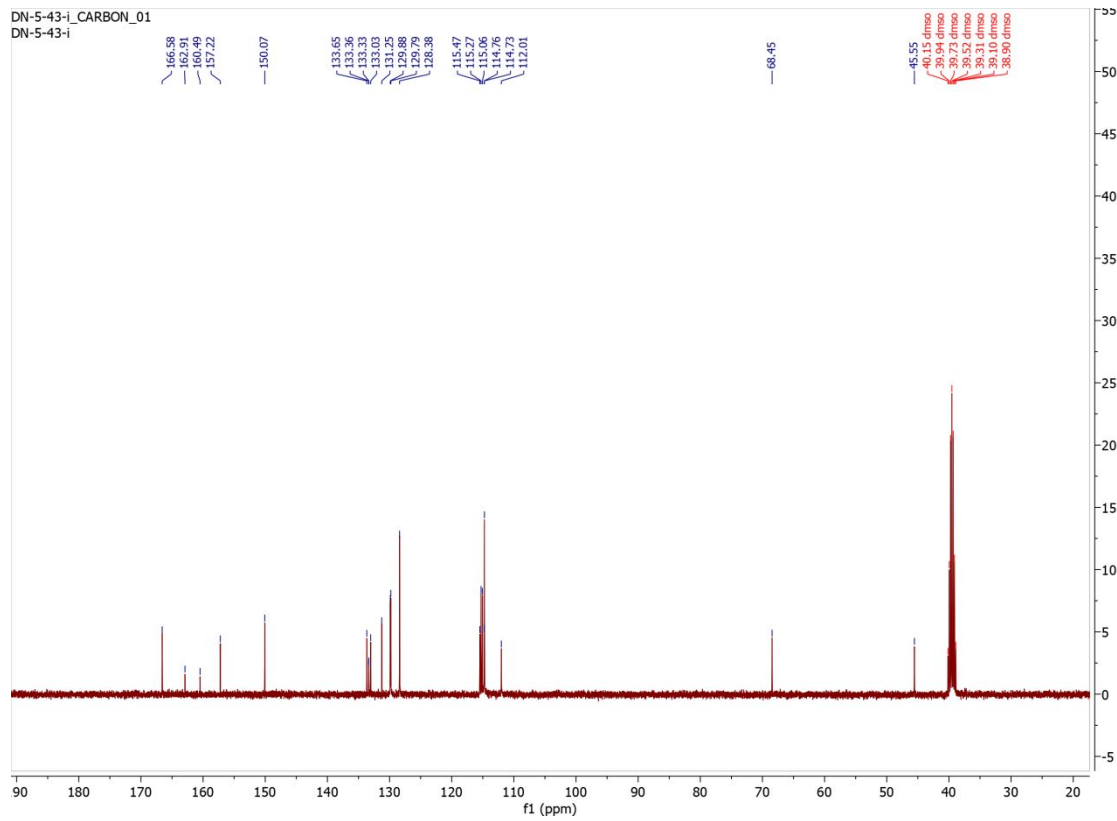


4r

DN-5-43-i_PROTON_01
DN-5-43-i

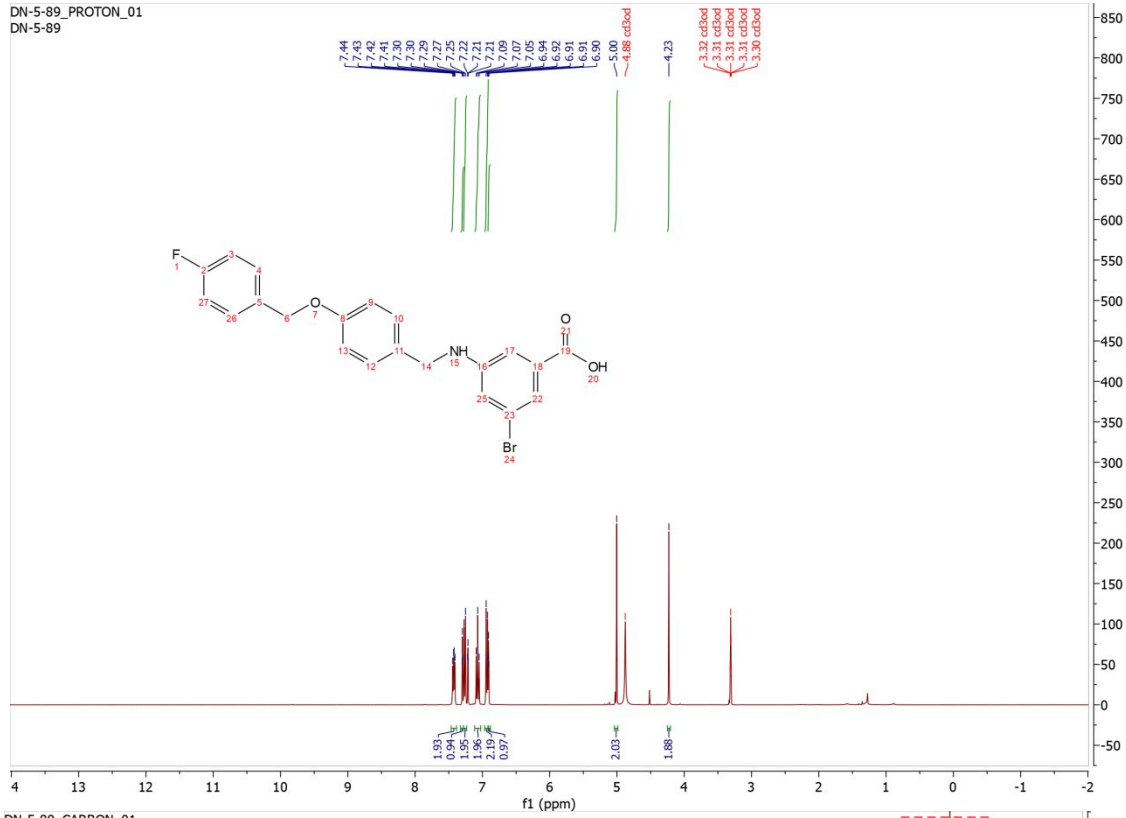


DN-5-43-i CARBON_01
DN-5-43-i

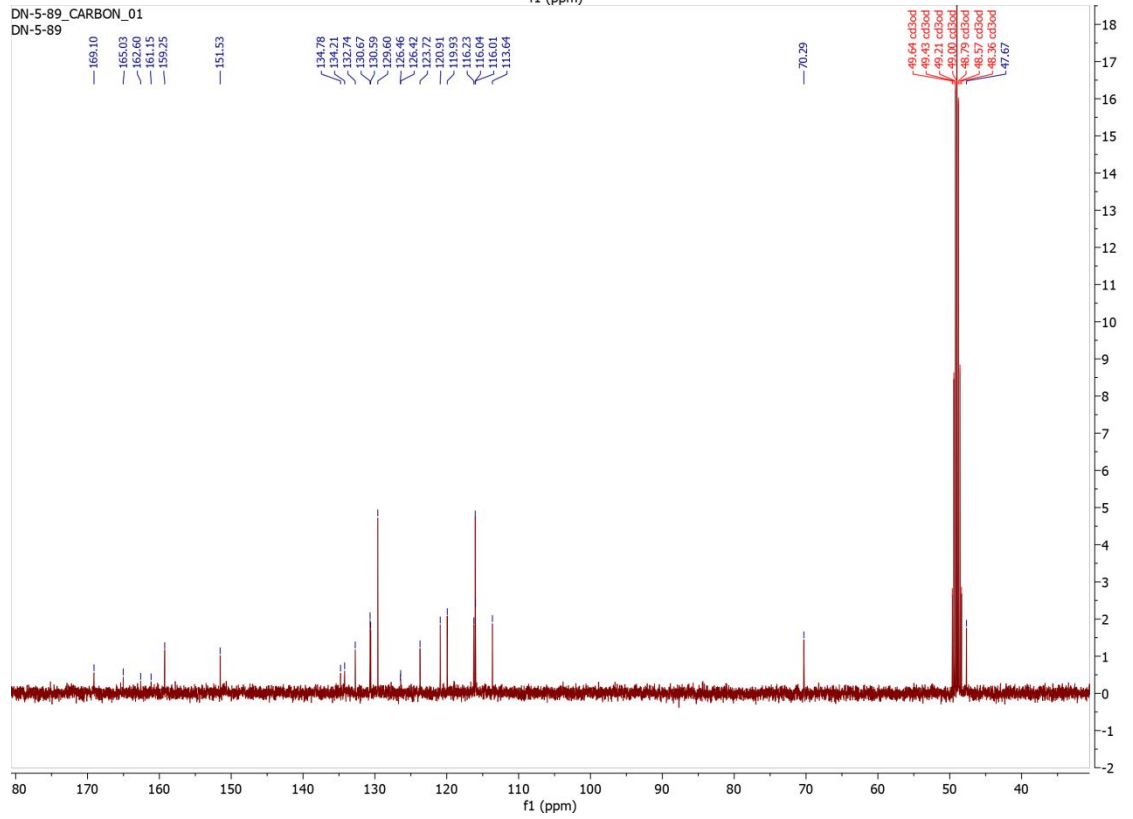


4s

DN-5-89_PROTON_01
DN-5-89

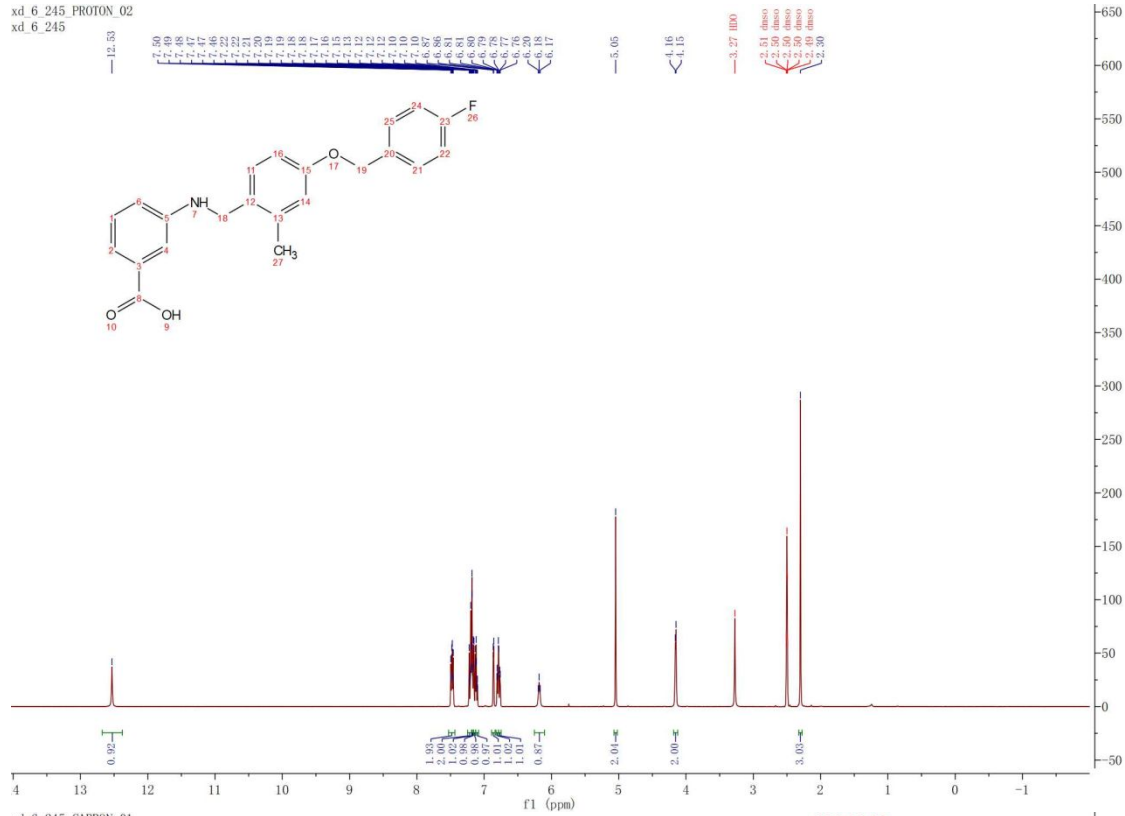


DN-5-89_CARBON_01
DN-5-89

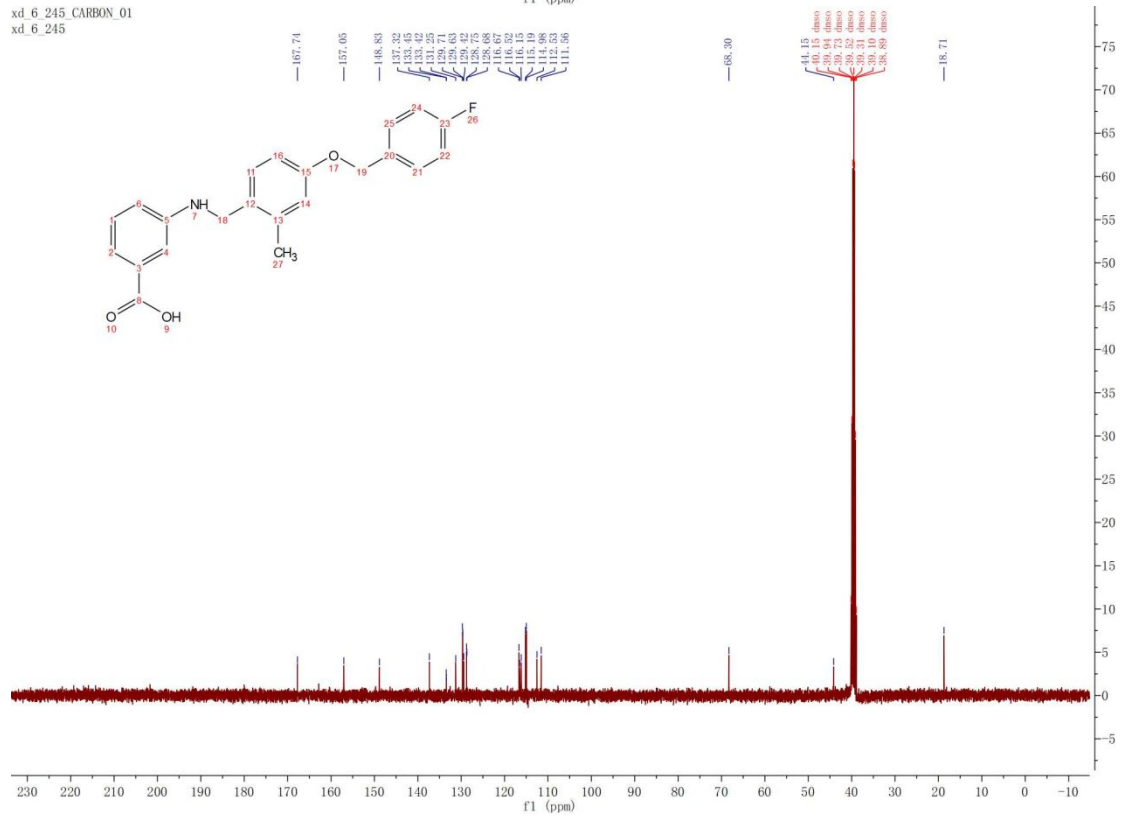


4t

xd_6_245 PROTON_02
xd_6_245

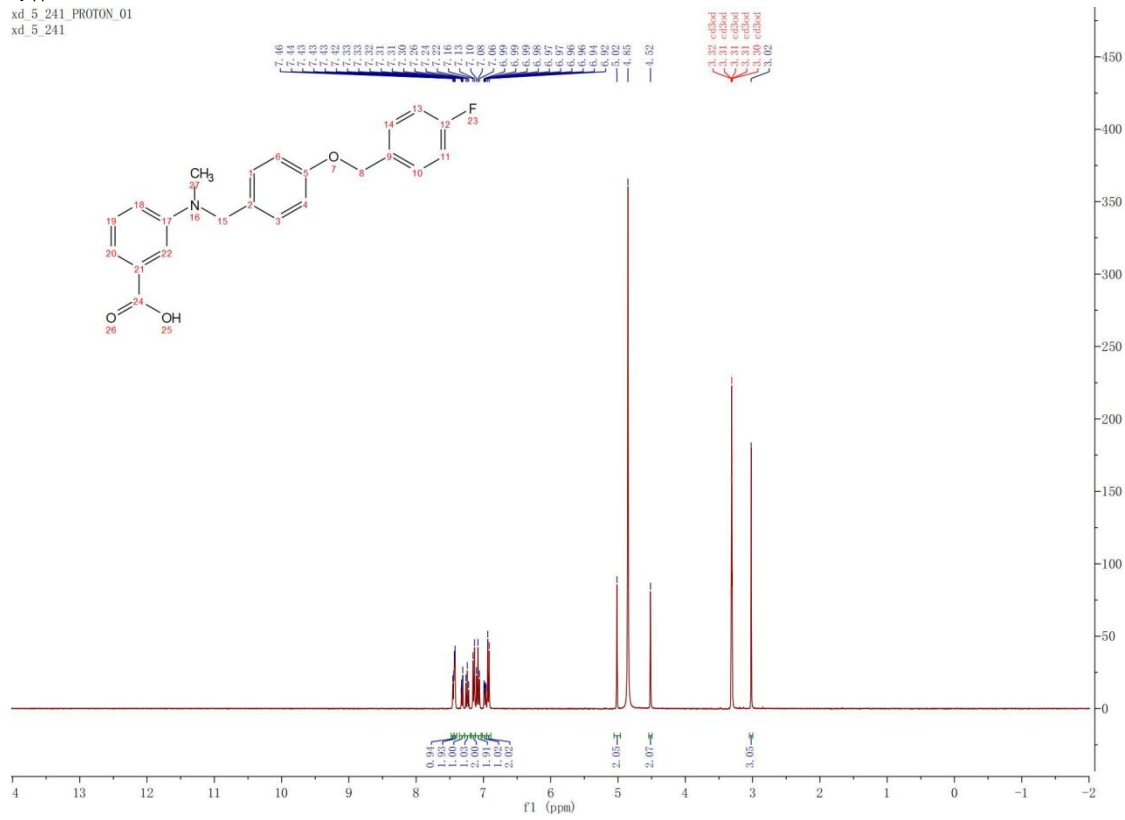


xd_6_245 CARBON_01
xd_6_245

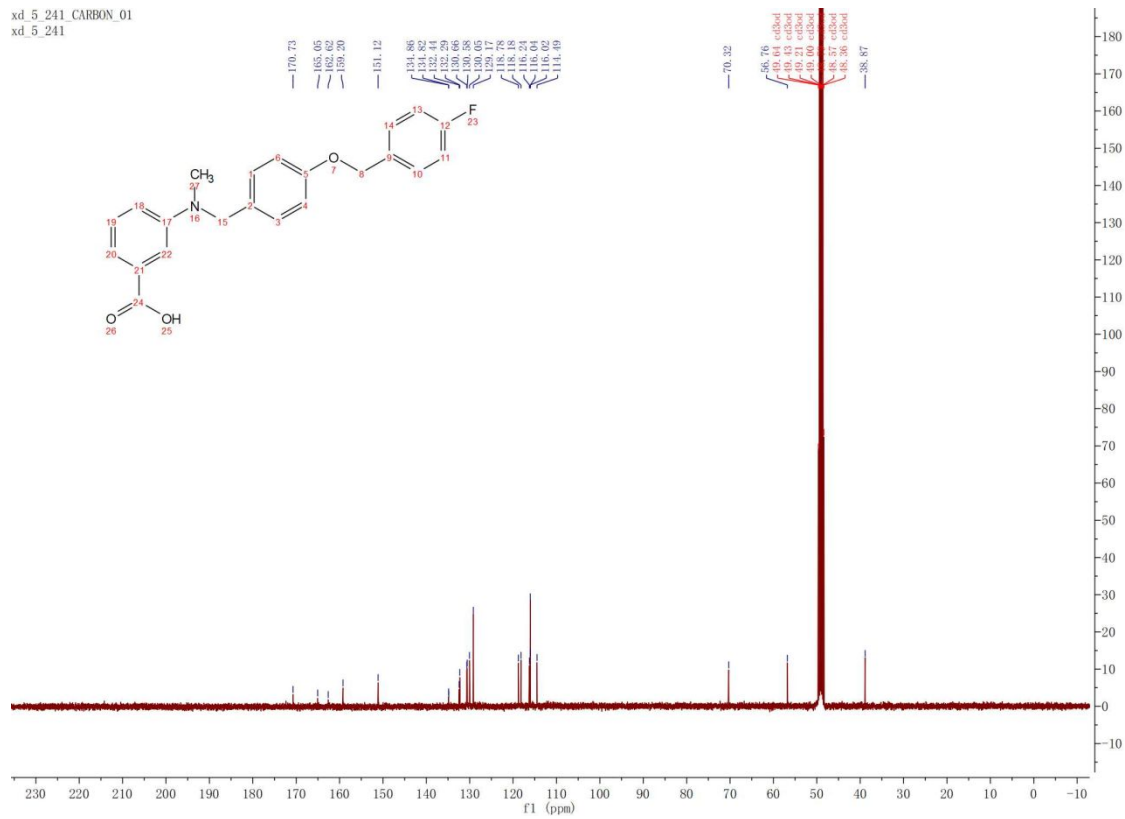


4w

xd_5_241_PROTON_01
xd_5_241

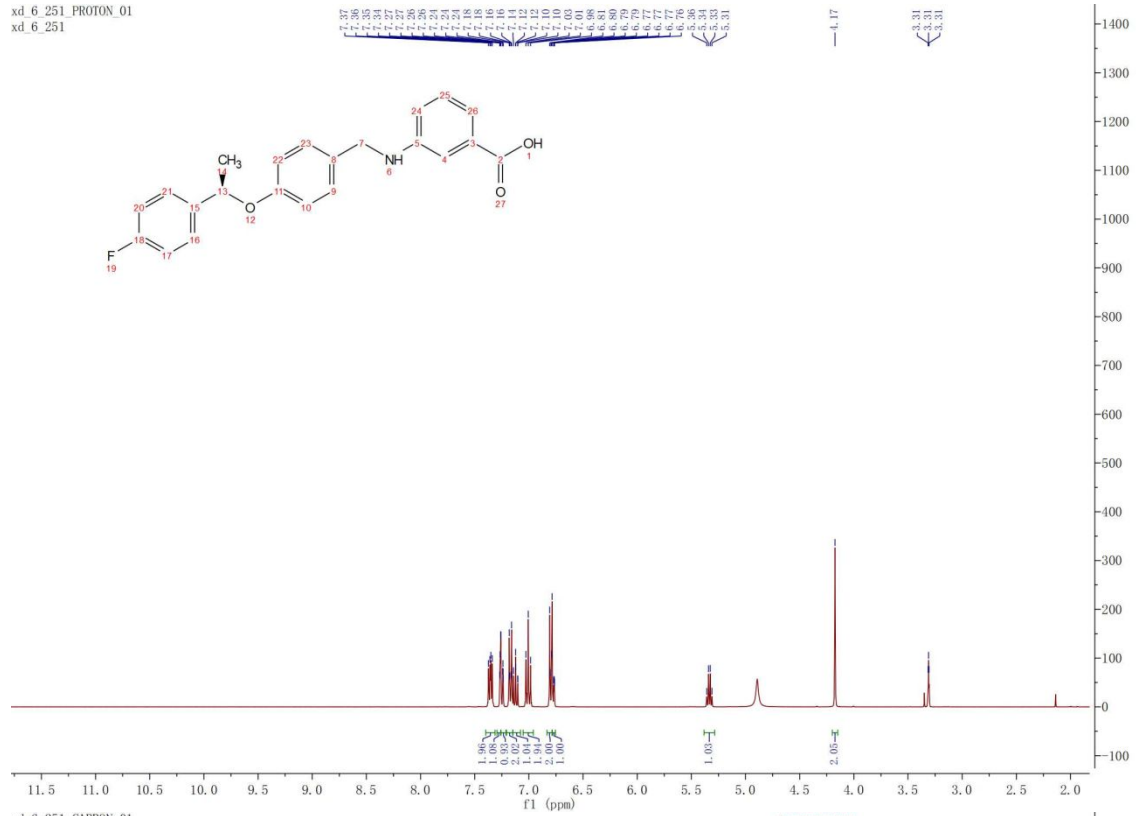


xd_5_241_CARBON_01
xd_5_241

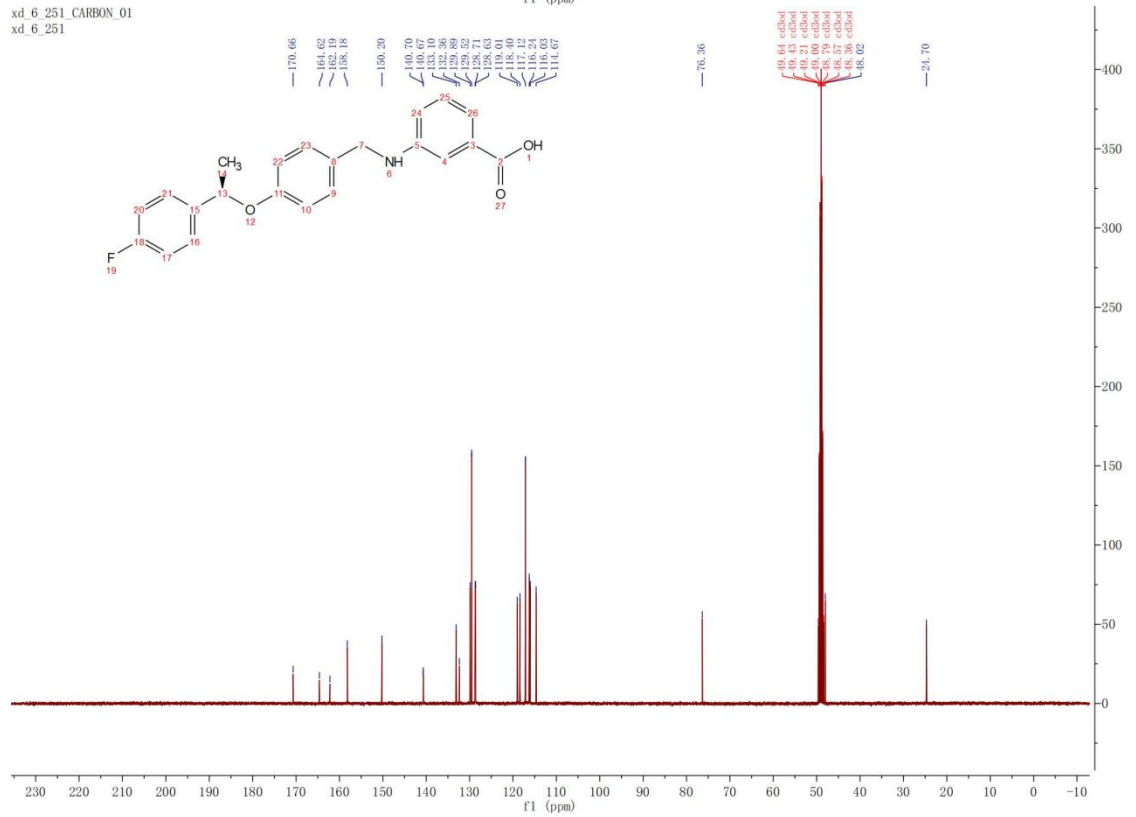


4x

xd_6_251_PROTON_01
xd_6_251

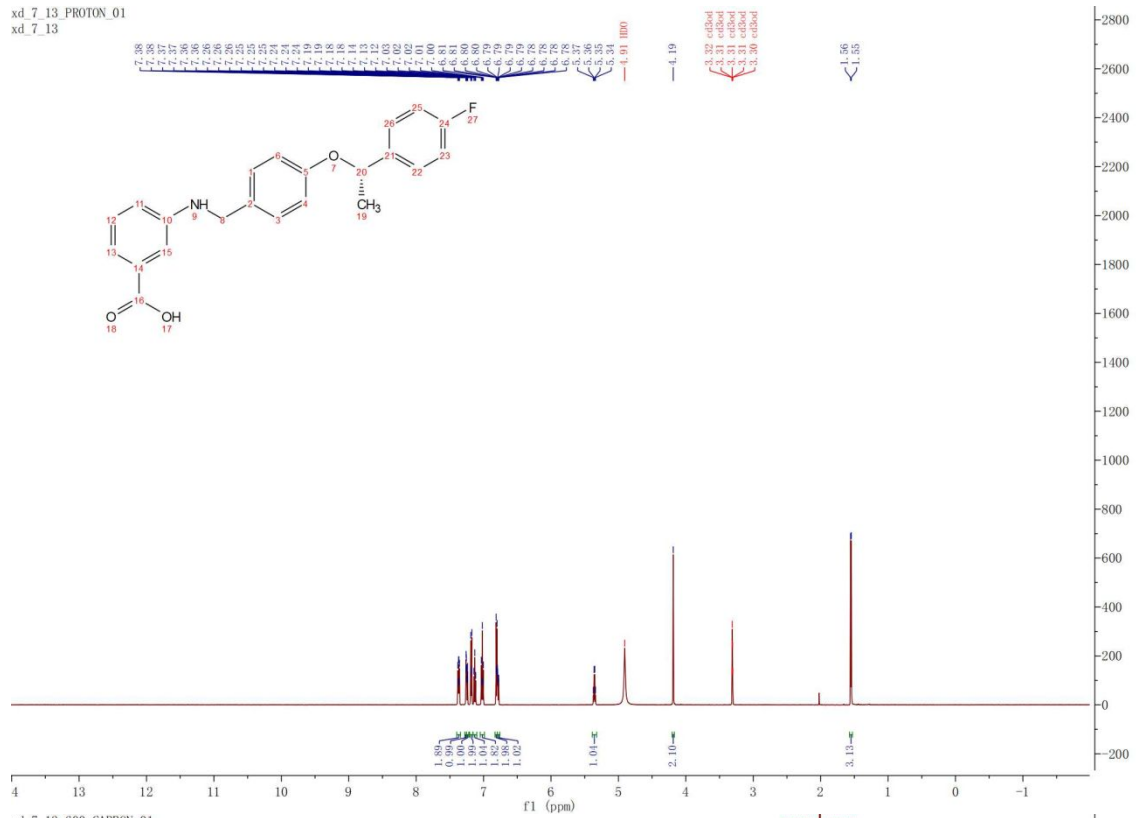


xd_6_251_CARBON_01
xd_6_251

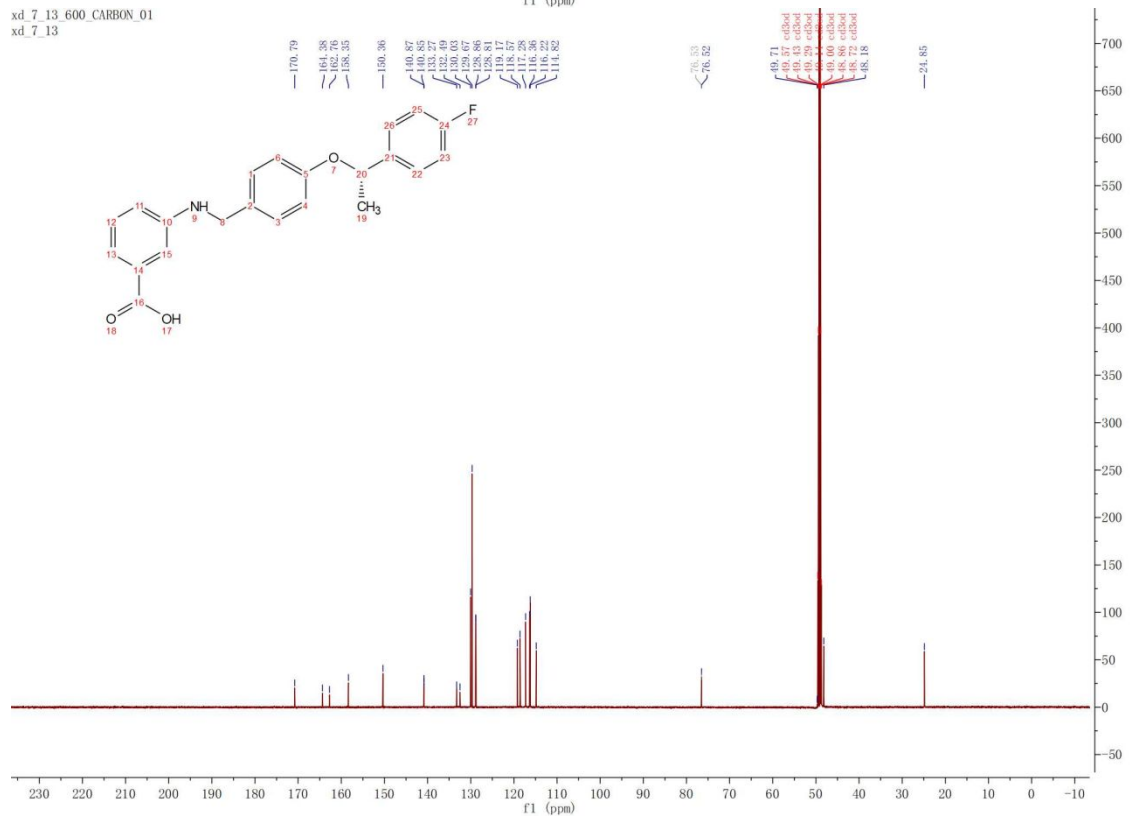


4y

xd_7_13_PROTON_01
xd_7_13

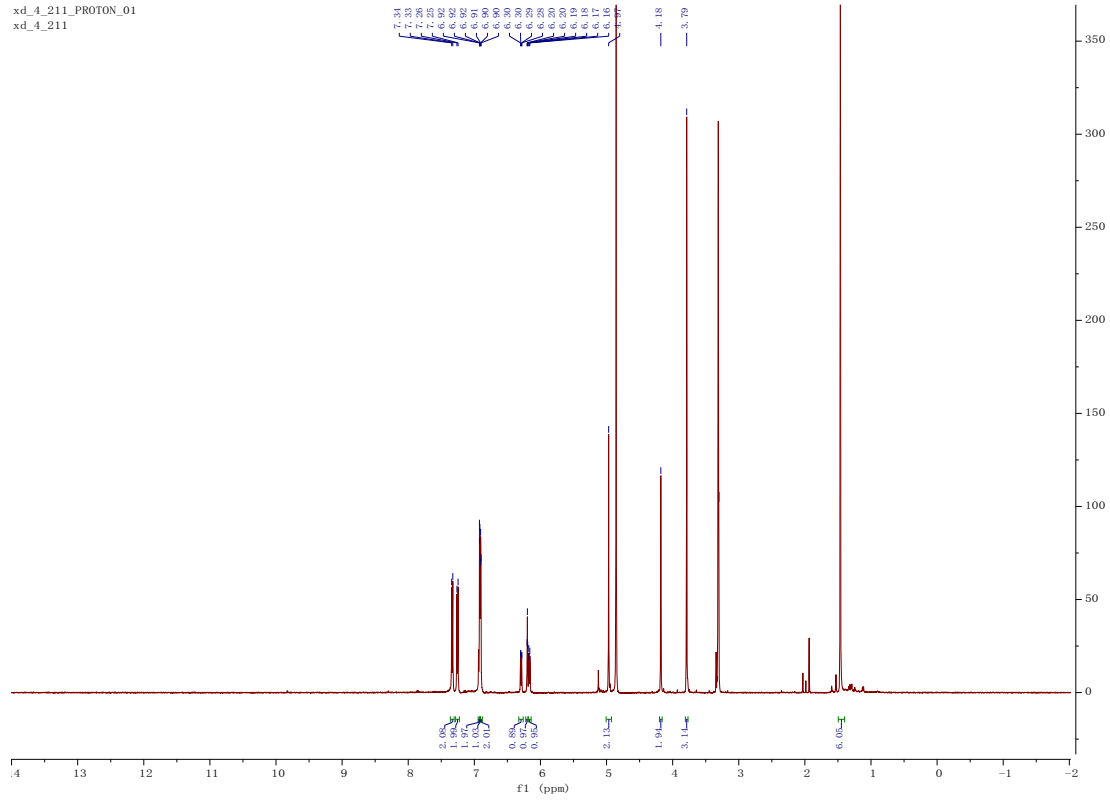


xd_7_13_600 CARBON_01
xd_7_13

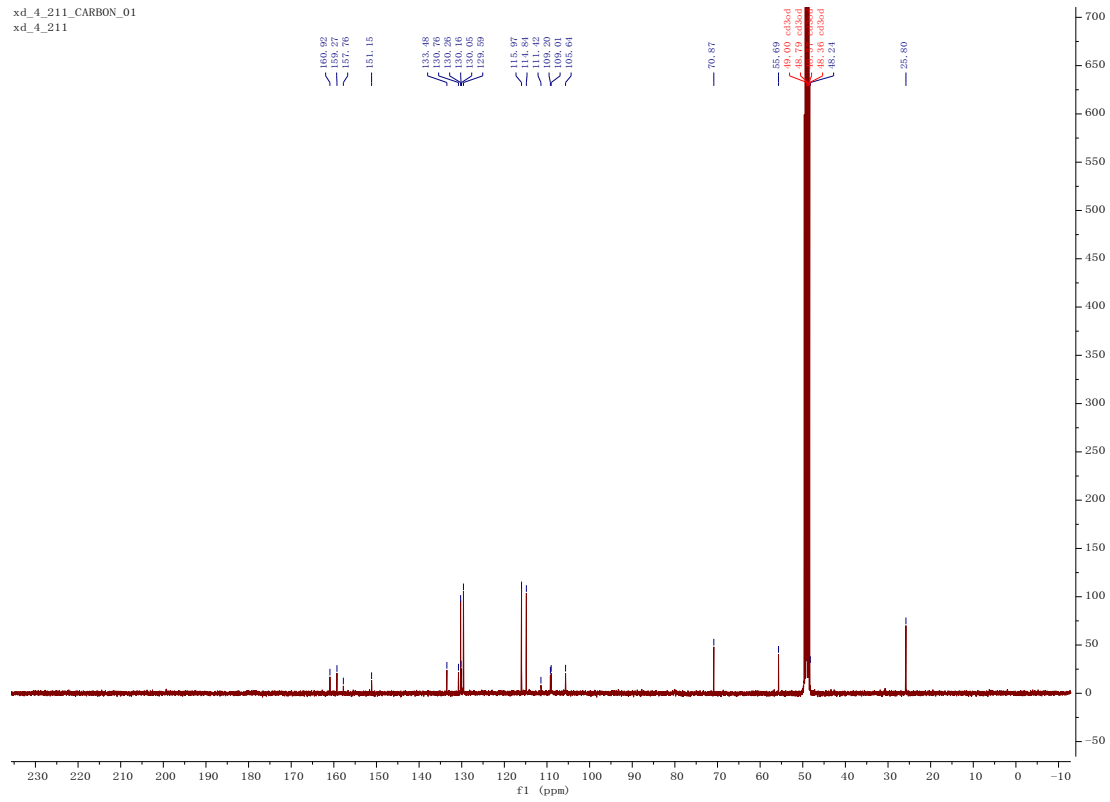


5a

xd_4_211_PROTON_01
xd_4_211

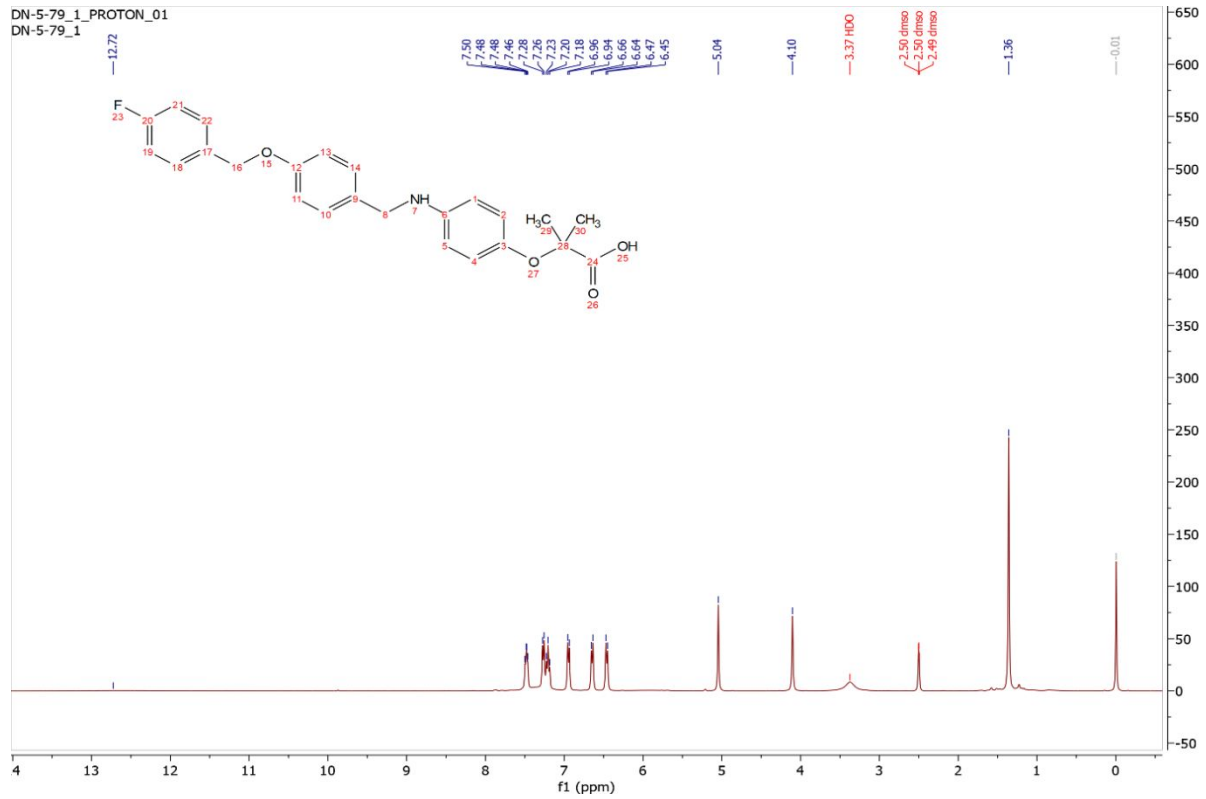


xd_4_211_CARBON_01
xd_4_211

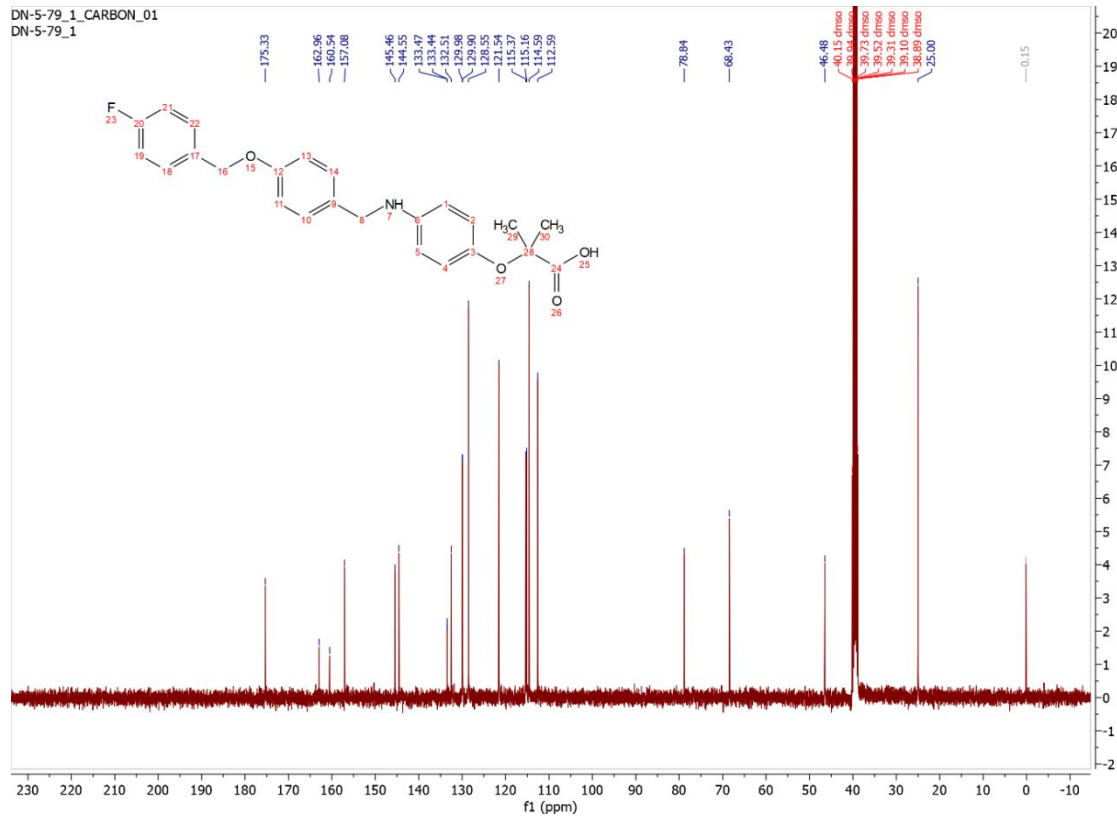


5b*

DN-5-79_1_PROTON_01
DN-5-79_1

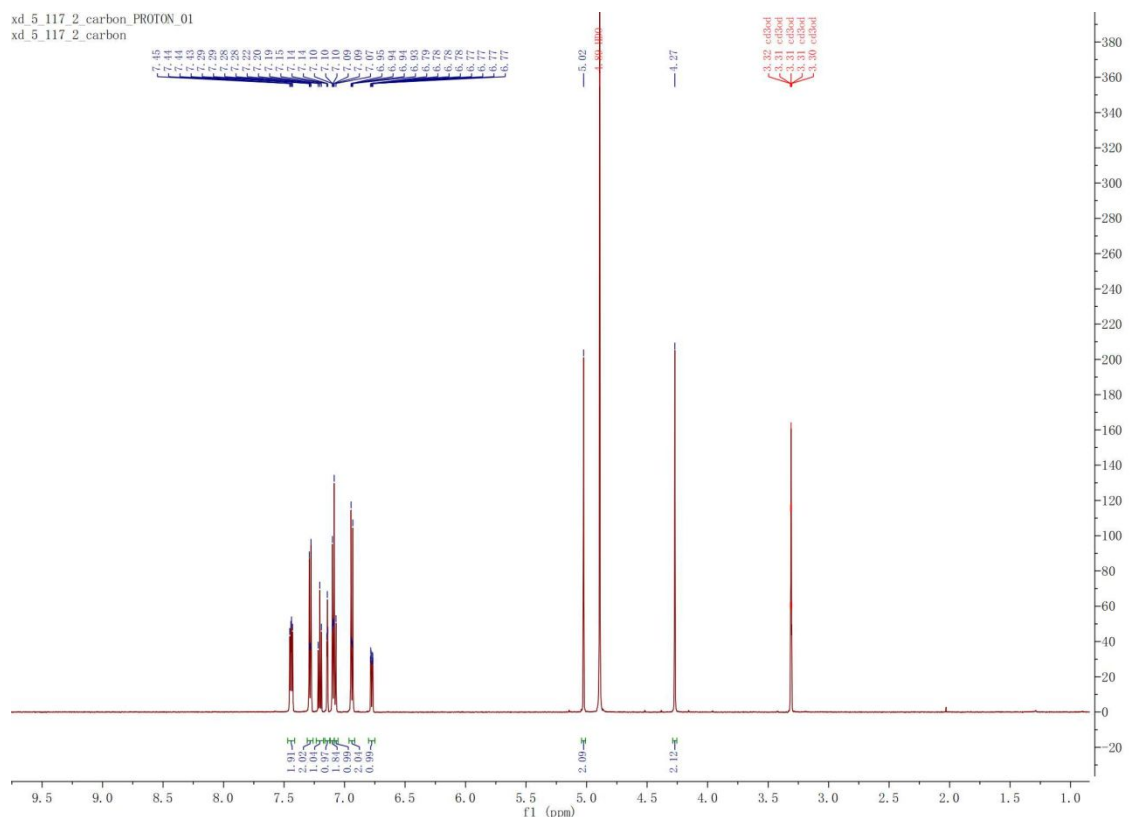


DN-5-79_1_CARBON_01
DN-5-79_1

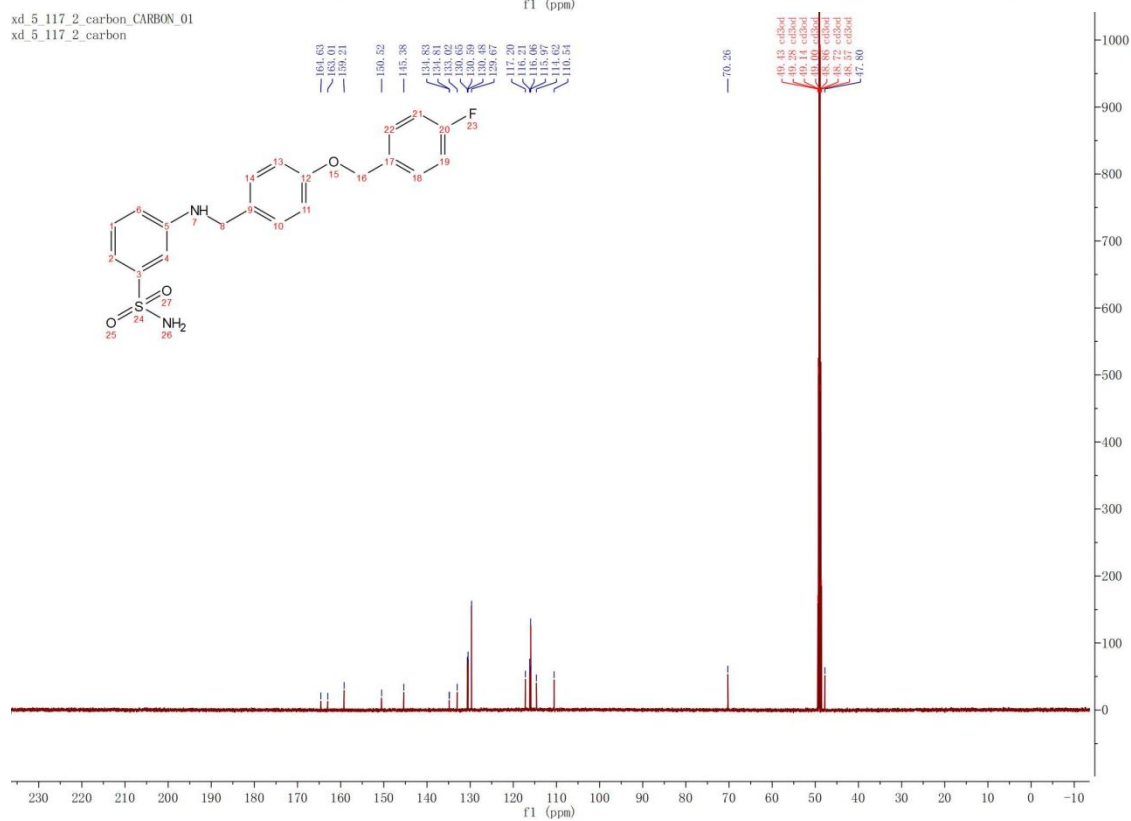


19c

xd_5_117_2_carbon_PROTON_01
xd_5_117_2_carbon

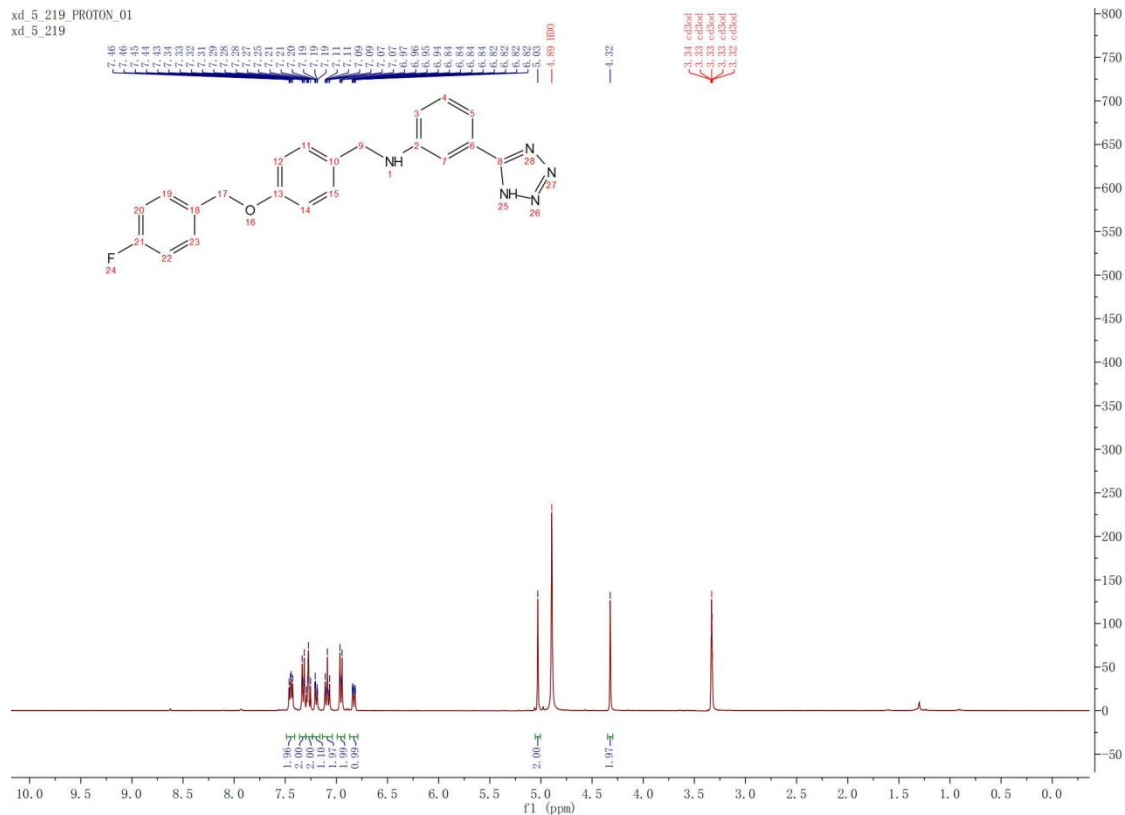


xd_5_117_2_carbon_CARBON_01
xd_5_117_2_carbon

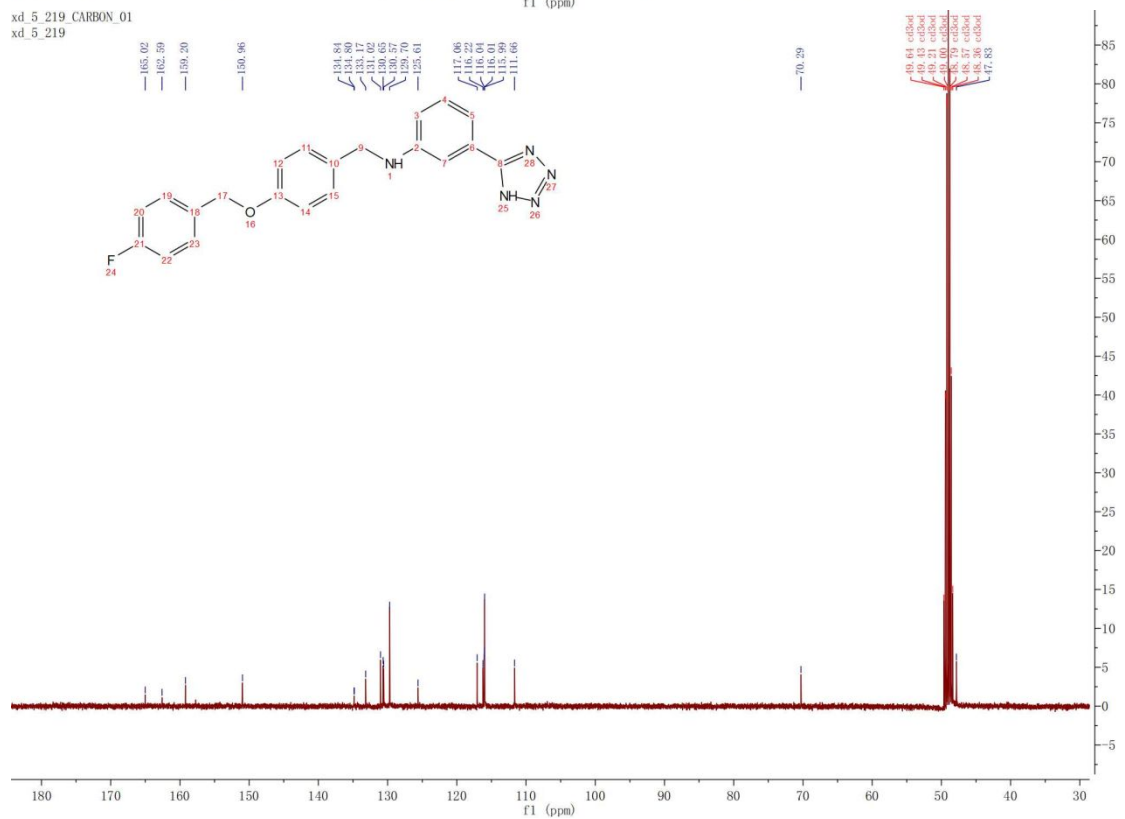


19d

xd_5_219_PROTON_01
xd_5_219

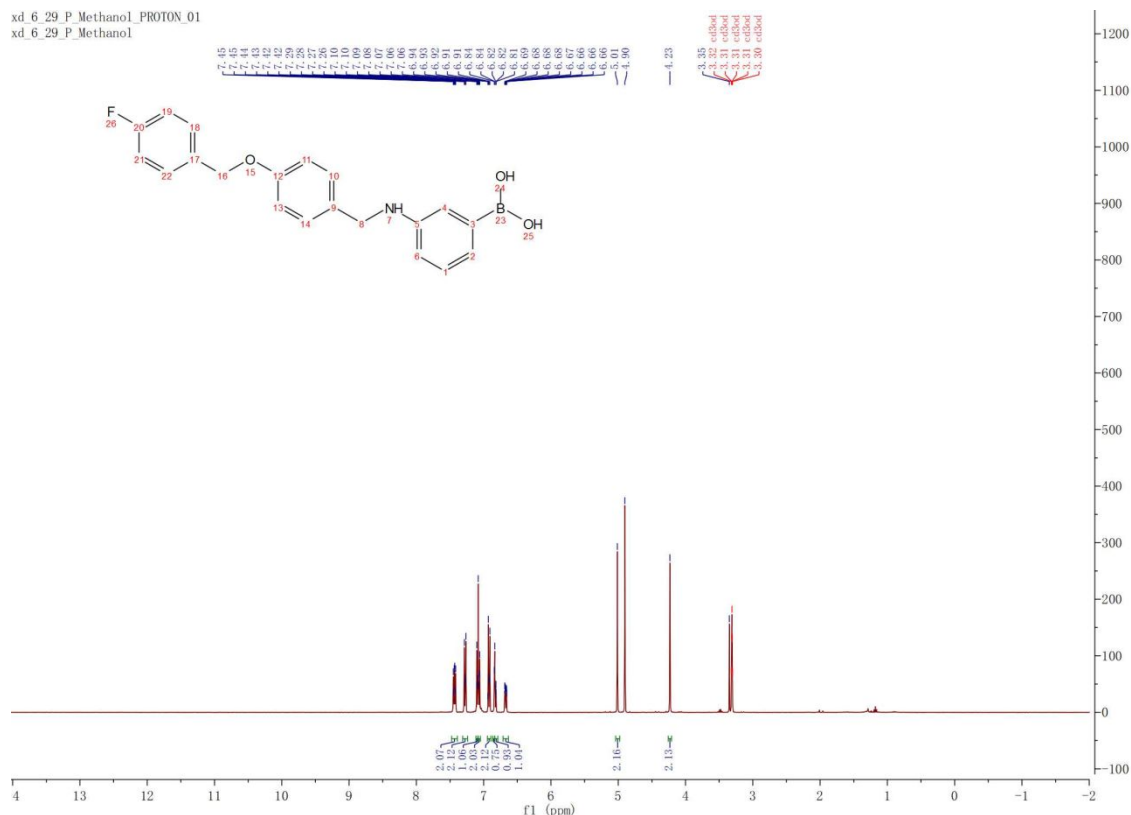


xd_5_219 CARBON_01
xd_5_219



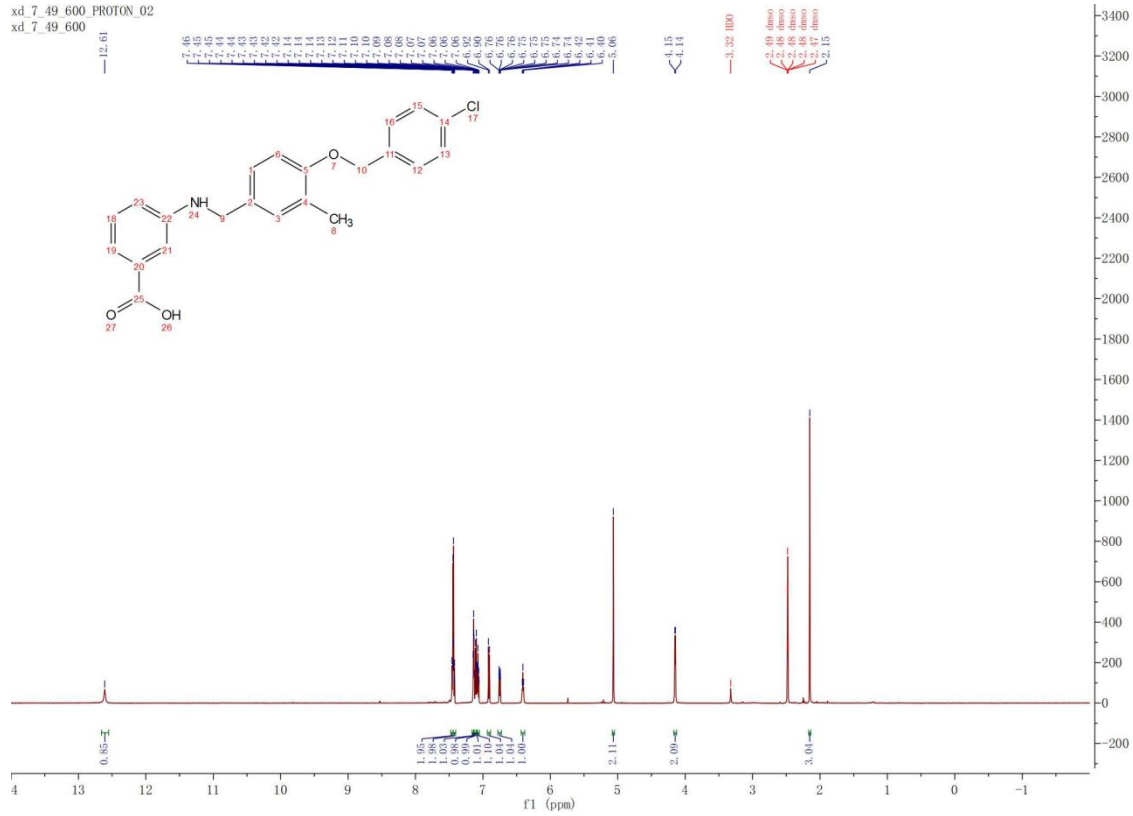
19e

xd_6_29_P_Methanol_PROTON_01
 xd_6_29_P_Methanol

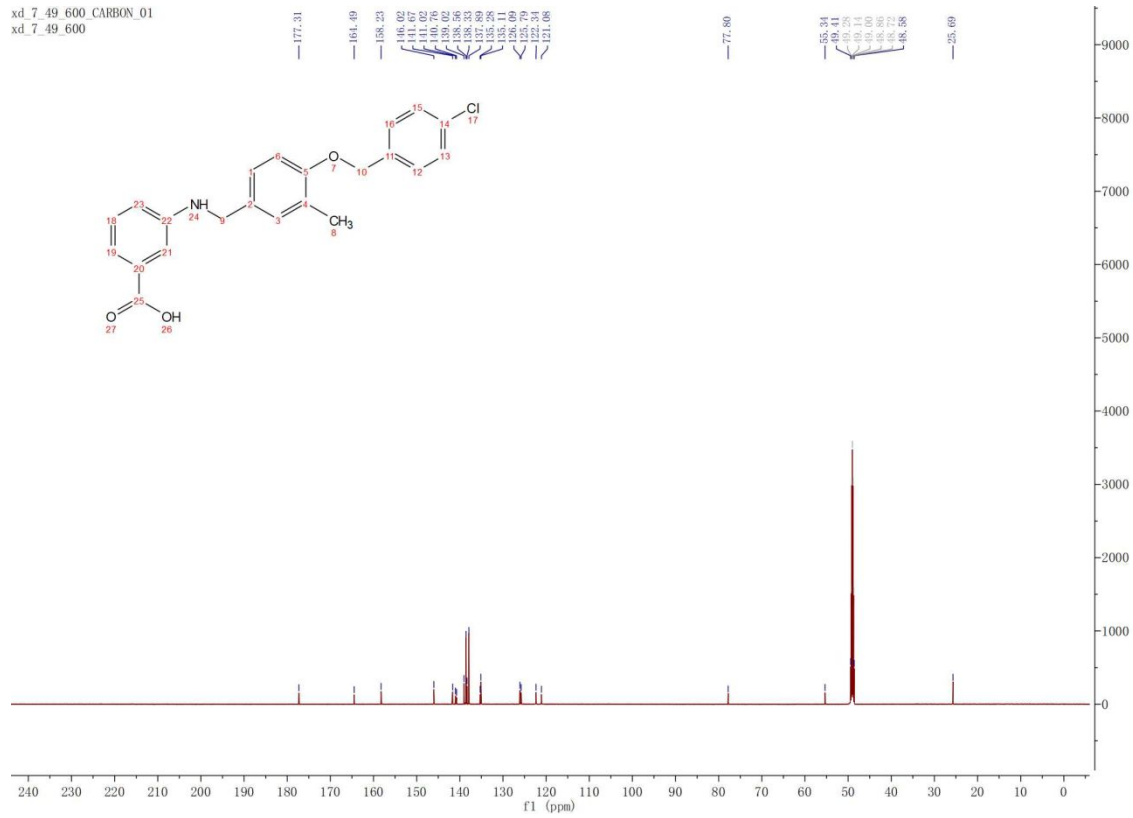


20

xd_7_49_600 PROTON_02
xd_7_49_600

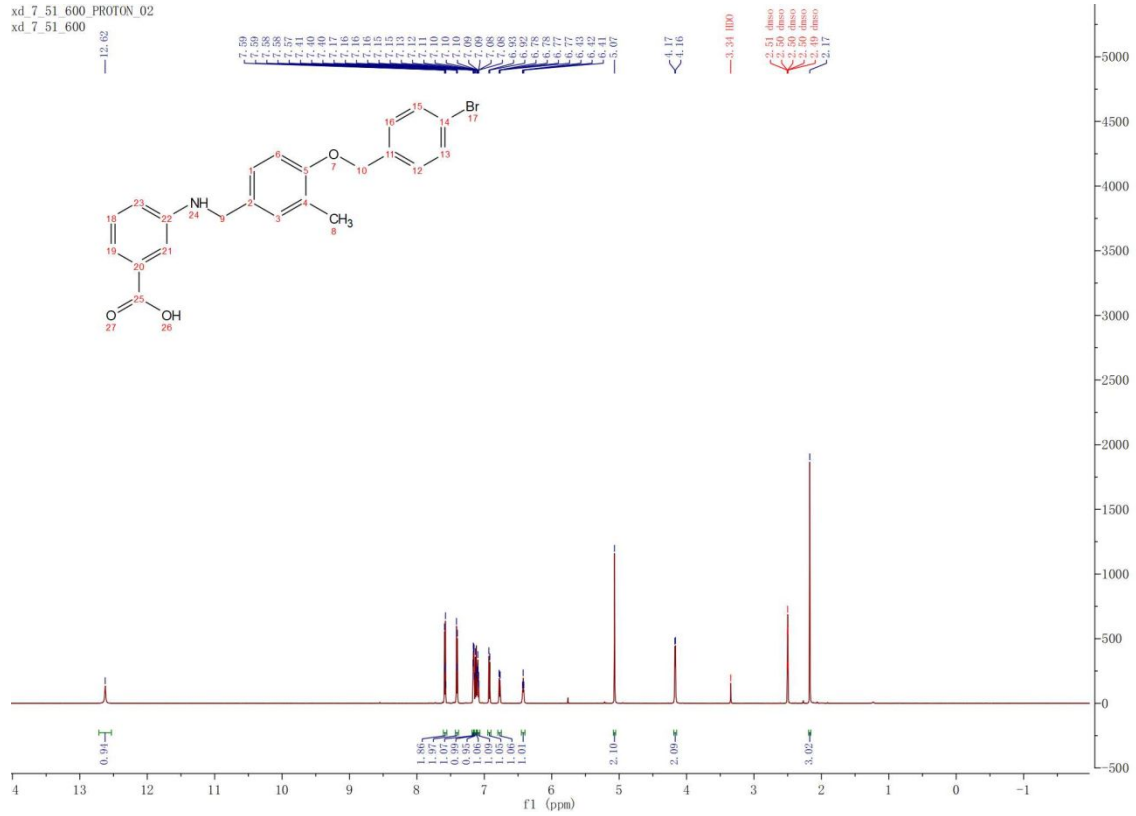


xd_7_49_600 CARBON_01
xd_7_49_600

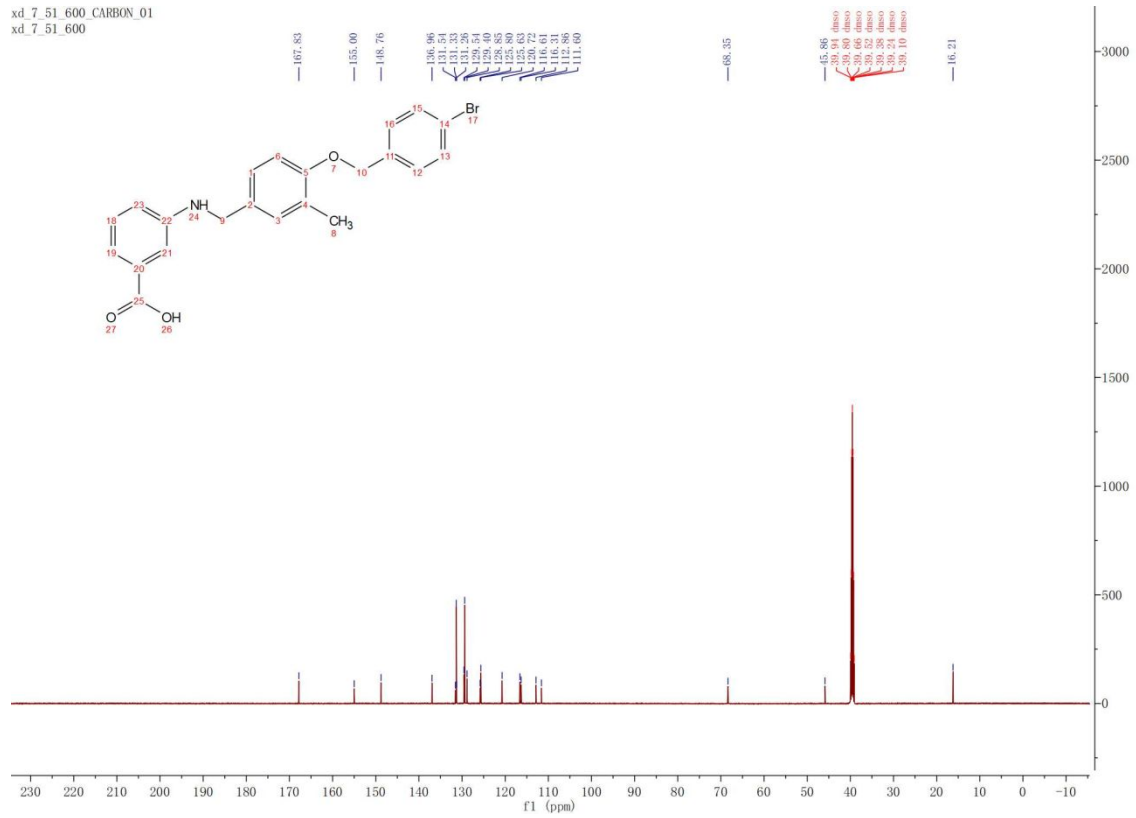


21

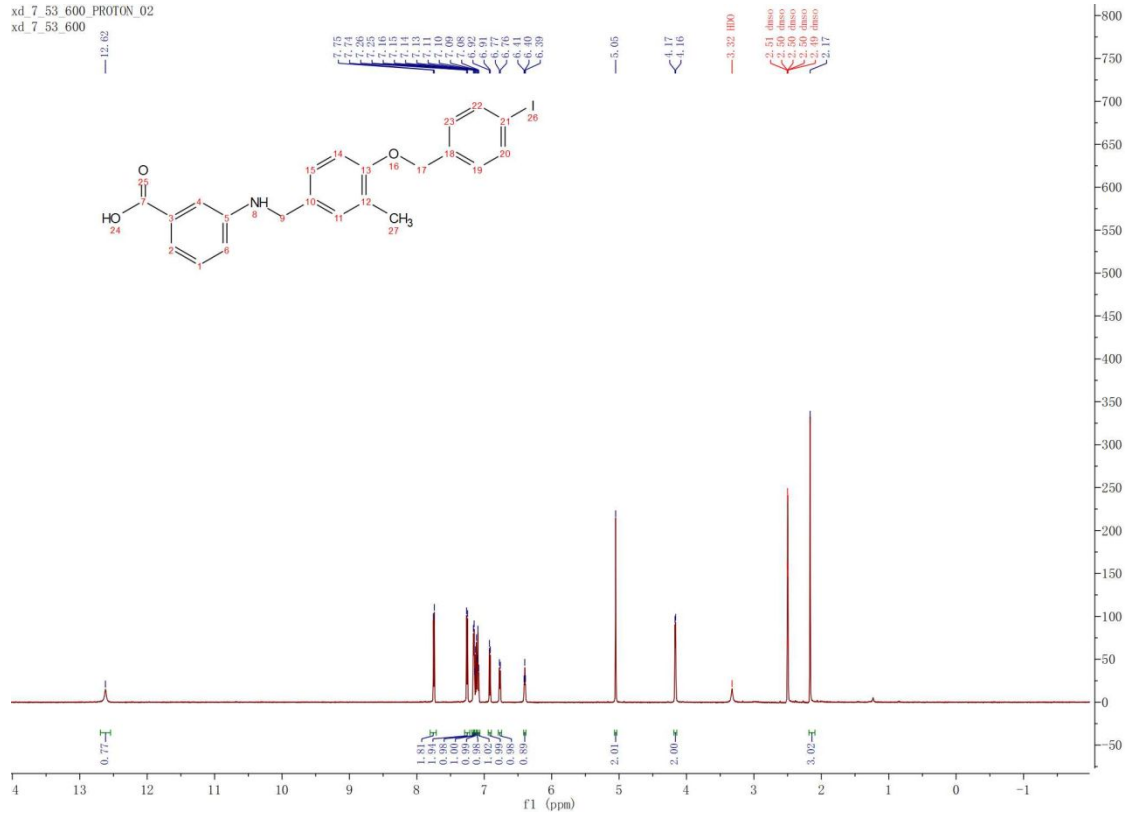
xd_7_51_600 PROTON_02
xd_7_51_600



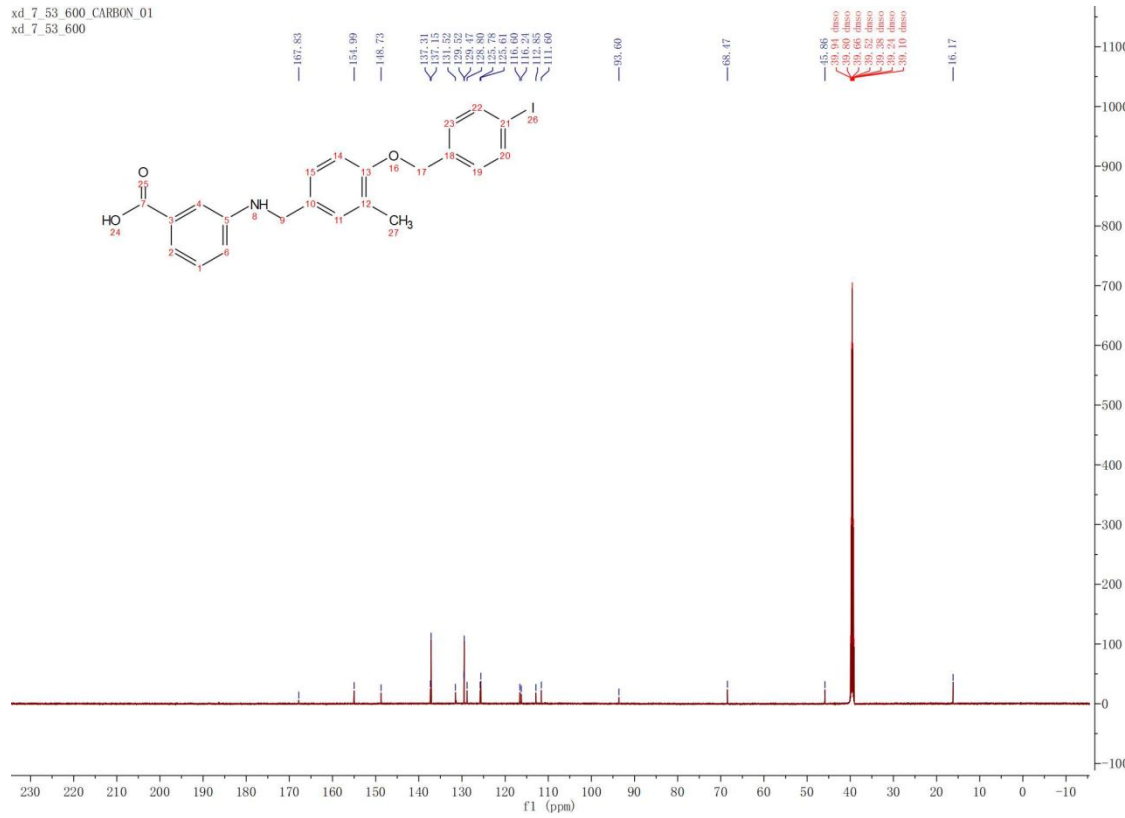
xd_7_51_600 CARBON_01
xd_7_51_600



xd_7_53_600 PROTON_02
 xd_7_53_600

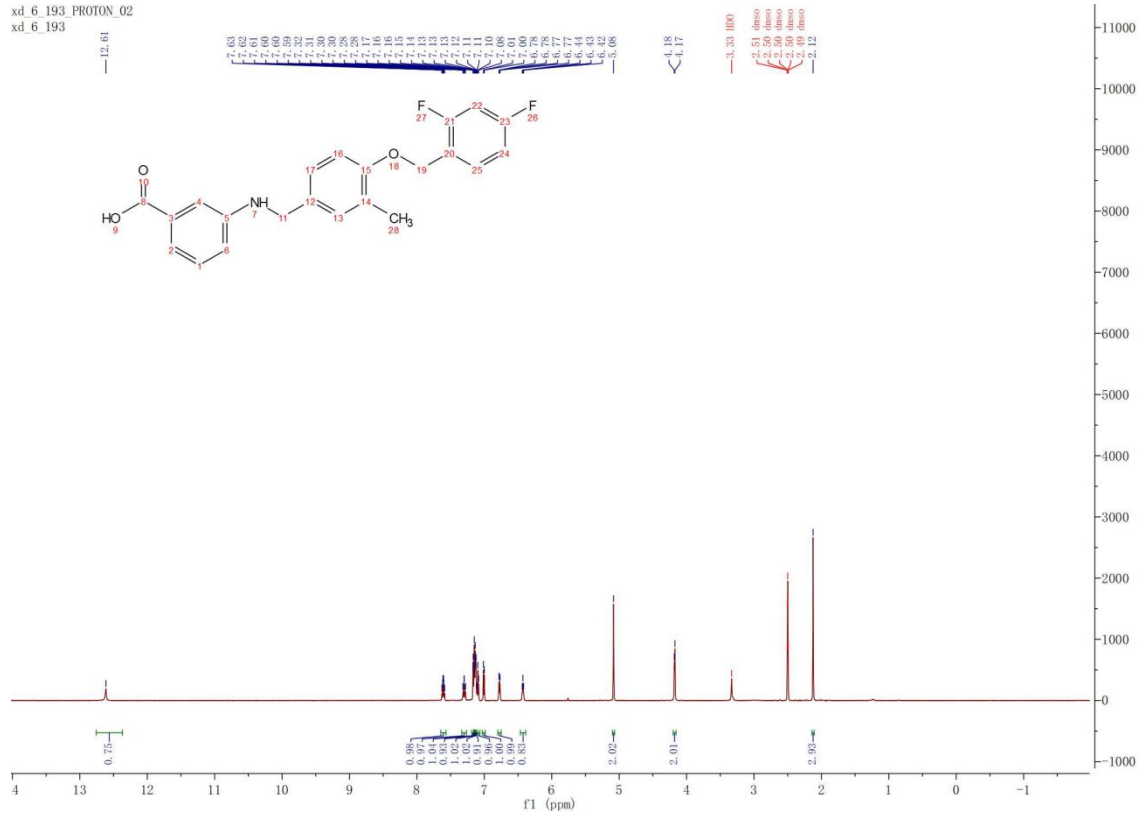


xd_7_53_600 CARBON_01
 xd_7_53_600

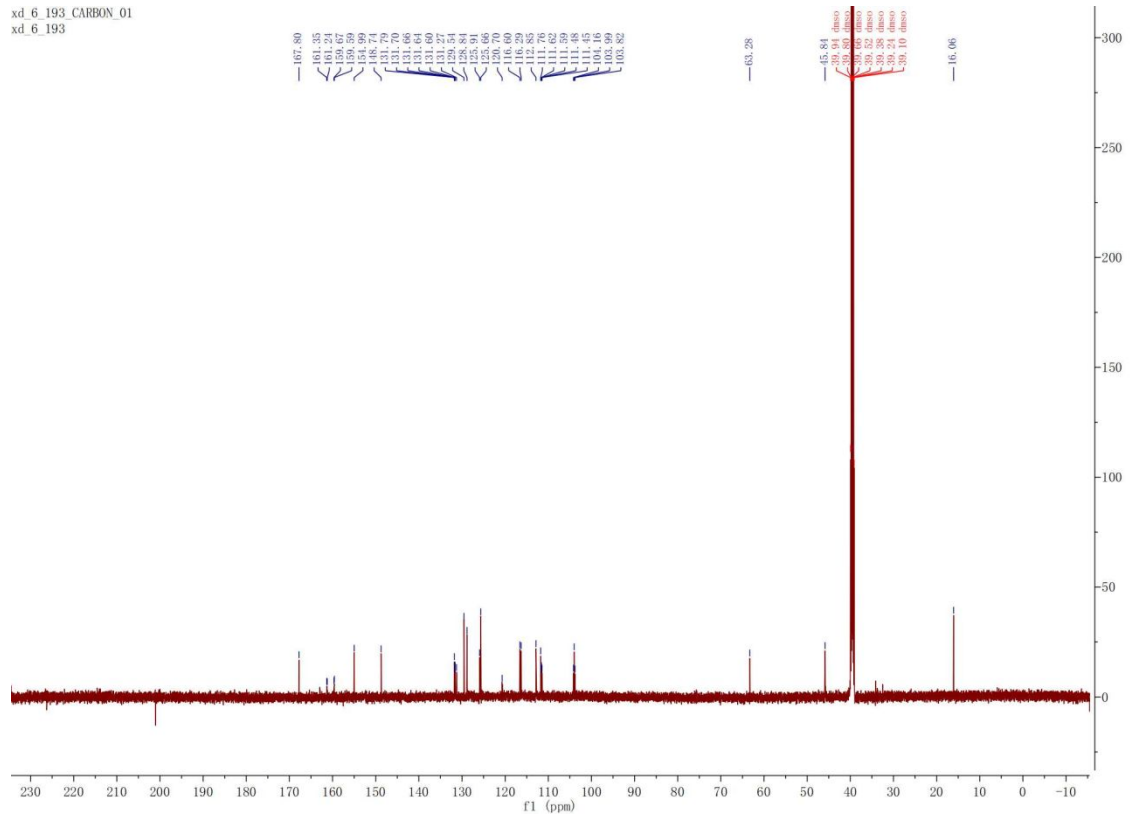


23

xd_6_193 PROTON_02
xd_6_193

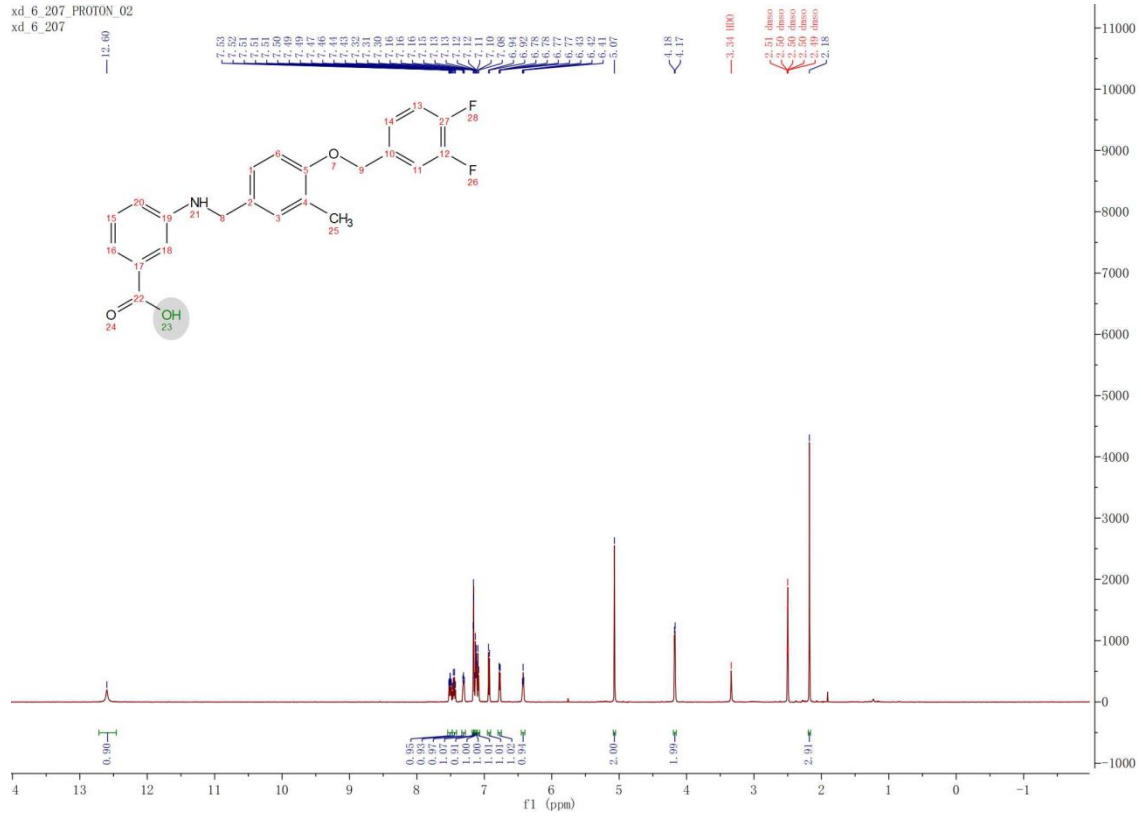


xd_6_193 CARBON_01
xd_6_193

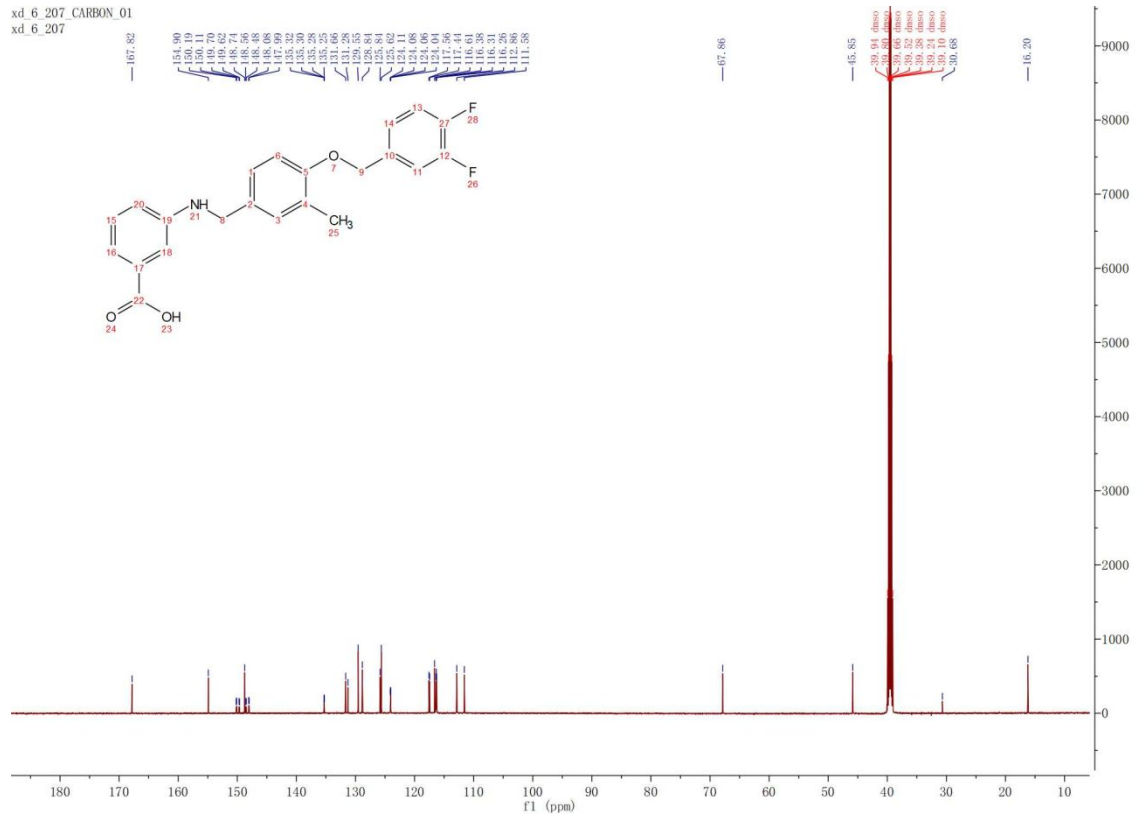


24

xd_6_207_PROTON_02
xd_6_207

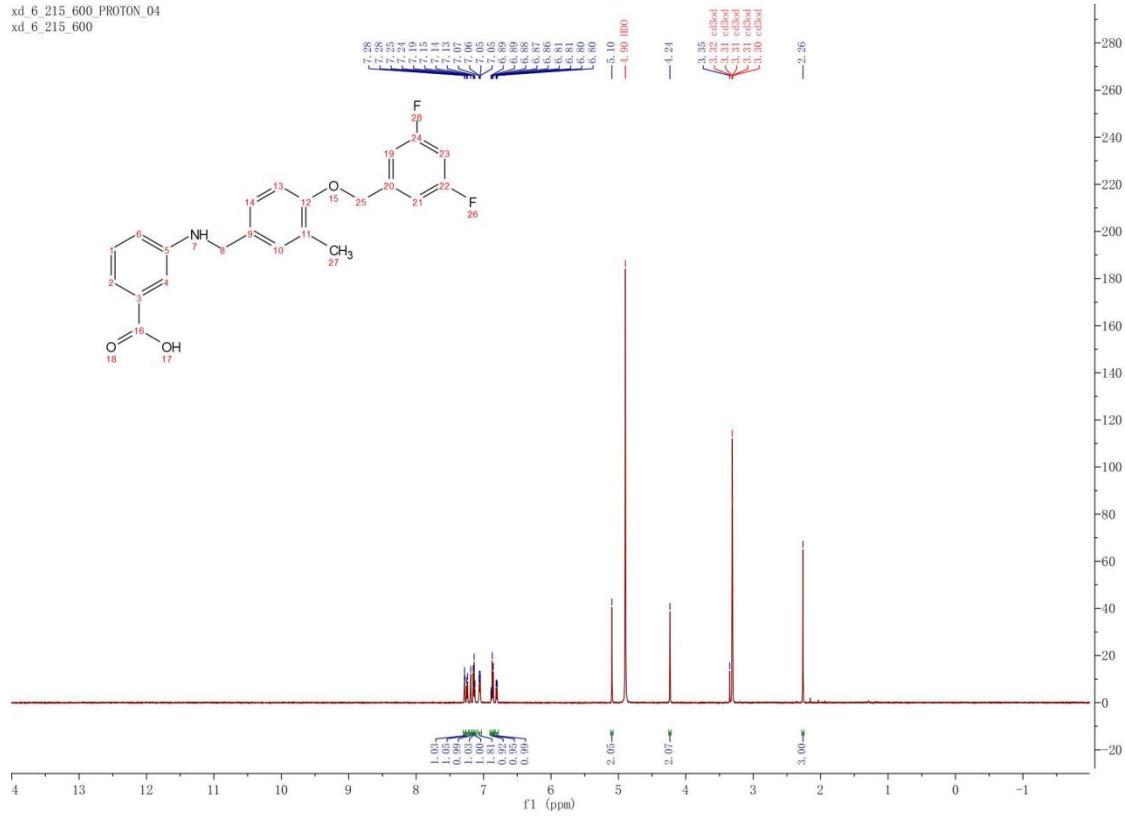


xd_6_207 CARBON_01
xd_6_207

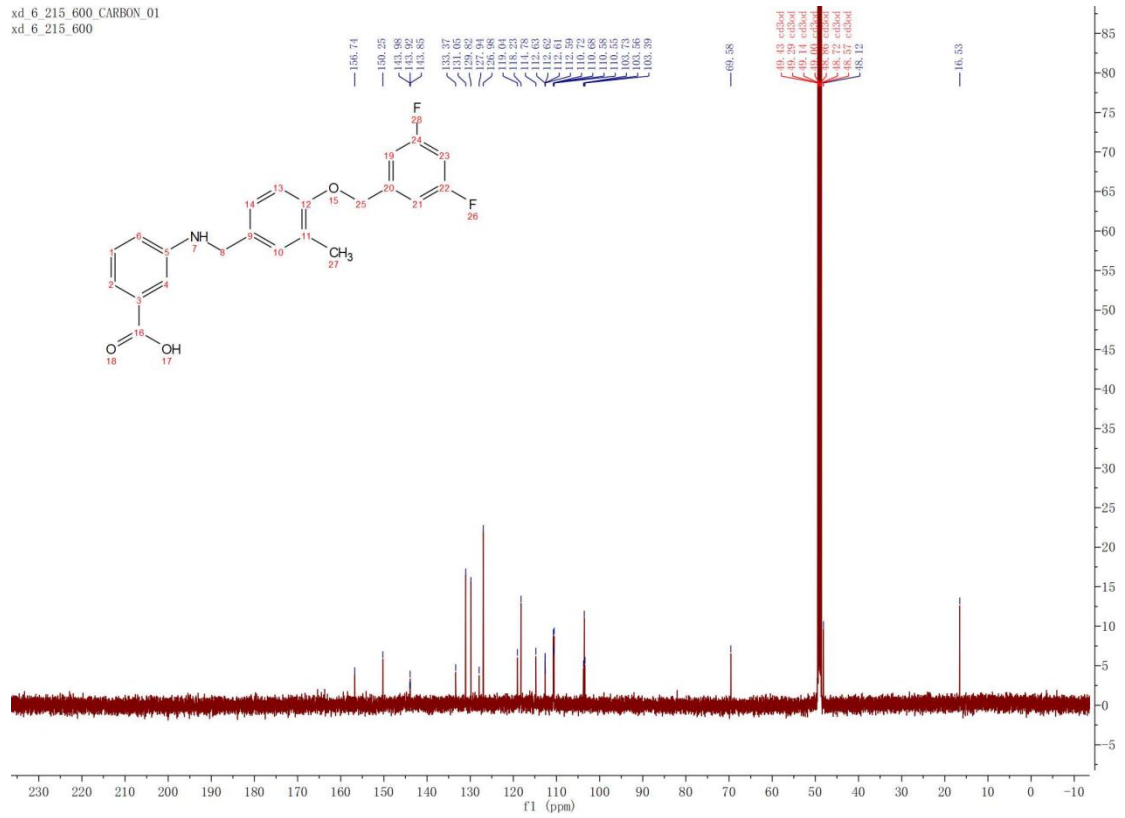


25

xd_6_215_600 PROTON_04
xd_6_215_600



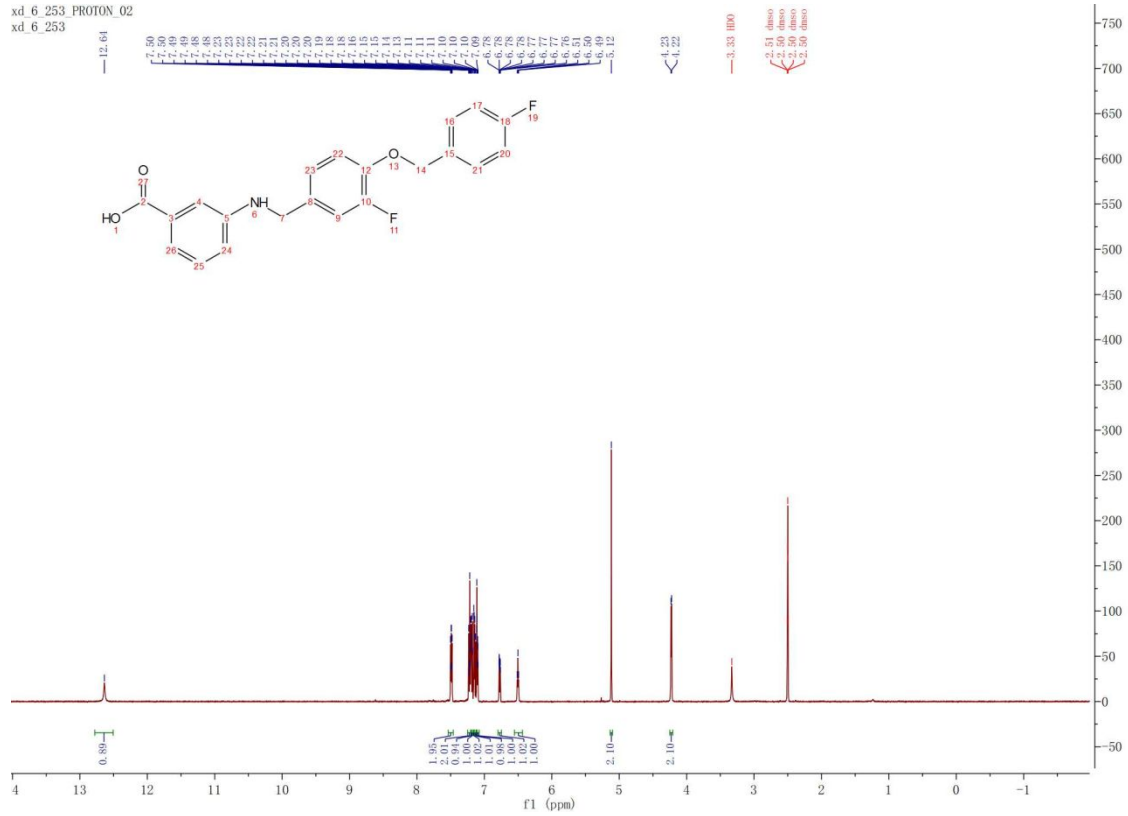
xd_6_215_600 CARBON_01
xd_6_215_600



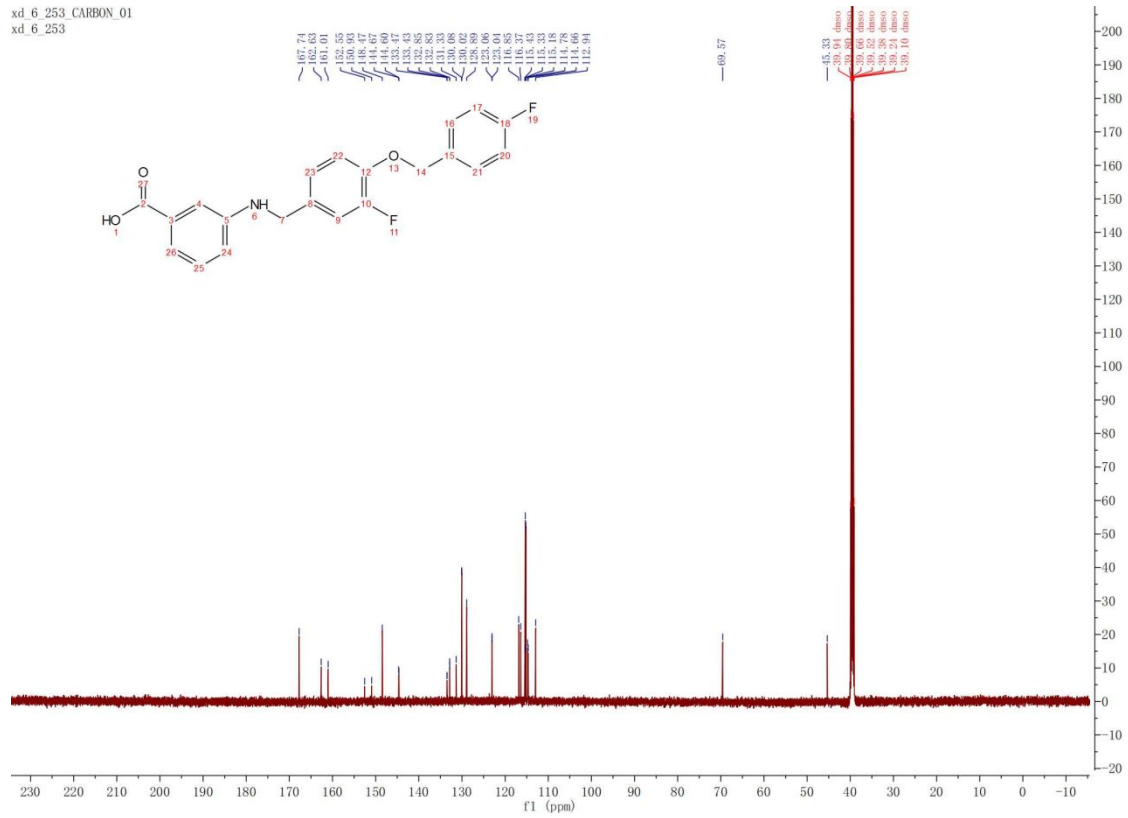
S50

26

xd_6_253 PROTON_02
xd_6_253



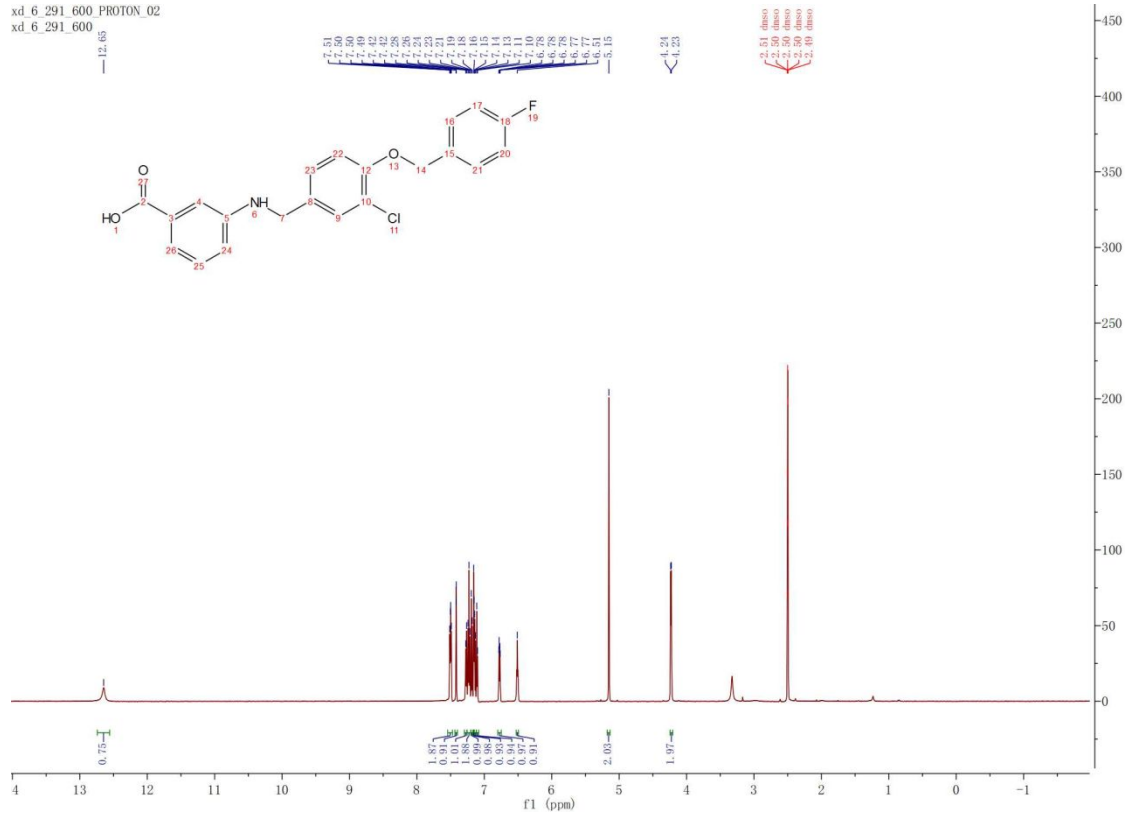
xd_6_253 CARBON_01
xd_6_253



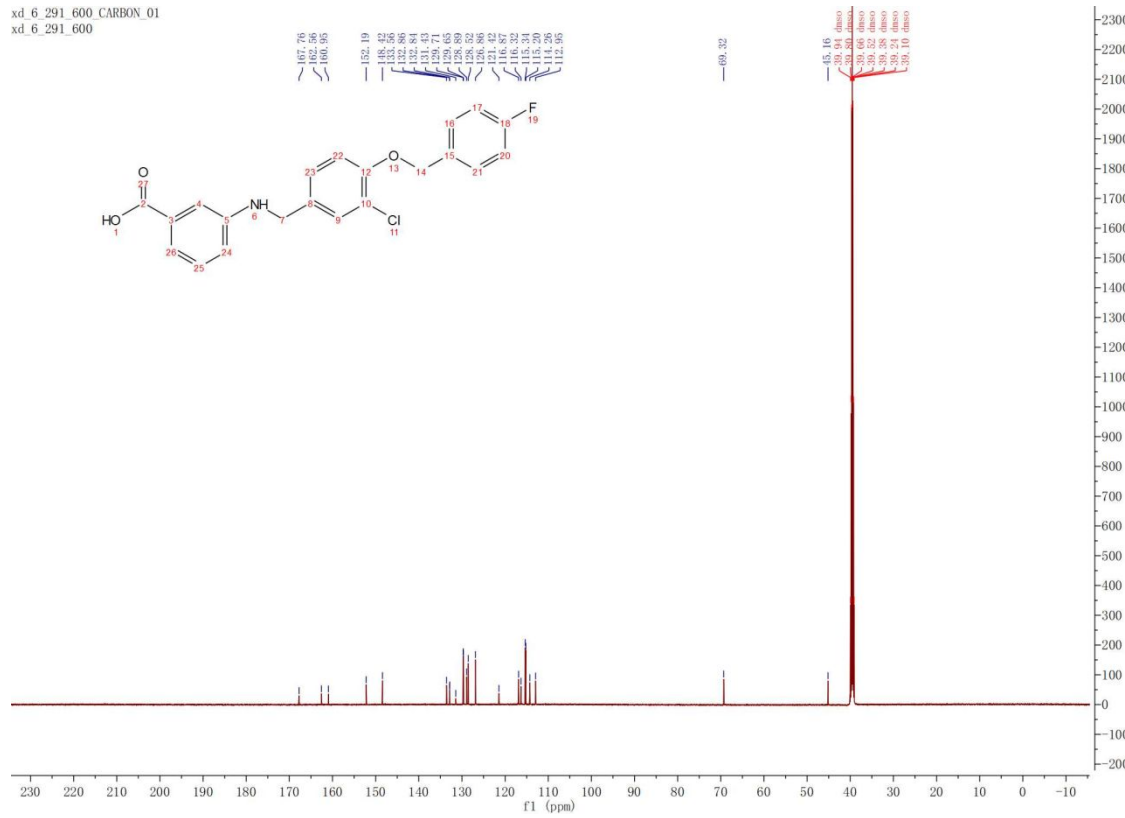
S51

27

xd_6_291_600 PROTON_02
xd_6_291_600

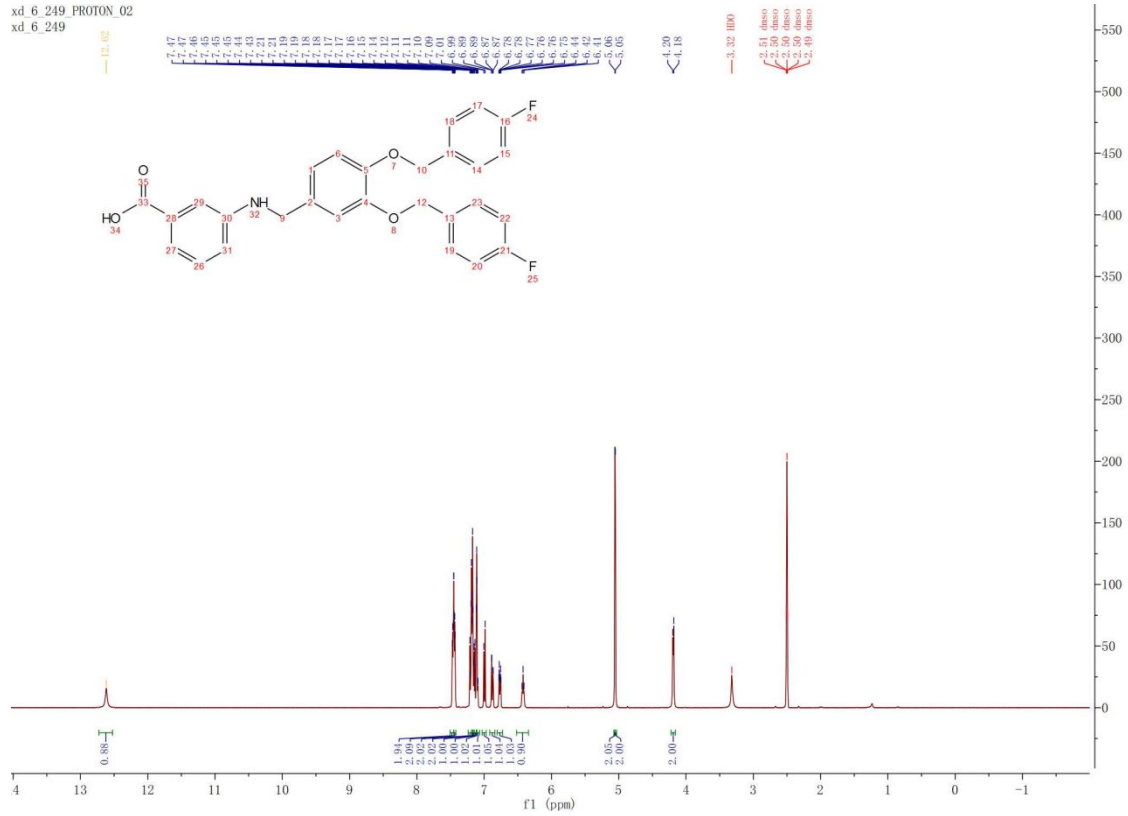


xd_6_291_600 CARBON_01
xd_6_291_600

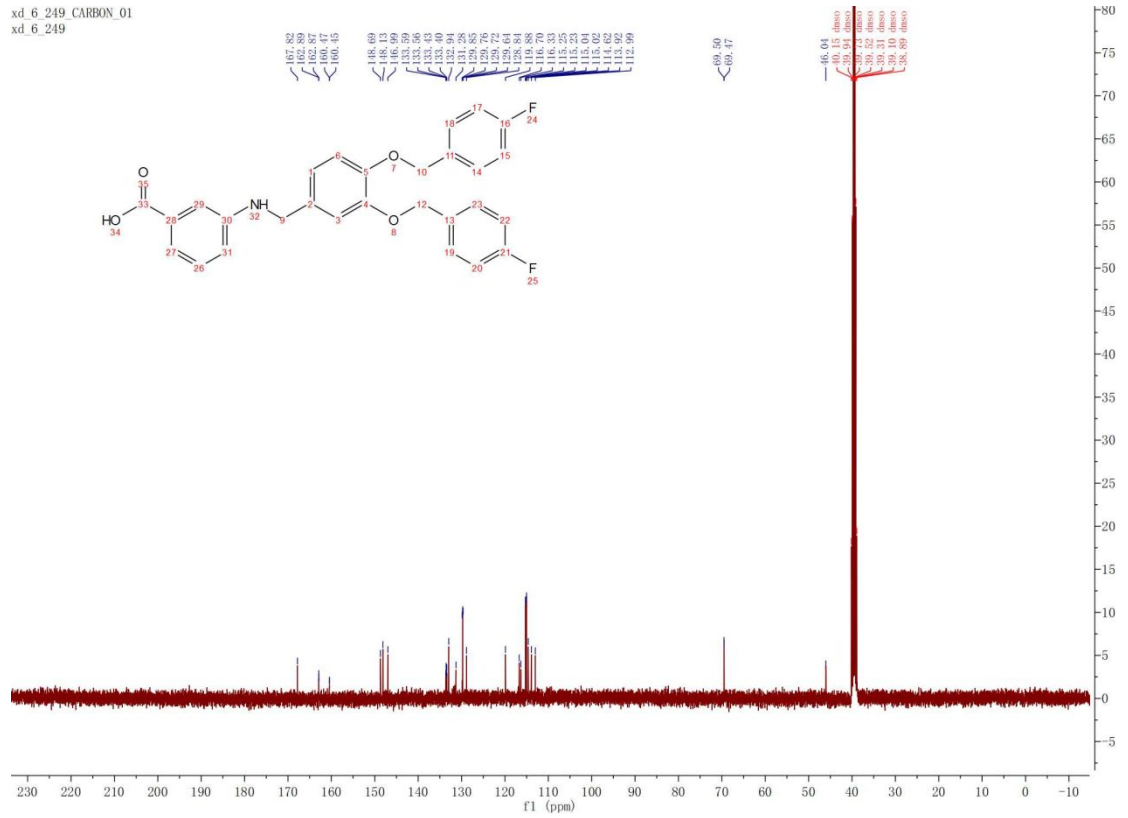


28

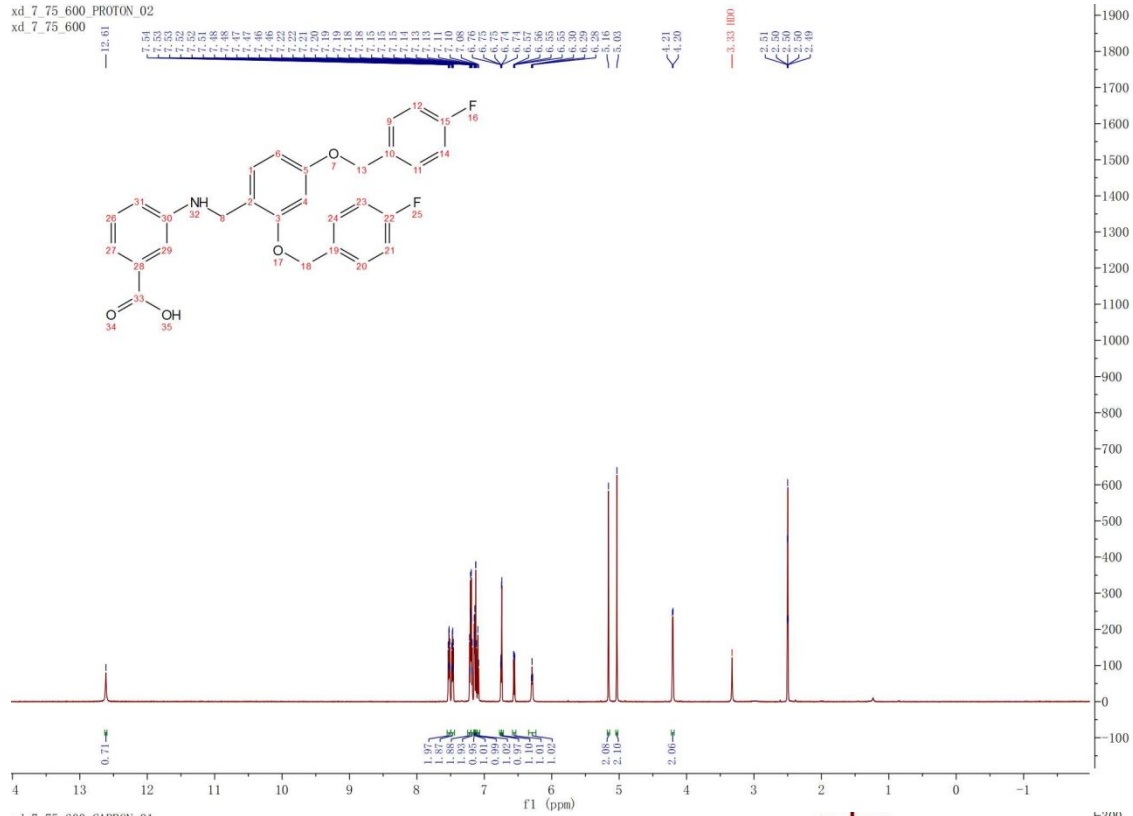
xd_6_249_PROTON_02
xd_6_249



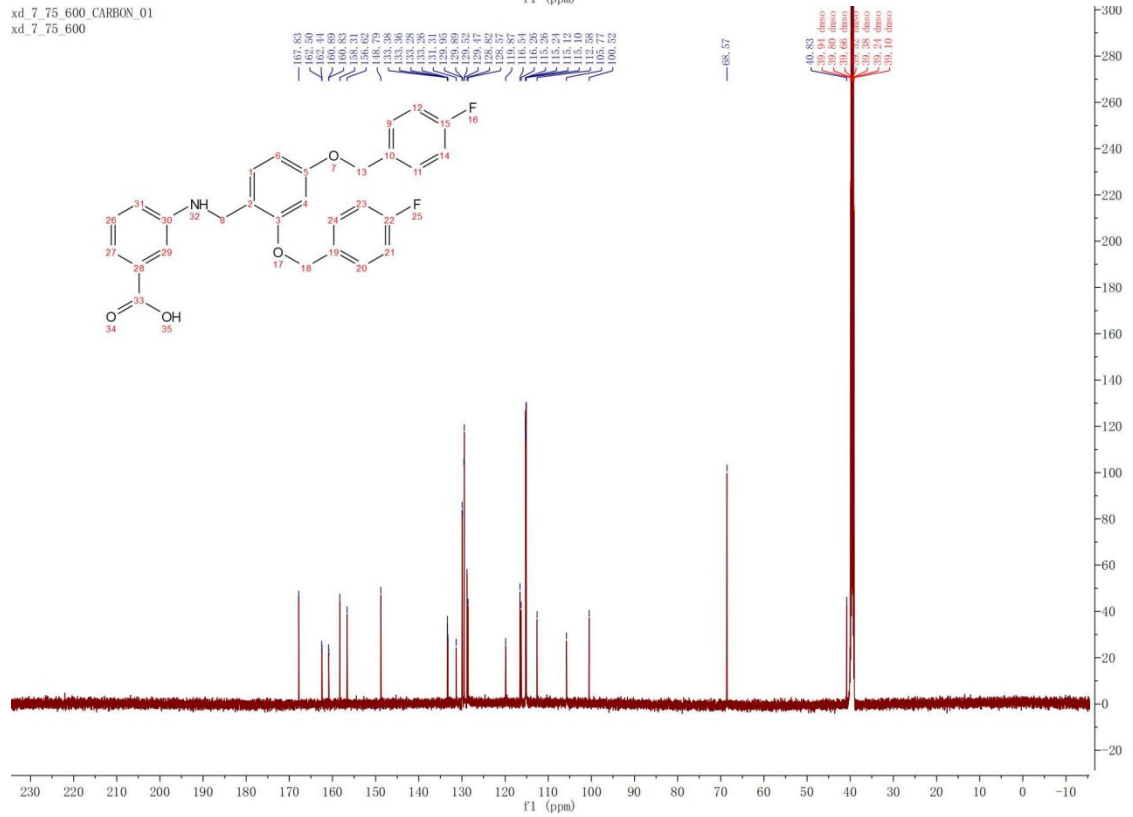
xd_6_249_CARBON_01
xd_6_249



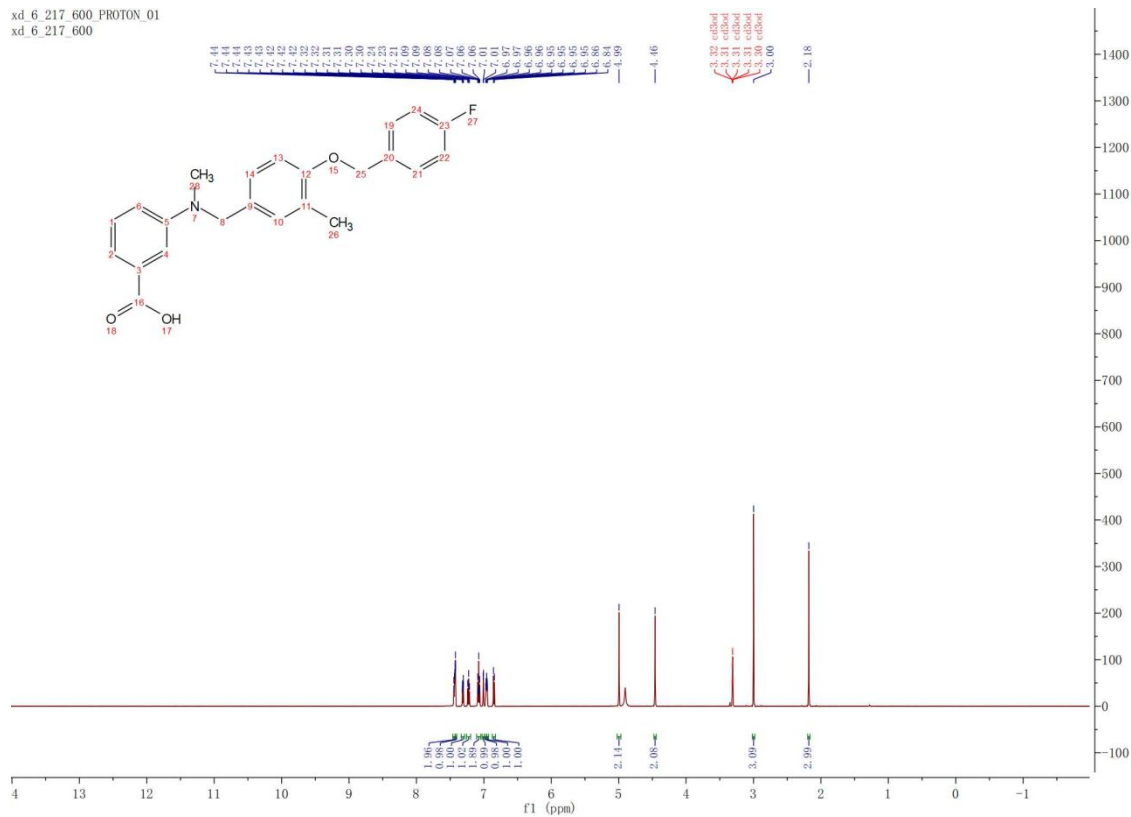
xd_7_75_600 PROTON_02
xd_7_75_600



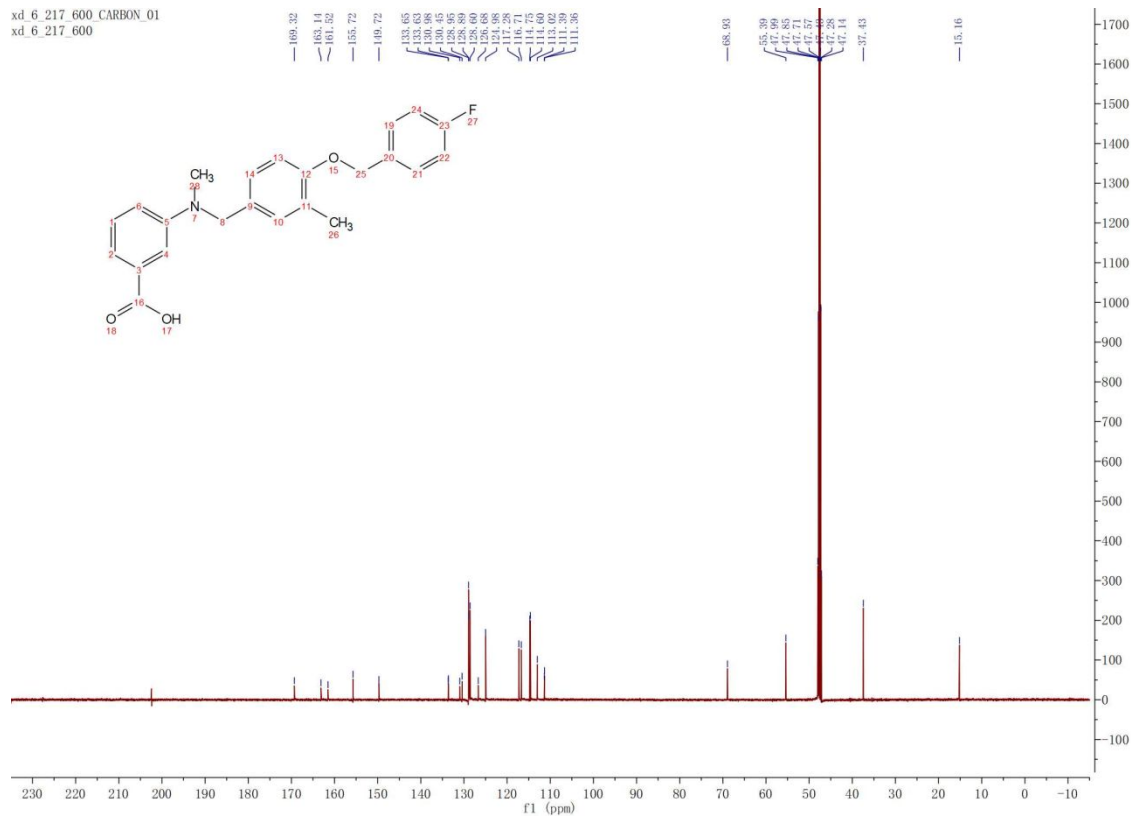
xd_7_75_600 CARBON_01
xd_7_75_600



xd_6_217_600_PROTON_01
xd_6_217_600

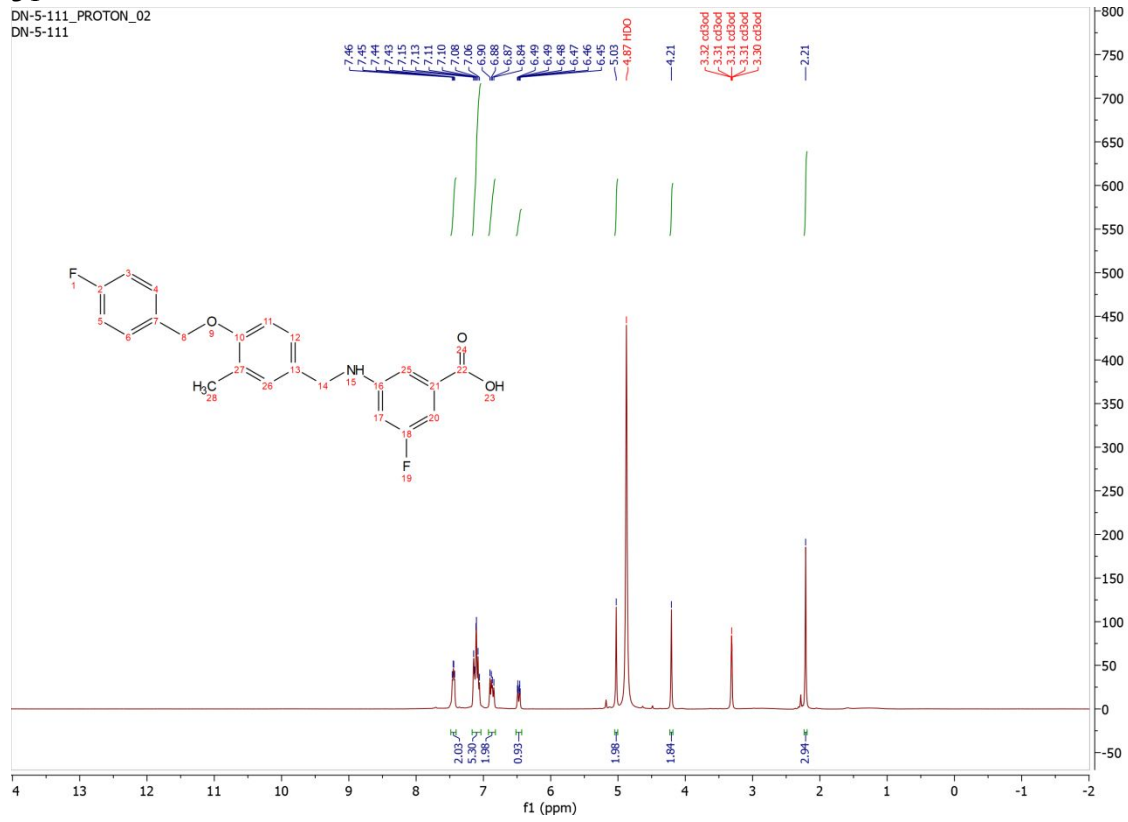


xd_6_217_600 CARBON_01
xd_6_217_600

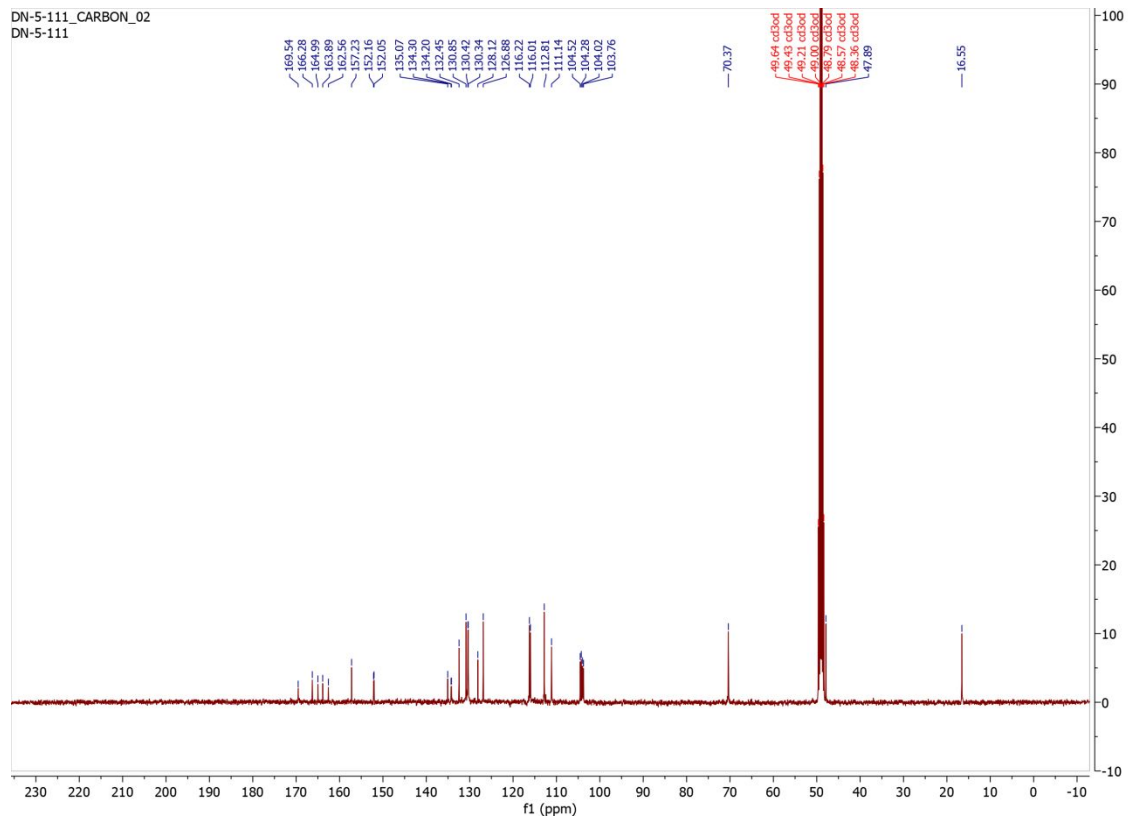


31

DN-5-111_PROTON_02
DN-5-111

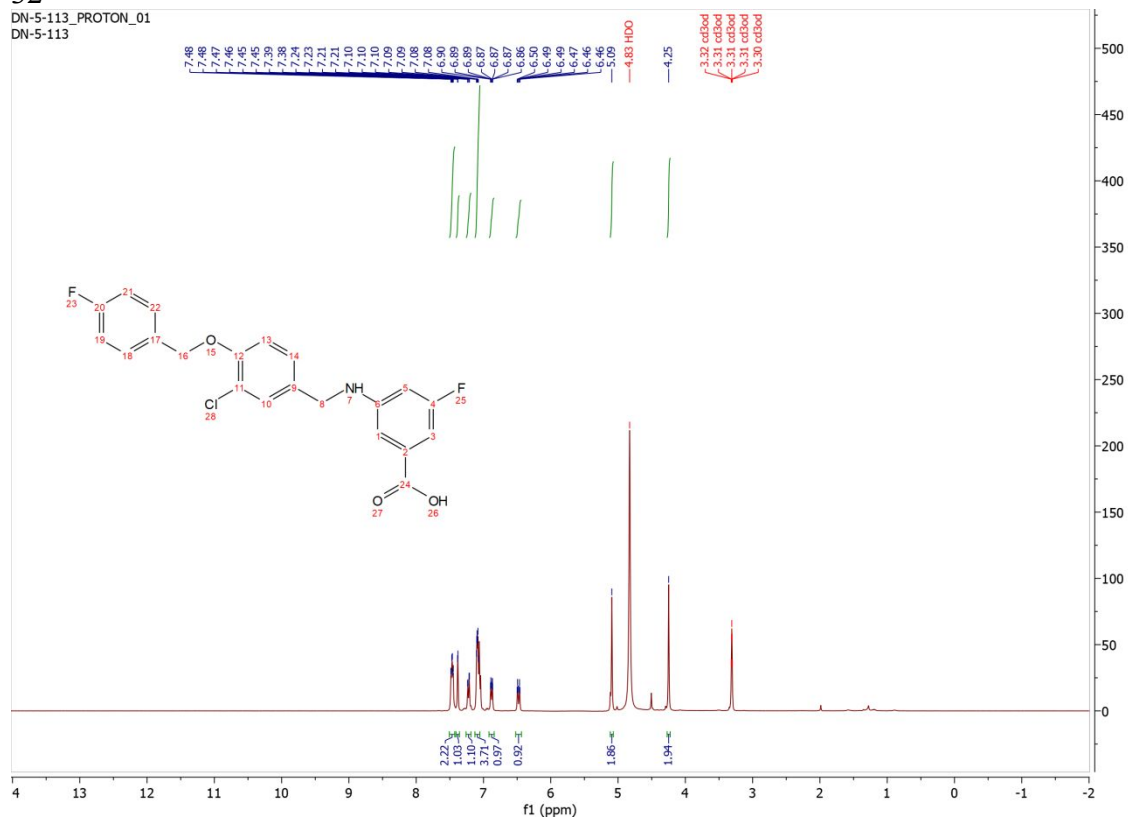


DN-5-111_CARBON_02
DN-5-111

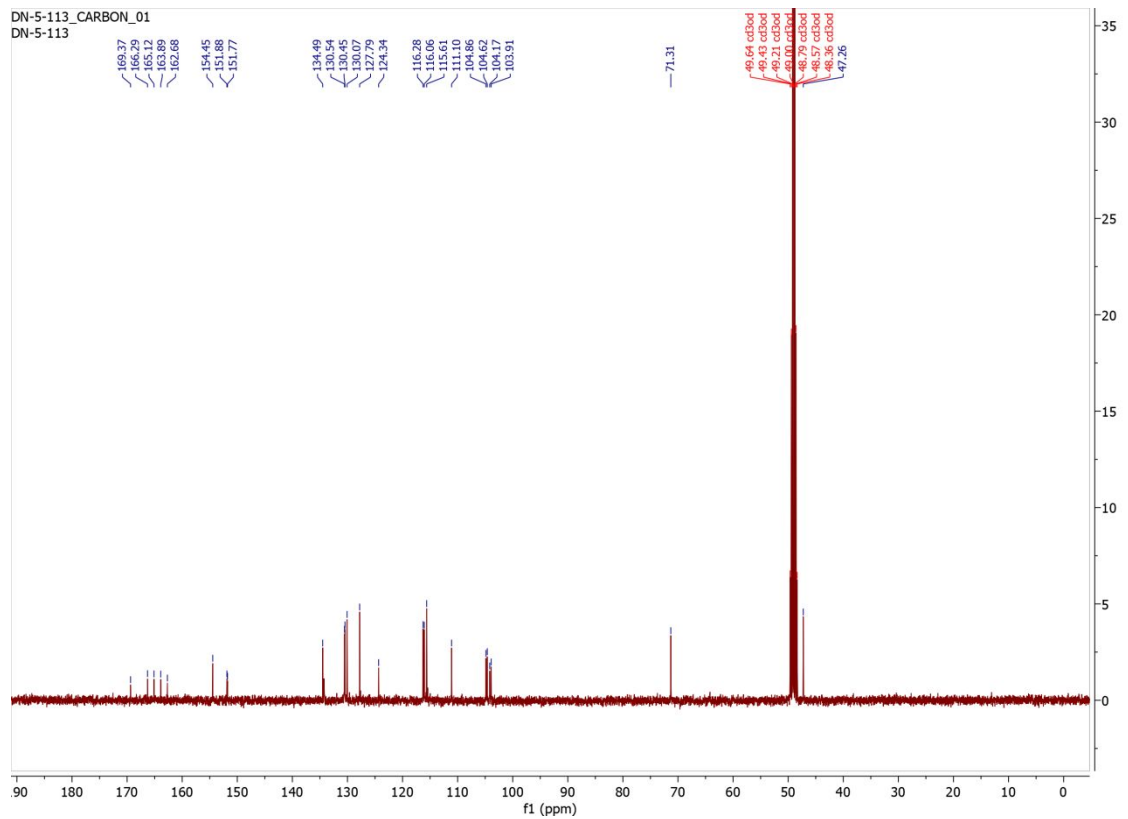


32

DN-5-113_PROTON_01
DN-5-113

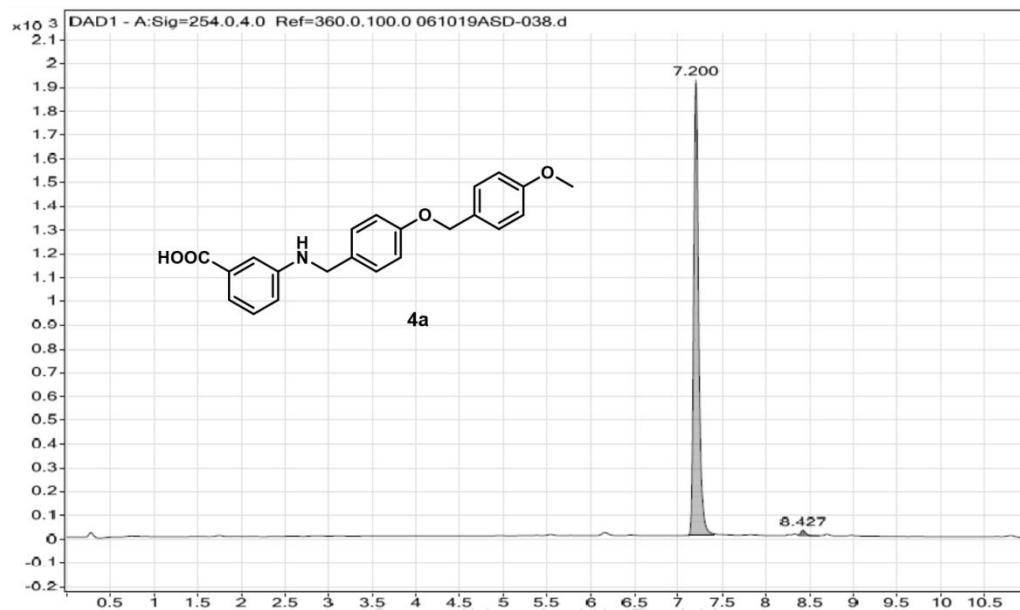


DN-5-113_CARBON_01
DN-5-113

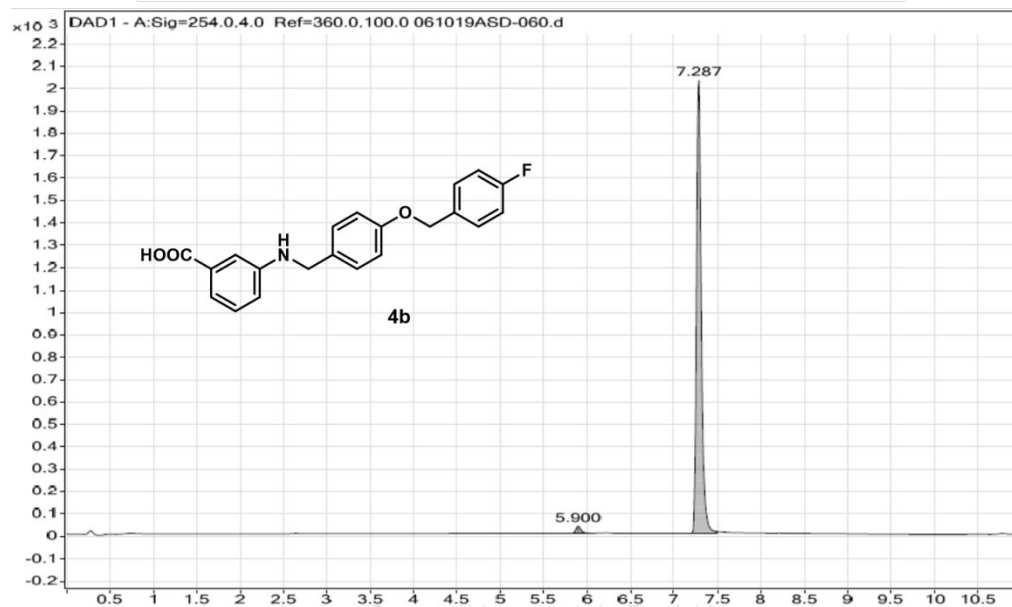


HPLC Traces

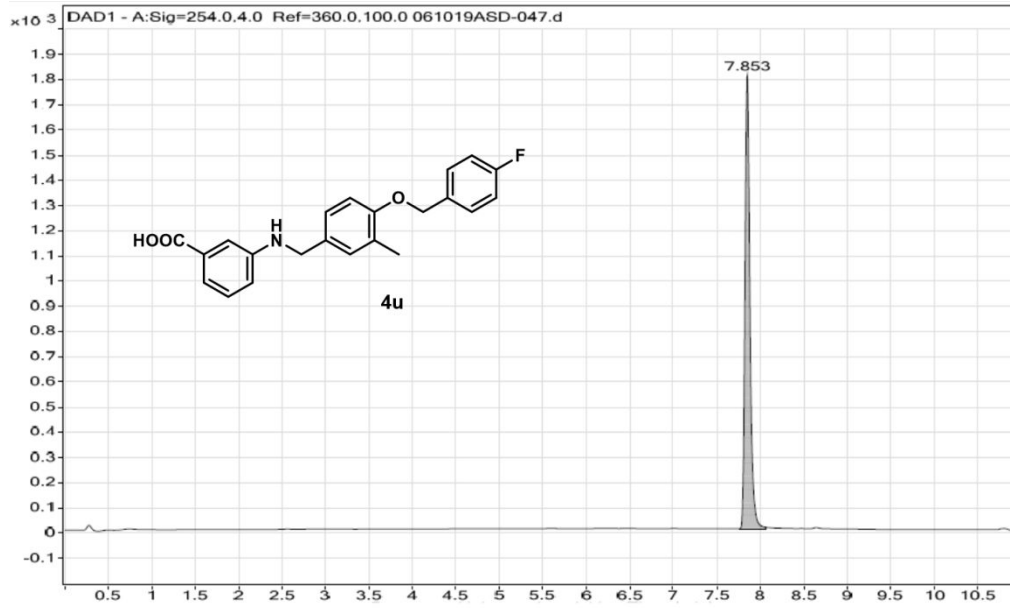
Peak	RT	Area	Height	Type	Saturated	Width	FWHM	SNR
1	7.2	7611.9	1917.3			0.293	0.059	
2	8.427	94.93	23.43			0.24	0.057	



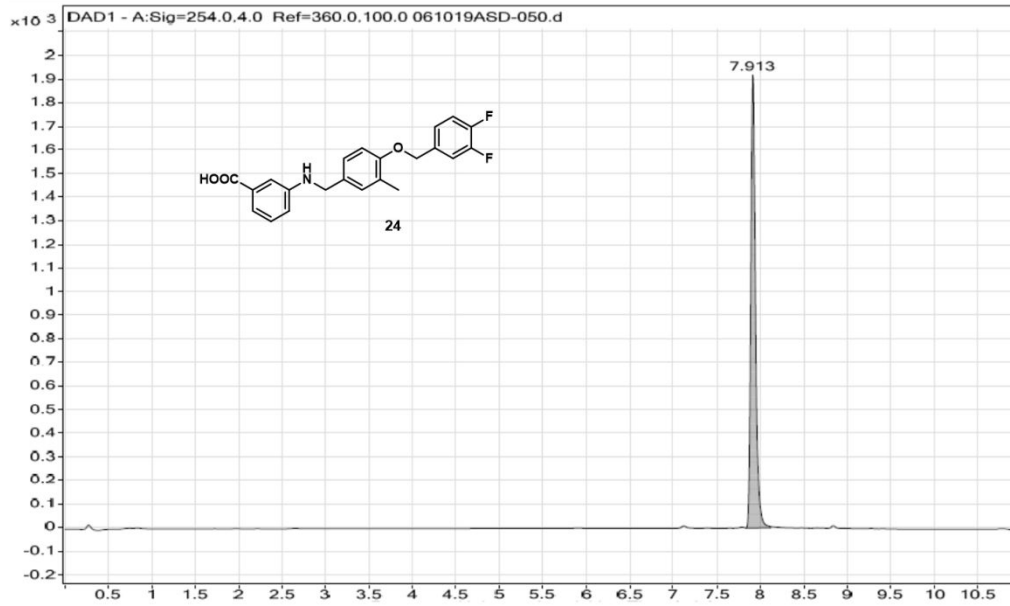
Peak	RT	Area	Height	Type	Saturated	Width	FWHM	SNR
1	5.9	135.02	32.58			0.247	0.061	
2	7.287	7833.3	2024.17			0.29	0.057	



Peak	RT	Area	Height	Type	Saturated	Width	FWHM	SNR
1	7.853	7214.4	1803.97			0.3	0.059	



Peak	RT	Area	Height	Type	Saturated	Width	FWHM	SNR
1	7.913	7258.6	1920.86			0.287	0.056	



Peak	RT	Area	Height	Type	Saturated	Width	FWHM	SNR
1	0.28	115.51	32.09			0.189	0.054	
2	3.867	62.05	16.78			0.193	0.052	
3	4.4	2570.6	805.61			0.226	0.048	

